2018-01-01

A Combined Field, Experimental And Modeling Approach To Understand The Impacts Of Flood Irrigation On Pedogenic CaCO3 And CO2 Dynamics In Drylands

Anna Cristina Ortiz
University of Texas at El Paso, anna.ortizc@gmail.com

A COMBINED FIELD, EXPERIMENTAL AND MODELING APPROACH TO UNDERSTAND THE IMPACTS OF FLOOD IRRIGATION ON PEDOGENIC $CaCO_3$ AND CO_2 DYNAMICS IN DRYLANDS

ANNA CRISTINA ORTIZ

Doctoral Program in Geological Sciences

APPROVED:

Lixin Jin, Ph.D., Chair

Lin Ma, Ph.D.

Mark Engle, Ph.D.

Craig Tweedie, Ph.D.

Anthony Darrouzet-Nardi, Ph.D.

Charles Ambler, Ph.D.
Dean of the Graduate School

Dedication

To all my family and friends and their constant support.

A COMBINED FIELD, EXPERIMENTAL AND MODELING APPROACH TO UNDERSTAND THE IMPACTS OF FLOOD IRRIGATION ON PEDOGENIC $CaCO_3$ AND CO_2 DYNAMICS IN DRYLANDS

by

ANNA CRISTINA ORTIZ

B.S., M.S.

DISSERTATION

Presented to the Faculty of the Graduate School of

The University of Texas at El Paso

in Partial Fulfillment

of the Requirements

for the Degree of

DOCTOR OF PHILOSOPHY

Department of Geological Sciences

THE UNIVERSITY OF TEXAS AT EL PASO

December 2018

Acknowledgements

I would like to acknowledge all of the amazing people that have helped review and prepare this dissertation research for the last four and a half years. I am grateful to all of the lab mates that have helped me, particularly Sandra Garcia, Syprose Nyachoti and Manny Sosa. This work would not have been possible without the help of all of the undergraduate researchers that aided in sample analyses and data collection: Karen Valles, Andrea Lopez, Paola Soto-Moreno, Frank Chavez and Isaac Martinez. I want to acknowledge all the help received by Gesuri Ramirez in helping set up all the sensor hardware and software appropriately for the column flow-through experiments. I would also like to thank the Ivey Family for allowing us to work extensively in their pecan and alfalfa orchards over the years. Furthermore, I am particularly grateful to Dr. Niu, Triston Hooks and Christina Perez of Texas A&M Agrilife for allowing us to use their greenhouses to run our flow-through column experiments.

Abstract

Soil salinization is a global problem affecting 10% of agricultural soils, particularly in irrigated arid-lands. This study investigated salt loading through flood-irrigation, particularly of calcite ($CaCO_3$) salt in the southwest of the United States. To evaluate the impact that flood-irrigation has on $CaCO_3$ buildup and its effect on C-cycling, a natural soil and two agricultural soils were sampled: a pecan orchard and an alfalfa field in the El Paso, TX region. Agricultural soils in this study are flood irrigated by the Rio Grande river and by ground waters in its absence, both of which are oversaturated with calcite.

To trace for Ca^{2+}, $^{87}Sr/^{86}Sr$ characterizations of irrigation water, dust, soil, soil water, and soil amendment samples were conducted to determine controlling sources pedogenic carbonates in agricultural soils. By also characterizing $\delta^{13}C$ in SOC, carbonates in the soil profiles, DIC, major ions in the irrigation waters, soil waters, and CO_2 in soil gases from the highly managed pecan orchard, the relative impact of flood-irrigation and natural processes with mass balance modeling was constrained. Flow-through column experiments of varying textures and flood water salinities helped elucidate physical and abiotic processes that control calcite kinetics and CO_2 efflux.

This work highlights flood irrigation as the major mechanism of soil salinization and C-cycling in our sample sites. All soils were found to have high salinity and sodicity, are controlled by the quantity/quality of irrigation waters and by variations in soil-texture. Pedogenic carbonate precipitation in agricultural fields is driven by Ca^{2+} loadings of irrigation practices and not by natural processes. This dissertation shows a previously unmeasured CO_2 flux as a consequence of agricultural calcite formation and propose that these are a function of soil moisture loss in combination with atmospheric pressure pumping. Furthermore, this work suggests that pore-fluid

EC can be used successfully a proxy to determine calcite-sourced CO_2 efflux. Supplementary work is suggested to determine if CO_2 emissions are significant in regional and global carbon budgets.

Table of Contents

List of Tables

List of Figures

Chapter 1: Introduction

The critical zone is defined as the land surface layer extending from the canopy to the lower boundary of the groundwater and is crucial in providing ecosystem functions and services especially in managed agricultural lands (Chorover et al., 2007; Amundson et al., 2007). More than 40% of the Earth's land coverage are designated as arid-lands where rainfall is exceeded by potential evaporation and transpiration, resulting in a water deficit (e.g., Reynolds et al. 2007). Some arid-lands are cultivated for crops as a result of the pressures exerted by growing food demand (MEA 2005; Reynolds et al. 2007). The application of irrigation water makes these particular critical zones more dynamic hydrologically and biogeochemically as shifts in their system functions and services are driven by agriculture. However, such agricultural practices are unsustainable because arid-lands are freshwater limited environments (Rozema and Flowers, 2008; Assouline et al., 2015). In addition, salt loading through irrigation and reduced leaching capacity of fine textured soils, combine to increase soil salinity, deteriorate overall soil quality, and lower crop yields (Pannell and Ewing, 2006; Shrivastava and Kumar, 2015; Cox et al., 2018). Soil salinization affects more than 830M ha of land globally, or ~10% of the global arable land (Szabolcs, 1989; Martinez-Beltran and Manzur, 2005). Soil salinization has been recorded worldwide including countries such as Argentina and in the North China Plain (Falasca et al., 2014; Shrivastava and Kumar, 2015; Wang et al., 2015). Furthermore, it is expected that by the year 2050, 50% of the world's arable land will be salinized (Jamil et al., 2011). In the U.S. alone, crop yield has reduced by approximately 30% in irrigated soils as a result of salinization (ars.usda.gov).

In the regions surrounding El Paso, Texas, Rio Grande river water and groundwater are typically used for flood irrigation, where both water types are of high salinity. High

evapotranspiration and reduced water infiltration in soils lead to supersaturation with respect to evaporate salts and facilitates their precipitation in soils (Szynkiewicz et al., 2015; Assouline et al., 2015). High soil salinity and sodicity have been previously observed in soils of the major crops in the region: cotton, alfalfa and pecan (Cox et al., 2018).

Pedogenic carbonates, specifically $CaCO_3$, commonly form naturally in hot drylands when soil waters become supersaturated with calcite as a result of evapotranspiration, CO_2 degassing, and/or microbial activity (Reardon et al., 1980; Kempe et al., 1991; Cerling and Quade, 1993; Lorah and Herman, 1988; Ku, 2001; Szramek and Walter, 2004; Jin et al., 2008). In natural systems, the accumulation of pedogenic carbonate is limited by available Ca^{2+} from the dissolution of primary Ca-bearing carbonate and silicate bedrocks, as well as wet and dry aeolian depositions (Capo & Chadwick, 1999; Hoven & Quade, 2002; Naiman, Quade, & Patchett, 2000; Zamanian et al., 2016). With limited rainfall, irrigation becomes an essential practice, loading additional Ca and promoting precipitation of secondary calcite and other salts (Cox et al., 2018; Falasca et al., 2014; Squires and Glenn, 2004). However, few studies have focused on the impact that calcite deposition and precipitation in agricultural fields has on carbon cycling. Irrigation supplies significant amounts of Ca^{2+} and HCO_3^- to soils annually and could dramatically alter carbon cycles as it is intrinsically linked to emission of CO_2 (Reaction 1) (Suarez, 2000; Schlesinger, 2000; Sanderman, 2012; Nyachoti et al., 2017; Cox et al., 2018).

$$Ca^{+2}{}_{(aq)} + 2HCO^-_{3(aq)} \leftrightarrow CaCO_{3(s)} + CO_{2(g)} + H_2O_{(l)} \quad \text{Reaction (1.1)}$$

Emission of CO_2 from soils to the atmosphere is considered to be a major global C flux. The abiotic release of CO_2 to the atmosphere has not been directly measured; although, soils have been established to be important CO_2 reservoirs. (Schlesinger and Andrews, 2000; Serrano-Ortiz et al. 2010; Bourges et al., 2012; Fernandez-Cortes et al., 2015). Natural production of soil CO_2

has long been studied, where it is dominated by biotic sources including bacterial decomposition of organic matter, root respiration, and microbial activity, even in water-limited drylands (Trumbore et al., 1996; Davidson et al., 1998; Lal, 2004; Tang et al., 2005; Darrouzet-Nardi et al., 2015). Enhanced CO_2 production as a consequence of dryland agriculture would include an unexpected and otherwise unstudied source that could be widely impacting global carbon cycling, especially since dryland agriculture is so wide spread and is expected to continue to grow with present climate models.

This PhD dissertation focuses on accumulation of pedogenic carbonates and emission of abiotic CO_2 in irrigated arid-lands. It combines field, laboratory and modelling approaches to understand the controls on these geochemical processes and quantifies the magnitude of different carbon fluxes in the global cycles. The study sites are selected in southwestern United States, along the Rio Grande valley, in two major crops alfalfa and pecan.

Chapter 2 addresses the physical and chemical controls on soil salinization by flood irrigation in arid-lands. Salt loading is quantified and irrigation is shown to be much more important than wet and dry deposition or soil amendments. As a result of more than 90 years of cultivation, soils become saline and sodic. Application of soil amendments such as gypsum lowers soil sodicity, but only temporarily. This study also identifies water quality and soil texture as the primary control on the magnitude of salt accumulation in soils, including pedogenic carbonates.

Sediments along the Rio Grande are a several thousand years old, where pedogenic carbonates accumulated naturally but are now also driven by irrigation practices. Chapter 3 and Chapter 4 use Sr and C isotopes respectively to differentiate “old” and natural versus “young” and anthropogenic carbonates, then quantify their relative contribution. Chapter 3 collected and characterized $^{87}Sr/^{86}Sr$ ratios of different endmembers (natural endmembers: local and regional

dust and rainfall; anthropogenic endmembers: irrigation and soil amendments) and quantified the sources of Ca in pedogenic carbonates.

Chapter 4 evaluates the impact of irrigation on C cycles, using carbon isotopic analyses of soil pedogenic carbonate, organic matter and soil gases. Carbon isotopes in pedogenic carbonate can elucidate the contribution from irrigation-derived dissolved inorganic carbon and natural C3-type and C4-type vegetation. Soil CO_2 are evaluated as a mixture of three sources, atmospheric CO_2, soil respired CO_2 and calcite-derived CO_2. This chapter highlights the impact of irrigation on atmosphere-land carbon exchange, through organic and inorganic carbon cycles.

Chapter 5 reports a series of flow-through column experiments, with contrasting soil texture and different salinity of irrigation water. These controlled experiments use only sands and clays to eliminate the influence of biological processes and focus on the calcite accumulation and abiotic CO_2 production. Field conditions (i.e., flood irrigation) are simulated and the physical and chemical controls on CO_2 movement and production are studied through nested soil CO_2 and soil moisture sensors. Results from these experiments shed light on the impact of irrigation on soil carbonate in the future scenarios of climate change.

REFERENCES:

Amundson R, Richter DD, Humphreys GS, Jobbagy EG, and Gaillardet J. (2007) Coupling between biota and Earth materials in the Critical Zone. Elements 3: 327-332.

Assouline S., Russo D., Silber A., et al. (2015) Balancing water scarcity and quality for sustainable irrigated agriculture, *Water Resources Research*, 51. 9127-9140

Capo, R.C. and Chadwick, O.A. (1999) Sources of strontium and calcium in desert soil and calcrete. Earth and Planetary Letters 170, 61-72.

Cerling T.E., and Quade J. (1993) Stable Carbon and Oxygen Isotopes in Soil Carbonates. *Geophysical Monograph Series.* https://doi.org/10.1029/GM078p0217

Chorover J, Kretzschmar R, Garcia-Pichel F and Sparks DL. (2007) Soil biogeochemical processes within the Critical Zone. Elements 3: 321-326.

Cox, C., Jin, L., Ganjegunte, G., Borrok, D., Lougheed, V., and Ma, L. (2018) Changes of soil quality due to flood irrigation in agricultural fields along the Rio Grande in western Texas. *Applied Geochemistry* 90, 87-100, doi.org/10.1016/j.apgeochem.2017.12.019.

Davidson, E.A., Belk, E. and Boone, R.D. (1998) Soil water content and temperature as independent or confounded factors controlling soil respiration in a temperate mixed hardwood forest. *Glob. Change Biol.* 4(2), 217-227.

Darrouzet-Nardi, A., Reed, S., Grote, E. and Belnap, J. (2015) Observations of net soil exchange of CO2 in a dryland show experimental warming increases carbon losses in biocrust soils. *Biogeochemistry* 1-16.

Falasca S.L., Ulberich A., and Acevedo A. (2014) Identification of Argentinian saline drylands suitable for growing *Salicornia bigelovii* for bioenergy, *International Journal of Hydrogen Energy* 39, 8692-8689

Jamil A., Riaz S., Ashraf M., Foolad M.R. (2011) Gene expression profiling of plants under salt stress. Crit. Rev. Plant Sci 30(5): 435-458.

Jin, L., Williams, E., Szramek, K., Walter, L. M. and Hamilton, S. K. (2008) Silicate and carbonate mineral weathering in soil profiles developed on Pleistocene glacial drift (Michigan, USA): Mass balances based on soil water geochemistry. *Geochimica et Cosmochimica Acta* 72, 1027-1042.

Kempe, S., Pettine, M., and Cauwet, G. (1991) Biogeochemistry of European rivers. In Biogeochemistry of Major World Rivers (eds. S. Kempe, E. T. Degens, J. E. Richey). John Wiley & Sons, New York, SCOPE/UNEP 42, 169–211.

Ku, T.C.W. (2001) Organic carbon–mineral interactions in near surface environments: implications for the global carbon cycles. Ph.D. Dissertation, University of Michigan, Ann Arbor, MI.

Lal, R. (2004) Soil carbon sequestration to mitigate climate change. *Geoderma* 123 (1-2), 1-22.

Lorah, M.M. and Herman, J.S. (1988) The chemical evolution of a travertine-depositing stream: geochemical processes and a mass transfer reaction. *Water Resources Research* 24, 1541–1552.

Naiman, Z., Quade, J. and Patchett, P.J. (2000) Isotopic evidence for eolian recycling of pedogenic carbonate and variations in carbonate dust sources throughout the southwest United States. *Geochim. Cosmochim. Acta* 64, 3099–3109.

Nyachoti, S., Jin, L., Tweedie, C.E. and Ma, L. (2017) Formation of pedogenic carbonates in the semi-arid Rio Grande valley: insights from carbon, major elements, and U-series isotopes in natural and agricultural soils of southern New Mexico and western Texas. Chemical

Geology, doi.org/10.1016/j.chemgeo.2017.10.014.
Serrano-Ortiz, P., Roland, M., Sanchez-Moral, S., JanssenS, I.A., Domingo, F., Goddéris, Y. and Kowalski, A.S. (2010), Hidden, abiotic CO_2 flows and gaseous reservoirs in the terrestrial carbon cycle: Review and perspectives. *Agricultural and Forest Meteorology* 150 (3), 321-329.
Martinez-Beltran J, Manzur CL. (2005). Overview of salinity problems in the world and FAO strategies to address the problem. *Proceedings of the international salinity forum, Riverside, California*, April 2005, 311–313.
Pannell D., and Ewing M, (2006) Managing secondary dryland salinity: Options and challenges. Agricultural Water Management v. 80 41-56
Reardon, E.J., Mozeto, A.A. and Fritz, P. (1980) Recharge in northern clime calcareous sandy soils: chemical and carbon-14 evolution. *Geochimica et Cosmochimica Acta* 44, 1723–1735.
Reynolds, J. F., Stafford Smith, D. M., Lambin, E. F., Turner, B. L., Mortimore, M., Batterbury, S. P. J., Downing, T. E., Dowlatabadi, H., Fernandez, R. J., Herrick, J. E., Huber-Sannwald, E., Jiang, H., Leemans, R., Lynam, T., Maestre, F. T., Ayarza, M., and Walker, B. (2007) Global desertification: building a science for dryland development, Science, 316, 847–851.
Rozema, J., and Flowers T. (2008) Crops for a Salinized World, Science v.322, 1478-1481.
Sanderman, J. (2012) Can management induced changes in the carbonate system drive soil carbon sequestration? A review with particular focus on Australia. *Agriculture, Ecosystems and environment* 155, 70-77.
Schlesinger, W.H. (2000) Carbon sequestration in soils: some cautions amidst optimism. *Agriculture, Ecosystems and Environment* 82, 121-127.
Shrivastava P., Kumar R. (2015) Soil salinity: A serious environmental issue and plant growth promoting bacteria as one of the tools for its alleviation. Saudi Journal of Biological Sciences (22)123-131.
Squires V.R., and Glenn E.P. (2004) Salinization, Desertification and Soil Erosion. V.R Squires (Ed.), The Role of Food, Agriculture, Forestry and Fisheries in Human Nutrition, UNESCO, EOLSS Publishers, Oxford UK
Suarez, D. L. (2000) Impact of Agriculture on CO_2 as Affected by Changes in Inorganic Carbon', in Lal, R., Kimble, J. M., Eswaran, H., and Stewart, B. A. (eds.), Global Climate Change and Pedogenic Carbonates, CRC/Lewis Publishers, Boca Raton, FL, pp. 257–272.
Szablocs, I. (1989) Salt affected soils, Boca Raton, CRC Press.
Szramek, K., McIntosh, J.C., Williams, E.L., Kanduc, T., Ogrinc, N., Walter, L.M. (2007) Relative weathering intensity of calcite vs. dolomite in carbonate-bearing temperate zone watersheds: carbonate geochemistry and fluxes from catchments within the St. Lawrence and Danube River Basin. Geochemistry, Geophysics, and Geosystems 8, Q04002, doi: 10.1029/2006GC001337.
Szynkiewicz A., et al. (2015) Isotopic studies of the Upper and Middle Rio Grande. Part 2- Salt loads and human impacts in south New Mexico and west Texas. Chemical Geology v.411, 336-350.
Tang, J., Misson, L., Gershenson, A., Cheng, W. and Goldstein, A.H. (2005) Continuous measurements of soil respiration with and without roots in a ponderosa pine plantation in the Sierra Nevada Mountains. *Agricultural and Forest Meteorology* 132, 212-227.

Trumbore, S.E., Chadwick, O.A. and Amundson, R. (1996) Rapid exchange between soil carbon and atmospheric carbon dioxide driven by temperature change. *Science* 272 (5260), 393-396.

Van der Hoven S.J. and Quade, J (2002) Tracing spatial and temporal variations in the sources of calcium in pedogenic carbonates in semiarid environment, *Geoderma*, 108, 259-276

Wang, Y., Deng C., Liu, Y., Niu Z., Li, Y.(2015) Identifying change in spatial accumulation of sol salinity in an inland river watershed, China *Science of the Total Environment 621*, 177-185

Zamanian K., et al., (2016) Pedogenic carbonates: Forms and formation processes, *Earth-Science Reviews 157*, 1-17

Chapter 2: Physical and Chemical Controls of Salt Movement and Accumulation in Natural versus Irrigated Soils in arid-lands of southwestern U.S.: a case study in El Paso, TX

1. INTRODUCTION

1.1 Agriculture in arid lands: opportunities and challenges

The critical zone is defined as the land surface layer extending from the canopy to the lower groundwater boundary and is essential for ecosystem function and service (Chorover et al., 2007; Amundson et al., 2007). However, human activities, especially since the Industrial Revolution, have significantly modified the critical zone (Crutzen, 2002). Agriculture occurs within the critical zone, impacting the its ecosystem services. More than 40% of the Earth's land coverage are designated as arid-lands (e.g., Reynolds et al. 2007). These are defined by as those terrestrial regions where current precipitation is exceeded by potential evaporation and transpiration, resulting in water deficit and lower biomass. A significant portion of arid lands have undergone land-use change from natural ecosystems into cultivated agriculture, so as to provide food for growing demands, while providing home to more than 38% of the world's population (MEA 2005; Reynolds et al. 2007). However, crop cultivation and the application of irrigation water, drives these particular critical zones into becoming more hydro-bio-geo-chemically dynamic, as their original ecosystem functions are modified.

Irrigated agriculture in arid-lands is problematic as the vast use of freshwater resources in such water-limited environments is not sustainable (Rozema and Flowers, 2008; Assouline et al., 2015). In addition, water used for irrigation is typically high in salinity in arid-lands, and high evapotranspiration and reduced infiltration lead to supersaturation with respect to evaporite salts and thus their precipitation in soils (Szynkiewicz et al., 2015; Assouline et al., 2015; Cox et al., 2018). Soil salinization resulting from irrigated agriculture has been recorded worldwide,

including Argentina and the north China plain ((Falasca et al., 2014; Shrivastava and Kumar, 2015; Wang et al., 2015), lowering crop yield, and deteriorating the overall soil quality (Pannell and Ewing, 2006; Shrivastava and Kumar, 2015; Cox et al., 2018). Salinization affects more than 830M ha of land globally, or ~10% of the world's arable land (Szabolcs, 1989; Martinez-Beltran and Manzur, 2005). It is expected that by the year 2050, 50% of the world's arable land will be salinized (Jamil et al., 2011). In the U.S. alone, crop yield from irrigated soils is reduced by approximately 30% relative to historic yields as a result of salinization (ars.usda.gov).

Soil salinity can be approximated by the electrical conductivity (EC) in water leachates and a soil is considered saline with EC values greater than 4 dS m^{-1}, approximately equivalent to 40 mM of NaCl (Marscher, 1995). Sodicity is a term given to soil with and excess of available Na^{+} adsorbed onto clay particles. As a result, it weakens soil structure by dispersing clay particles and limiting their aggregation and greatly decreasing soil permeability and hydraulic conductivity as a consequence (Assouline et al., 2015; Qi et al., 2018). Sodicity is and additional measure of soil quality because it controls clay structure and soil permeability (Richards, 1954). A proxy of soil sodicity is the sodium adsorption ratio (SAR), which is the concentration ratio of sodium concentrations over the square root of the sum of calcium and magnesium concentrations in soil leachates. Sodic soils are typified by SAR values >13 (Essington, 2003; Chaganti & Crohn, 2015). Soils that are saline and sodic can undergo a positive feedback loop, where increased sodic conditions lead to increased clay dispersion, limiting water movement through the profile, which in turn increases the amount of salt that is retained in the dispersed clays, and diminishes the functionality of the critical zone. To lower soil sodicity and salinity, soil amendments are applied to the field; however best management practices to minimize salt accumulation are essential for improving soil quality and sustaining irrigated agriculture in arid-lands.

1.2. The Rio Grande Valley

Rio Grande is the 5th largest river in the United States, and ~ 80% of its annual flow is diverted for municipal and agricultural use for over 5 million people throughout its course (Woodhouse et al., 2012; Hall and Peterson, 2013). Climate change induced decreased snowfall in the Rio Grande headwaters in Colorado is projected leading to predicted reduced recharge to the river (Elias et al., 2015; Pascolini-Campbell et al., 2017). Diminished water availability will make stakeholders, including municipalities, industries and farmers compete for increasingly limited freshwater resources (Szynkiewicz et al., 2015). Moreover, recharge of saline groundwater, wastewater source points and agricultural runoff increase the salinity of Rio Grande (Hogan et al., 2007; Williams et al., 2013; Szynkiewicz et al., 2015). Human activities threaten the water quality of the Rio Grande river by increasing its contaminant levels downstream (e.g., Ordoñez et al., 2011; Cayan et al., 2013; Borrok and Engle 2014; Elias et al., 2015).

Along the mid-Rio Grande, large portions of land surrounding the river are used for cultivation, including two agricultural hotspots in New Mexico, US : Albuquerque and Las Cruces and El Paso in Texas, USA. In 2012, 25.4% of land-use in the El Paso County, Texas was registered as cropland and El Paso was ranked 1st in pima cotton production and 2nd in pecan production for the State of Texas (agcensus.usda.gov). To ensure crop yields, large amounts of fertilizers are applied to crops in the region. Flood-irrigation is a common, low infrastructure practice in the region for intensive cultivation, from Rio Grande surface water and local ground water. The EC values of irrigation water near the El Paso, TX region were reported at ~1.4-4.6 dS m^{-1} with the Rio Grande water approaching saturation or being oversaturated for calcite ($CaCO_3$), near saturation for gypsum ($CaSO_4*2H_2O$) and under-saturated for halite (NaCl) (Szynkiewicz et al. 2015). Thus, $CaCO_3$ is predicted to precipitate in agricultural soils after irrigation events (Szynkiewicz et al., 2015) and is observed in agricultural soils (Cox et al., 2018). Although near

saturation, gypsum and halite, co-precipitation of these can easily occur in soils due to high concentrations of Na^+, Cl^-, and SO_4^{2-} in arid-land soils and high evapotranspiration rates (Graham and O'Green 2010). Cox et al. (2018) also confirmed overall high soil sodicity and salinity as common problems in agricultural soils along Rio Grande valley. Thus, agricultural practices such as tilling, application of soil amendments, and irrigation during non-growing seasons are commonly used to combat high soil salinity and sodicity.

Rio Grande river is hydrochemically closely linked to agricultural soils along the Rio Grande valley. Incoming irrigation waters leach evaporite salts out of the soil fields and return these into the surface waters through return flow, contributing to water salinity (Szynkiewicz et al., 2015; Cox et al., 2018). Indeed, Rio Grande water chemistry was shown to shift from Na^+-Cl^--type to SO_4^{2-}-Mg^{2+}-Ca^{2+}-type due to agricultural practices (Szynkiewicz et al 2011).

Irrigated agriculture in El Paso supports salt-tolerant crops such as alfalfa (*Medicago sativa*), cotton *(Gossypium barbadense)* and pecan *(Carya illinoinensis*) (ars.usda.gov). Soils along the Rio Grande valley are typically alkaline entisols, with no discernable horizons (Miyamoto 2010). Because downstream sediment deposits are controlled by flooding (Hall and Peterson 2013), present variability in sediment composition can be accredited to antecedent natural flooding. Moreover, historic river flooding and meandering have left a variety of inter-fingerings of sand, silt and clay sediment particles (Doser et al., 2007), and thus, soil texture in the agricultural fields is heterogeneous, controlling water flowpaths and residence time, and thus magnitude of salt accumulation.

This study aims to: (1) quantify natural (i.e., atmospheric wet and dry deposition) versus anthropogenic (i.e., agricultural amendments, and flood irrigation) salt inputs to local agricultural

soils; (2) investigate the importance of different controls on salt accumulation rates; and (3) determine if soil amendments improve soil quality.

2. METHODS

2.1. Site description

The agricultural study sites were selected on two typical crops in the region (alfalfa and pecan). Where the alfalfa site is located in El Paso, Texas and the pecan site is located in Tornillo, Texas, USA (Figure 1). The pecan orchard has grown pecans for the last 50 years and cotton for 30 years before that. The majority of fertilizers used are liquid or easily soluble salts. These include potassium carbonate, urea, gypsum and humic acids, to improve nutrient retention and crop yield (Appendix Table 2.1). To combat sodicity, 500lbs $acre^{-1}$ of elemental sulfur pellets have been annually over the past 20 years. Gypsum is added periodically to specific soils in the site with severe salinity and sodicity at the beginning of the growing season. During the growing season for pecans (April-September), the fields are flooded with about 10cm of irrigation waters every 2 to 3 weeks, or approximately 1.5m of water per growing season (Appendix Table 2.1). Waters used for irrigation include Rio Grande river, agricultural drainage waters and local groundwaters, when surface waters are not sufficient. Soils are tilled every spring to expose the low salinity and sandy sediments at depth, thus limiting sediment packing and increasing porosity.

Sediments in the pecan orchard belong to the Saneli silty-clay loam, Harkey loam, and Tigua silty-clay soil series. These Holocene-aged clayey and sandy alluvium soils are a result of natural flooding events in the Rio Grande basin (NRCS Custom Soil Report). Two soil profiles were chosen within the pecan orchard (Figure 2.1), one with visually stunted pecan tree growth (referred to as Pecan_Fine) and the other with visually lush growth (referred to as Pecan_Coarse). Furthermore, two additional soil profiles were collected before and after gypsum soil treatments

(referred to as Pecan_BG and Pecan_AG) amendments to determine the impact of such soil amendments on soil quality. The agricultural soils in this study have no O-horizon; total organic matter content is < 1.2 wt% at the surface and rapidly decrease with depth (Cox et al., 2018).

The alfalfa site is located in southeastern El Paso, Texas (Figure 2.1). These soils belong to Harkey-aged silty clay loam alluvium (NRCS Custom Soil Report). Different from the pecan site, the alfalfa site has not been fertilized, amended, or tilled. In addition, groundwaters have never been used for irrigation at alfalfa site. If Rio Grande water is not sufficient for irrigation, the alfalfa fields are left fallow. Two soil profiles (Alfalfa_Fine and Alfalfa_Coarse) were chosen by naturally stunted and lush crop growth when the alfalfa field was fallowed. In addition, a 60cm soil profile Alfalfa_Fine_D was collected next to Alfalfa_Fine as duplicate. The Alfalfa_Coarse profile is located in a visually high crop-yield location (Figure 2.1).

A natural site, with no current or historic documented agricultural development and located in the outskirts of Fabens, Texas is used as a comparison (Figure 2.1). Dominant sediments at the natural site are wind-modified sandy alluvium with surrounding soils of Pleistocene-age (NRSC Custom Soil Report). The natural site is characterized by Chihuahuan Desert scrub, dominated by mesquite (*Prosopis glandulosa*) and creosote bush (*Larrea tridentata*) among bare lands of eolian deposits and a few sand-dune mounds.

2.2. Dust collection

Dust samples were collected with passive dust-pans in both the pecan and natural sites for exactly one year, following Ganor (1975) and Shannak et al. (2014). Specifically, an aluminum pan filled with glass beads was attached to a vertical pole that was 1.5m above the ground surface. Presumably, the dust-pan samples contain both wet and dry deposition. The sample from each pan was weighed, then the annual flux was calculated using the dimension of the dust-pan (0.14 m^2)

and the duration of the dust deposition (one year). Elemental analyses of dust samples will be discussed below along with soil samples.

2.3. Amendment and fertilizer collection

An assortment of nine solid amendments and fertilizers applied for soil and foliar application were collected from the pecan orchard in 2018, approximately 150mg were dissolved in 15mL of de-ionized water and analyzed for major ions as described in detail in following sections (Appendix Table 2.1). Gypsum, elemental sulfur pellets and all other liquid amendments and fertilizers with known chemistry were not analyzed.

2.4. Soil collection and characterization

Soil samples at the pecan sites were collected with a soil auger in 10 cm intervals until 300 cm below the surface and or just above the water table. Pecan_BG and Pecan_AG profiles reached 70 and 80cm, respectively with 10 cm resolution. For the alfalfa sites, two soil profiles were collected with 10 to 20 cm resolution in February of 2013: Alfalfa_Coarse and Alfalfa_Fine. Soil profiles at the Alfalfa_Coarse and Alfalfa_Fine are 300 cm deep and the Alfalfa_Fine_D is only 60 cm. Soil samples at ~10 to 20 cm intervals were collected from the natural site to a depth of 109cm. All soils were air-dried and split with a riffle splitter, to produce representative samples.

Soil texture: particle size analysis

The bulk soil sample was ground gently with a mortar and pestle to break aggregates and all particles were less than 2mm. The sand fraction was separated from silt and clay by wet sieving (0.063 mm, Mesh # 230). All finer particles in a slurry were then centrifuged at 3500 rpm for ten minutes. The supernatant contained the clay fraction and was separated from the pellet at the bottom of the centrifuge tube, the silt fraction. All three fractions (sand, silt and clay) were air dried and then weighed to determine soil texture.

Sequential extraction of soil, dust and amendment/fertilizer samples

The sequential extraction of water-soluble (WS), and acid leachable (AC) fractions (described below) was conducted for the dust, pecan soils, natural soils, and the Alfalfa_Fine_D soils. The pecan amendments/fertilizers, soil profiles from Pecan_Coarse, Alfalfa_Fine1A, Pecan_BG and Pecan_AG were only characterized for the WS fraction.

Water soluble (WS)*:* De-ionized water was used to extract water-soluble salts, such as $CaCl_2$, NaCl, $CaSO_4*2H_2O$ or Na_2SO_4 from the samples. The resulting WS fraction is directly linked to irrigation and evaluates the salt buildup, as well as soil salinity and sodicity. For the WS extraction, 10g of a soil sample was weighed into a centrifuge tube, and mixed with 30 ml of de-ionized water (18.2 MΩ, DI). The slurry was shaken for 15 minutes on a shaker and centrifuged at 3500 rpm for ten minutes. The supernatant was passed through with a 0.45μm paper filter and weighed. The leachate was analyzed for electrical conductivity (EC) and pH. The sympHony VWR EC and pH electrodes and meters were calibrated using 1413 μS cm^{-1} and 12900 μS cm^{-1} standards, and pH 4 and pH 7 buffer solutions, respectively. Before elemental analyses, the leachate was diluted to 1:100 with de-ionized water. Aliquots used for cation concentrations were acidified with 3-4 drops of ultra-pure HNO_3 and analyzed in a Perkin Elmer 5300DV inductively coupled plasma-optical emission spectrometer (ICP-OES). Aliquots for anion concentrations remained un-acidified and run on a Dionex ICS-2100 ion chromatography (IC).

Exchangeable cation extraction (CEC): The exchangeable cations were removed from the residual soil pellets after the WS extraction and before the next AC extraction. The soil residues were mixed with 25ml of 0.1M $BaCl_2$-0.1M NH_4Cl, shaken for 15 minutes, and then centrifuged at 3500rpm

for five minutes. Residue soils were separated from supernatants, rinsed with 5 mL of DI water, and centrifuged for 5 minutes at 3500 rpm. The supernatants were discarded.

Acid Leachable extraction (AC): The acid leachable extraction (AC) is designed to dissolve carbonate minerals, i.e., pedogenic calcite in this study. 20mL of dilute acetic acid were added onto soil residue from the CEC fraction, (1M or 2M depending on calcite contents, estimated from the soil inorganic carbon contents). The mixture was shaken for six hours and centrifuged at 2500 rpm for 20 minutes and the supernatant filtered with a 0.45μm paper filter. The soil residue was washed again with 3mL of 1M or 2M acetic acid. Two aliquots of acetic acid leachates were combined, dried and re-dissolved in 2% HNO_3, before analysis of cation concentrations on the ICP-OES.

Finally, 20mL of dilute acetic acid were added onto soil residue from the CEC fraction, (1M or 2M depending on calcite contents, estimated from the soil inorganic carbon contents). The mixture was shaken for six hours and centrifuged at 2500 rpm for 20 minutes and the supernatant filtered with a 0.45μm paper filter. The soil residue was washed again with 3mL of 1M or 2M acetic acid. Two aliquots of acetic acid leachates were combined, dried and re-dissolved in 2% HNO_3, before analysis of cation concentrations on the ICP-OES.

2.5. Water sample collection and characterization

Three types of water samples were collected from the pecan orchard only, irrigation waters, soil waters and drainage waters. Irrigation waters were collected prior to flooding from the irrigation canals or from the groundwater wells. Soil waters were collected after irrigation, using 1900-series tension lysimeters (Soil Moisture Ltc, Barbara, CA) installed at four depths (15, 30, 60 and 120 cm). A vacuum of -50 centibar was pulled on the lysimeters one day before irrigation.

Drainage waters were collected seven days after irrigation from the drainage canals. Irrigation and drainage water samples were filtrated in the field using 0.45 μm filters and analyzed for alkalinity and concentrations of major ions. The ceramic cups in the lysimeters have maximum pore size of 1.3 μm, so soil water samples were not further filtered. All samples were collected in acid washed bottles and were rinsed in the field with water as that which was sampled. All samples were refrigerated at 4°C before analysis. Samples for cation analysis were acidified using several drops of ultrapure nitric acid. Water alkalinities were titrated with dilute hydrochloric (HCl) acid and calculated using the Gran-alkalinity method with the DL15 Mettler-Toledo titrator (Drever, 1997). Major cations were analyzed by the ICP-OES, and major anions were analyzed in the IC.

Saturation indices (SI) for calcite, gypsum and halite were calculated from pH, elemental chemistry and temperature of water samples using Visual MINTEQ ver 3.1. Saturation Indices for a given sample is the ratio of the ion activity product (IAP) to solubility product ratio in a log unit for a given mineral:

$$SI = log_{10}(\frac{IAP}{K_{sp}}) \qquad \text{Equation (2.1)}$$

Water samples are at equilibrium for any specific mineral if the SI equals zero, under-saturated if the SI is negative, and supersaturated if the SI is positive.

2.6. Quality assurance (QA) and quality control (QC) for water chemistry

Procedure blanks and sample replicates were included for QA/QC. The USGS Reference Materials M182 and M178 were run as checks on ICP-OES and an in-house water standard for IC. Quality assurance for major cation concentrations were conducted with multi-element water reference standards from NIST and U.S. Geological Survey and in-house standards for major anion concentrations. Errors were within 10% on all major element concentrations. The data quality of the leachates in water-leachable fractions were also evaluated by charge balance where

concentrations of major cations and anions and alkalinity are measured, as well as regressions between electrical conductivity and the sum of cation charges or anion charges. Charge balance was calculated for the water-soluble fraction for the Pecan_Fine soils and reported in Appendix Figures 2.1A and 2.1B.

2.7. Soil Sensor Network

A soil sensor network had been previously established in both the Pecan_Fine and the Alfalfa_Fine site by Cox et al. (2018), where soil volumetric moisture content, soil temperature and bulk soil electrical conductivity (EC) were recorded at depths of 15, 30, 60, and 120 cm with 5TE Decagon sensors and data loggers. Additional soil sensor network was established for Pecan_Coarse soils. A continuous dataset with five-minute resolution was collected for Pecan_Fine soils for two growing seasons (2014 and 2015) and for Pecan_Coarse soils for one growing season (2016). Only one irrigation event was captured for both Pecan_Fine and Pecan_Coarse soils during 2016.

Pore-fluid chemistry change due to evaporation, dissolution and precipitation of secondary salts can be better understood by calculating the real-time variation in pore-fluid EC, which can be calculated by bulk EC from the 5TE sensors (Hilhorst, 2000):

$$\sigma_p = \frac{\varepsilon'_p * \sigma_b}{\varepsilon'_b - \varepsilon'_{\sigma b=0}} \qquad \text{Equation (2.2)}$$

Where, σ_p is the pore-water EC (dS m^{-1}); ε'_p is the unitless real portion of the dielectric permittivity of the soil pore-water; σ_b is the bulk EC (dS m^{-1}); ε_b is the real portion of the bulk soil dielectric permittivity, unitless; $\varepsilon'_{\sigma b=0}$ is the real portion of the dielectric permittivity of the dry soil. ε'_p can be calculated from the soil temperature by:

$$\varepsilon_p = 80.3 - 0.37 * (T_{soil} - 20) \qquad \text{Equation (2.3)}$$

where T_{soil} is the soil temperature (ºC) and collected from the 5TE sensors. Furthermore, ε_b' is calculated using the raw VWC counts and converting these to bulk dielectric with a calibration:

$\varepsilon_b' = \frac{\varepsilon_{Raw}}{50}$ Equation (2.4)

$\varepsilon'_{\sigma b=0}$ is an offset term to represent the dielectric permittivity of dry soils, we used a generic offset of 4.1.

3. RESULTS

3.1. Soil Texture

The particle size distribution (PSD) changed dramatically with depth at each soil profile and also among different soil profiles (Table 2.1; Figure 2.2). PSD was different between the two pecan sites and also between two alfalfa sites (Figure 2.2A-D). The Pecan_Fine soils were loamy at shallow depths, contained up to 75 wt% clay and almost 0 wt% sand between 50 cm and 160 cm, and sandy below the clayey layer (Figure 2.2A). Similar fine-grained layer was observed at the same depth range of the Pecan_Coarse soil profile, but with much lower clay content and higher sand content (Figure 2.2B). Below 40 cm, more than 50% of sand was observed at Pecan_Coarse. A Wilcoxon Rank-Sum test showed that Pecan_Fine soils had significantly higher clay contents than Pecan_Coarse soils ($p<0.05$).

Shallow soils from Alfalfa_Coarse contained ~50% sands with a distinctive clay peak between 50-140cm depths, while the deep soils were sandy (Figure 2.2D). The soils from the Alfalfa_Fine site were dominated by finer silt and clay particles throughout the profile, with sand% decreasing with depth (Figure 2.2C). At the natural Fabens site, soils from the top 10 cm contained almost 90% sand and became finer towards deeper soils. As sand contents gradually decreased, silt contents increased with depth (Figure 2.2E).

3.2. Soil sequential extraction

Water Soluble Extraction

The pH, EC, and major ions concentrations of the WS fraction of all soils, dust and soil amendments are reported in Table 2.1.

All agricultural soils were slightly basic, with pH ranging narrowly from 7.0-8.0. In contrast, soil pH in the natural site changed quickly from 6.6 to 8.3 for the top 20 cm and remained around 7.5 after that (Figure 2.3A). Soil EC varied drastically with depth and also among different sites (Figure 2.3B). The Alfalfa_Coarse and the Pecan_Coarse sites had the lowest and the least variable EC among all soils. The entire Pecan_Fine soil profile showed consistently higher EC values between 0.96-3.68 dS/m. The soils at the Alfalfa_Fine site showed much lower EC values, than those at the Pecan_Fine, but had a peak of 3.86 dS/m around 150 to 250 cm depth. The highest EC values were observed in soils from the natural site; EC increased quickly with depth and reached 6.23 dS/m at around 90 cm.

Similar to EC, concentrations of water-soluble Na^+, Ca^{2+}, Cl^- and SO_4^{2-} were consistently higher in the Pecan_Fine soils than those in the Pecan_Coarse soils, for a given depth. The soils at the Alfalfa_Fine site also had consistently higher water-soluble concentrations than those at the Alfalfa_Coarse site (Figures 2.3C-2.3F), for a given depth. Concentrations of Na^+, Ca^{2+} and SO_4^{2-} in the water-soluble soil fraction at the natural site were even higher than all of the agricultural soils. For example, the highest Na^+ concentrations were observed in the natural soils, followed by those at the Pecan_Fine and Pecan_Coarse sites.

In general, the dominant cations in the water-soluble soil fraction were Na^+ and Ca^{2+}, followed by Mg^{2+} and K^+, and dominant anions SO_4^{2-} and Cl^- (Table 2.1; Figure 2.4A). Moreover, the Piper diagram revealed the soils in the Pecan_Coarse site have higher water-soluble Na^+ and K^+ and lower Ca^{2+} and Mg^{2+} than those in the Pecan_Fine site (Figure 2.4A). Soil SAR values

were calculated from water leachates, and were below the sodicity threshold of 13 (Figure 2.3G). However, because the soil profile samples are a one-time measurement, it is reasonable to assume most soils from the pecan and alfalfa sites are sodic or close to becoming sodic with continuous irrigation. Soil management practices at the pecan orchard have shown the improvement on soil sodicity as the SAR diminishes drastically after gypsum treatments (Figure 2.5). Soil extractions showed that gypsum-treated soils had an average of 60% lower SAR than untreated soils. Compared to soils from the Pecan_Coarse or Alfalfa_Coarse profiles, the soils from the corresponding Pecan_Fine and Alfalfa_Fine profiles had typically higher SAR values. The SAR values for the top 40cm soils of the natural site were much lower than those of any agricultural site, but quickly passed the threshold below 40 cm and remained almost constant throughout the rest of the profile (Figure2. 3G).

Acid Leachable

The predominant cation of the acid leachable extraction for all soils was Ca^{2+} with little addition of Mg^{2+} (Table 2.1; Figure 2.6A). Overall, soils at the Pecan_Fine had much higher Ca^{2+} than those at the Pecan_Coarse: Mg/Ca ratios of the acid leachates were 0.04 and 0.03 respectively, indicative of low-Mg calcite. Calcite contents in a soil were calculated from the acid leachable Ca^{2+} concentrations, assuming $CaCO_3$ stoichiometry. Soils from the Pecan_Fine soil profile contained up to 8 wt% of calcite and soils from the Pecan_Coarse soil had close to 3 wt% (Figure 2.6B). However, Alfalfa_Fine_D soils had more pedogenic carbonate that the pecan soils (Figure 2.6B; Table 2.1), averaging 13 wt% $CaCO_3$. Pedogenic carbonate contents at the natural soils were similar to those at the Pecan_Fine site, at ~8 and 6 wt% respectively. The acid leachable extraction of two dust samples from both the natural site and the pecan orchard measured 1.4 to 2.0 g Ca^{2+} m^{-2} yr^{-1} (Table 2.2).

3.3. Water chemistry

Water chemistry data were reported for the pecan sites in Table 2.3 and Figure 2.7. Charge balance for the water chemistry was calculated for samples with complete major cation and anion characterization and reported in Appendix Figures 2.1C and 2.1D. Irrigation water samples at the Pecan site were alkaline with pH ranging from 7.3-8.8 (Figure 2.7A). Soil water pH decreased slightly towards 60 cm depths for Pecan_Fine soils. For irrigation waters, four groundwater samples had similar pH values as Rio Grande surface waters. Alkalinities and EC increased as irrigation waters flowed downwards through the soil profiles. Drainage waters and irrigation waters had similar EC and alkalinity values (Figures 2.7B, 2.7C). Concentrations of major ions followed similar depth trends as alkalinity and EC for irrigation and soil waters (Ca^{2+}, Na^{+}, Cl^{-} and SO_4^{2-} in Figures 2.7D, 2.7E), increasing with depth. The Piper diagram for our pecan waters showed that both river irrigation and groundwaters typically had higher Na^{+} and K^{+} concentrations than Ca^{2+} and Mg^{2+} concentrations. River irrigation waters tend to have higher carbonate alkalinity and SO_4^{2-} and lower Cl^{-} than groundwaters (Figure 2.6B). Groundwater samples from the pecan field show that these usually have higher Cl^{-} and SO_4^{2-} and lower HCO_3^{-} than river waters.

Geochemical modeling indicated that SI values for gypsum were negative ~-2 and increased with depth to reach 0, suggesting that soil waters were under-saturated or near saturation. In contrast, irrigation waters and soil waters were near saturation or over-saturated with respect to calcite, with SI values from 0.06-0.42 (Figure 2.7F). All water samples were under-saturated with respect to halite, with SI values less than -5.

3.4. Soil Sensor Network

Soil moisture, temperature, bulk EC, and calculated fluid EC data at 15 cm depth were plotted for the Pecan_Fine and Pecan_Coarse sites, for one irrigation event in 2016 (Figure 2.8).

The soil moisture content at 15 cm was generally higher in soils at the Pecan-Fine site than those at the Pecan_Coarse site (Figure 82.A). Right after irrigation, soil moisture plateaued at 15 cm at 0.45 and 0.32 $m^3 m^{-3}$ at Pecan_Fine and Pecan_Coarse, respectively. This indicated higher porosity at Pecan_Fine soil than Pecan_Coarse soil at 15 cm. Although the differences in soil moisture were significant between two sites using Wilcoxon Rank-Sum test (p-value<0.05), soil moisture values for both soils returned to the same baseline values approximately 10 days after flooding (Figure 2.8A). Soil temperature remained relatively constant for the soil at 15 cm of the Pecan_Fine site, decreased upon irrigation, and then gradually increased after that (Figure 2.8B). For the same flood-irrigation event, Pecan_Fine soil had much higher bulk EC values than the Pecan_Coarse soil (Figure 2.8C). The bulk EC values peaked at the onset of irrigation for both soils and then gradually decreased. In contrast, pore-fluid EC decreased upon irrigation, increased after that, and then reached a baseline for Pecan_Fine soil (about 10 days after irrigation) and much sooner for Pecan_Coarse soil (approximately 1 day) (Figure 2.8D).

4. DISCUSSION

4.1. Salt loading at the agricultural and natural soils

Both human activities (irrigation and soil amendments) and natural processes (wet and dry deposition) load salt onto agricultural soils in arid-lands. Soils are amended and fertilized only in the pecan orchard and not in the alfalfa field (Table 2.2; Appendix Table 2.1). Water extraction of the soil amendments can be seen in Appendix Table 2.1. Extremely high loadings of Na^+, K^+ Ca^{2+}, Sr^{2+}, NO_3^-, Cl^-, and SO_4^{2-} in amendments and fertilizers are annually added onto the soils in order to prepare them for the growing season (Table 2.2). These loading of Ca and other species were estimated in Table 2.2 from four out of eight solid treatments applied at the pecan orchard in 2018. This is a source of salt loading but many orders of magnitude lower than irrigation waters and one

order of magnitude lower than loadings by dust, as discussed below (Table 2.2). Additional data on rates of application for the other amendments and fertilizers could most likely result in surpassing or at least equally high salt additions by dust.

Naturally, a total of 40 and 59g m^2 yr^{-1} of dust are accreted to agricultural and natural sites, respectively. Ca^{2+} was found to be the major water-soluble ion in the dust, consistent with previous studies that showed dusts to be an important source of Ca in soils (McFadden and Tinsley, 1985; Whipkey et al. 1999; Reheis et al, 1995; Reheis and Kihl, 1995). While rates of dust deposition for soluble Ca^{2+} are higher than that from soil amendment, they are at least two order of magnitude lower than that from irrigation waters (Table 2.2).

Our dust data agree with previous works that have recognized dust as a significant source of salts in desert environments (Monger and Gallegos, 2000; Gile et al., 1981; Capo and Chadwick, 1999; Reheis, 2006; Reheis and Urban, 2011; Floyd and Gill, 2011; White et al., 2015). Still, this dust deposition is much lower than irrigation loads, similar to what is observed in Cox et al. (2018). Indeed, the potential amount of salt loading from flood irrigation (~ 1.12 m of water per growing season) in the region around El Paso is significant: Cox et al. (2018) estimated 823g Na^+ m^{-2} yr^{-1}, 411g Ca^{2+} m^{-2} yr^{-1}, 906g Cl^- m^{-2} yr^{-1}, 1000 g SO_4^{2-} m^{-2} yr^{-1}, and 988 g HCO_3^- m^{-2} yr^{-1} are in local cotton, alfalfa and pecan fields. Similarly, our irrigation water characterizations found substantial loads of Ca^{2+} and other major ions reported in Table 2.2.

Major ion loads reported in Table 2 estimate loading from ground water or Rio Grande irrigation waters assuming these as only source for irrigation. As a result, sole-groundwater irrigation loading of major ions is higher than sole-Rio Grande irrigation loading, except SO_4^{2-} (Table 2.2).

4.2. Soil salinity and sodicity at the agricultural and natural soils

At the Fabens site, surface soils are only exposed to dust and meteoric waters; highlighting the importance of rain events in flushing salts with large quantities of fresh waters. However, the deep soils at the site are characterized by high salinity and sodicity, even higher than agricultural soils (Figure 2.3). This is beyond loading through rain and dust, even after thousands of years since sediments were deposited at Pleistocene (NRCS Custom Soil Report). A possible mechanism to form such a zone of high salinity is capillary rise of local groundwaters, and precipitation of salts above the water table after evaporative water loss (Daliakopoulos et al., 2016). However, such a hypothesis needs further investigation on local groundwater chemistries and seasonal movement to verify such a process. his needs further studies.

Continuous salt deposition affects the quality of soils in both the pecan and alfalfa sites, similar to what we have observed in other dryland irrigated soils (Assouline et al, 2015; Falasca et al., 2014; Cox et al., 2018). Indeed, EC values observed at some pecan and alfalfa sites are higher than 4 dS/m, even exceeding the salt tolerance levels of the pecan and alfalfa, 2.6 and 2.0 dS/m, respectively (Figure 2.3B) (Mass and Grattan, 1999; Picchioni et al., 2000).

4.3. Physical and chemical controls on salt buildup

Soil texture control

Soils used for cultivation along the Rio Grande valley developed from fluvial sediments thus exhibiting variable particle sizes due to antecedent flooding and river meanderings (Hall and Peterson 2013; Doser et al., 2007). This spatial heterogeneity in soil texture is both vertical and lateral, as observed in two soil profiles, that are less than 50 m apart, at the pecan orchard and the alfalfa field (Figures 2.1 and 2.2). Indeed, soil from Pecan_Fine, Pecan_Coarse and Alfalfa_Coarse site are characterized by finer texture at shallow depths, underlain by coarser and sandy texture. In

contrast, soils at the Alfalfa_Fine and the natural Fabens sites are relatively courser at top soils and become much finer at depth (Figure 2.2). Within the pecan orchard, both Pecan_Fine and Pecan_Coarse sites have a layer of finer particles between 100 and 150 cm; however, this layer is silty clayey at the Pecan_Fine but is still sandy at the Pecan_Coarse (Figure 2.2A, Figure 2.2B).

The absolute EC values measured on the soil leachates are sensitive to the soil: water mixing ratio in the slurry, but the same ratio is used for all soil samples in this study, so EC values are proxy for relative salt buildup among different sites (Table 2.1). The Pecan_Coarse soils, with relatively coarser soil texture, have lower EC than those Pecan_Fine soils; similarly, Alfalfa_Coarse soils have lower EC values than Alfalfa_Fine soils (Figure 2.3B). Within each soil profile, the EC peak is typically observed around the layer of finer texture (shaded areas in Figure 2.2). For both pecan sites, the highest EC values are around 100-150 cm; for alfalfa field, EC peaks are between 150-250 cm and between 50-100 cm for Alfalfa_Fine and Alfalfa_Coarse respectively (Figure 2.2). These findings suggest that soil texture exerts strong control on location and rates of salt accumulation in irrigated soils, similar to what others have observed (Eshel et al., 2007; Cox et al., 2018).

The salt buildup in agricultural soils is a balance of salt input and output fluxes. As discussed in last section, the inputs are predominantly through irrigation and soil amendments; the outputs are however sensitive to soil texture, soil permeability and thus salt leaching. Indeed, the soil at 15 cm below ground surface at the Pecan_Fine site has twice soil moisture content as the soil of the same depth at the Pecan_Coarse site right after the flood irrigation (Figure 2.8A). This indicates higher porosity in Pecan_Fine soil of finer texture than the Pecan_Coarse soil. Interestingly, soil moisture content at two soils decreases to the same level after ~14 days. Since water loss through transpiration and infiltration is expected to be lower in Pecan_Fine site due to

finer soil texture and smaller pecan trees, it is reasonable to conclude evaporation is higher at Pecan_Fine than Pecan_Coarse. If so, it will impact pore-water chemistry as discussed below.

Bulk soil EC increased dramatically at the onset of irrigation, highlighting the moisture in soils controlling conductivity of bulk soils (Figure 2.8C). Conversion of bulk soil EC to pore-water EC however allows us to focus on the soil water chemistry and its evolution with time through evaporation and chemical reactions. As shown in Figure 2.8D, soil water EC, probably similar to irrigation EC, was low right at the onset of flood irrigation and thus undersaturated with respect to gypsum and halite (Figure 2.7). After that irrigation event, pore-water EC continuously increases through dissolution of evaporate salts that have previously accumulated. Presumably equilibrium with existing salts is reached in two days in the Pecan_Fine soil and one day for Pecan_Coarse soil. After, evaporation continues lowering soil moisture content (Figure 2.8A), pore-water EC increased and reached mineral saturation, presumably leading towards secondary salt precipitation (Figure 8B).

Major ion concentrations and EC in soil waters increased with depth at the pecan orchard; as a result, SI of both gypsum and halite became less negative (Figure 2.7F). However, as discussed below, the floodplain mud interfingerings limit the depth at which waters leach salts and the connectivity of shallow soils and underlying aquifer. Furthermore, increased salt accumulation in these fine-textured layers should additionally decrease available pore space, lowering hydraulic connectivity and permeability. As restricted water movement occurs due to impermeable layers, lateral flow towards return and drainage waters is expected during saturated field conditions. With limited water infiltration, soil salt contents were much lower below the clayey layers in pecan soils. If so, drainage water chemistries are similar to those of shallow soils above the thick clay layers as in Figures (2.7D-E).

Soil practice control: Irrigation and soil amendments

Collectively, salt inputs are expected to be much lower in amount at the alfalfa fields than at the pecan orchard. Even so, the salt buildup is higher at Alfalfa_Fine than at Pecan_Coarse, as observed in large peaks in EC, Na^+, Cl^- etc in water-soluble soil fraction (Figure 2.3). This difference points to the texture as the primary control (finer texture at Alfalfa_Fine than Pecan_Coarse in Figure 2.2), and salt inputs as the secondary control. Indeed, the pedogenic carbonate content of the Alfalfa_Fine soils profile is higher than in the Pecan_Coarse soils.

Addition of gypsum onto land surface contributes to an important source of SO_4^{2-} and Ca^{2+} in soil waters and water-soluble fraction of soils. Indeed, gypsum can translocate to deep soils through dissolution and re-precipitation with infiltrating soil water. High concentrations of SO_4^{2-} are retained in the Pecan_Fine soils, showing surficial accumulation with up to 4.3g/kg of soil occurring in the top most soils, and retaining high concentrations throughout the rest of the profile. Whereas, Pecan_Coarse soils, which were treated with the same amendments, irrigation quantities and schedules, retain a maximum of 0.12g/kg SO_4^{2-} at a peak at depth. Certainly, soil particle size distribution impacts the retention of amendments, similar to salts in irrigation waters.

The pecan orchard primarily uses Rio Grande surface water for irrigation, but when it is insufficient, local groundwater is pumped to irrigate. As shown in Table 2.3 and Figure 2.7, groundwaters typically have higher EC values than Rio Grande, with average 4.0 and 1.5 dS/m respectively and will potentially load more salts. Pumping of groundwater in the Rio Grande valley has significantly lowered the water table and increased ground water salinity (Sheng, 2013).

Solubility control

Soil waters were only sampled during initial irrigation, and an evolution of elemental chemistry from irrigation and soil waters is observed: as irrigation waters infiltrate pecan soils, soil waters have evolved dramatically higher Ca^{2+} and SO_4^{2-} concentrations and slightly higher

Na^+ and Cl^- concentrations (Figure 2.7). We consider this evolution to be a result of dissolution of gypsum and halite salts previously accumulated in the soil zone. Towards the end of this irrigation, gypsum and minor halite will precipitate back to soils. In contrast, irrigation waters have been oversaturated or near saturation with respect to calcite and so are soil waters (Figure 2.7F). Thus, calcite is expected to accumulate throughout the irrigation reason. Similar to what have reported in Cox et al. (2018), up to 8wt% of calcite is observed in the soils of our study sites (Figure 2.6B). Combined with loaded ion concentrations, soil texture is the physical control that dictates the precipitation of water-soluble salts and also that of secondary calcite (Figure 2.6B). Indeed, the Pecan_Fine soils contain higher calcite than the Pecan_Coarse soils. Peaks in calcite coincide with peaks in clay for the Pecan_Coarse profile, where calcite explained by soil texture was higher than Pecan_Fine (linear regression R^2=0.30; R^2=0.24, respectively).

Contrasting solubility in secondary salt phases also explains the different composition of water- soluble soil fraction and irrigation water as observed in Piper diagrams (Figure 2.6). The irrigation water is clustered near Na^+/K^+ for cations; however, the water-soluble fraction in soils has slightly higher contribution from Ca^{2+}. This is due to both addition of Ca from soil amendments, but more importantly due to lower solubility of gypsum than halite. As such, Na^+ is more likely to remain in the water and leached out from soils than Ca^{2+}.

4.4. Short-term and long-term effects of using soil amendments

After 90 years of soil cultivation in the study region, soil quality deteriorates and salinization is expected to accelerate. The accumulation of secondary salts including calcite clogs soil pores, lowering soil porosity and permeability and accelerating more salt buildup. Water used for irrigation, Rio Grande or local groundwater, is sodic, and thus the agricultural soils in the study sites have both high salinity sodicity (Figure 2.4, Figure 2.3G). The improvement in soil quality

due to application of gypsum amendments appears to be effectively for less than one year. Hence, annual application of soil amendment is needed to maintain the agricultural functionality, as done in the pecan orchard.

4.5. Potential impacts on Groundwater and Rio Grande water quality

Increased regional temperatures and reduced snowpack at the headwaters, as well as human activities, are anticipated to impact the water quality and quantity of Rio Grande water (Phillips et al., 2003; 2011; Swetnam and Betancourt, 1998; Seager et al., 2007; Gutzler and Robbins, 2010). Not only is the Rio Grande expected to become more saline as these climate changes occur (Borrok and Engle, 2014), but the limited water availability will make it more competitive among water users and lead farmers to increase their use of groundwater for irrigation. The variability in groundwater TDS can fluctuate between fresh to brackish waters depending on pumping depths of the Hueco Bolson or Mesilla Bolson (Ashworth, 1990). Such changes in water sources and quality will impact soil salinization rates, groundwater table depth and regional cones of depression (Sheng, 2013) (Figure 2.9). Soil salinization can lead to low crop productivity, economic returns and thus vulnerability in the market (Hu and Schmidhalter 2002).

Longstanding impacts can result in high soil salinity, which can affect surface and groundwater quality. This can lead to decreased critical zone functions and services such as nutrient cycling and crop cultivation, requiring more intensive soil management practices. Irrigation water is connected with groundwater and Rio Grande through return flow (Cox et al., 2018). Nutrients from fertilizers and complex organometallic from pesticide and salts through irrigation and other soil amendments can be leached from soils and released to other water bodies.

5. CONCLUSION

Findings from this study suggest that continuous irrigation is the major source of salinization in the agricultural soils of the Rio Grande valley. Results from the study sites show that salt-loading onto agricultural soils is irrigation by groundwater > > irrigation by Rio Grande > dust > agricultural amendments. Better land-management can limit the amount of salts that accumulate in soils, especially by reduced saline water use. High sodicity has potential to break soil aggregates and disperse clays, thus lowering permeability and limiting water and salt leaching. Application of gypsum and other amendments greatly decrease sodicity but only temporarily, as irrigation with Na^+-rich Rio Grande or local groundwater will increase soil sodicity again. High soil salinity and soil sodicity are combined to deteriorate soil quality and lower crop production. Soil texture is a major control on water and salt movement, controlling soil water flow paths and its residence time, and thus the rates and locations of salt buildup. Among all secondary salt phases, calcite precipitation is the most significant, due to its low solubility, followed by gypsum and halite. Predicted increases in surface water salinity and decreases in its availability due to climate changes will lead to more use of groundwaters and elevated soil salinization in agricultural soils, making the Rio Grande region's agriculture vulnerable economically.

Table 2.1: Particle size distribution and chemistry of water soluble and acid leachable fractions of soils at the Pecan, Alfalfa and natural sites.

Depth	Sand	Silt	Clay	Water soluble fraction (EC in ds/m; concentrations in mg/kg soil; charge in meq/kg soil; SAR in mmole/$L^{0.5}$)														Acid leachable fraction (mg/kg soil)			$CaCO_3$*
(cm)	wt%	wt%	wt%	pH	EC	Mg^{2+}	Ca^{2+}	Na^{+}	K^{+}	Sr^{2+}	Cl^{-}	SO_4^{2-}	PO_4^{3-}	NO_3^{-}	Charge +	Charge -	SAR	Ca	Mg	Sr	wt%
Site: Pecan_Fine																					
10	37	50	13	7.33	1.80	180	1103	364	4	9	262	2456	11	167	86	61	2	23093	959	66	5.77
20	36	49	15	7.42	2.85	240	1636	473	4	15	373	4363	9	209	123	105	2	26895	1275	98	6.72
30	32	63	6	7.54	2.25	235	1075	522	4	11	335	3391	10	77	96	81	2	28474	1268	89	7.12
39	35	57	8	7.62	2.30	221	843	612	3	9	452	3190	5	43	88	80	3	28667	1570	114	7.17
49	32	55	14	7.62	2.76	266	1076	941	4	12	506	3845	0	41	117	95	4	26986	1042	89	6.75
59	52	40	8	7.74	1.24	137	331	499	3	3	370	1241	0	37	50	37	3	25075	661	62	6.27
69	30	46	25	7.77	2.29	195	653	955	3	7	589	2675	0	67	91	73	5	25906	1238	96	6.48
79	24	51	26	7.61	3.68	285	1194	1144	4	14	782	4967	0	77	134	127	4	27574	1306	99	6.89
88	6	52	43	7.51	3.33	205	627	1511	3	7	1041	3620	0	81	114	106	8	26521	1905	122	6.63
98	1	50	49	7.75	2.78	148	355	1404	3	3	991	2412	0	75	91	79	9	28998	2027	137	7.25
108	1	24	75	7.63	3.00	149	358	1508	3	3	1231	2463	0	110	96	88	10	28259	2006	136	7.06
118	1	39	61	7.73	3.28	160	410	1733	3	4	1235	2837	0	97	109	95	11	27328	1819	129	6.83
128	1	48	51	7.70	3.63	175	487	1696	3	5	1239	3259	9	109	113	105	10	27337	1939	136	6.83
137	1	68	31	7.77	3.45	165	412	1828	3	4	1430	2795	0	114	114	100	11	30163	1663	138	7.54
147	31	61	8	7.74	1.74	130	296	712	3	2	853	1112	0	77	57	48	5	17190	397	51	4.30
157	66	29	5	7.76	1.62	128	301	752	3	2	814	1068	0	75	59	46	5	25130	612	57	6.28
167	49	39	12	7.58	1.85	132	285	930	3	2	980	1123	0	72	66	52	7	31540	688	86	7.88
177	49	48	4	7.38	1.88	130	297	907	3	2	959	1176	0	64	65	53	6	30824	668	75	7.71
186	74	24	1	7.53	1.70	123	260	689	3	2	915	1094	0	54	53	49	5	24728	554	46	6.18
196	78	13	9	7.42	1.45	114	211	683	3	1	750	856	0	45	50	40	5	22731	525	40	5.68
206	80	14	6	7.32	1.28	117	236	583	3	1	579	876	0	38	47	35	4	21488	495	35	5.37
216	78	19	3	7.29	1.38	119	251	556	3	1	586	1023	0	32	47	38	4	22370	499	39	5.59
226	76	22	2	7.26	1.51	123	264	627	3	2	613	1140	0	1	51	41	5	21036	538	35	5.26
235	78	18	4	7.48	2.09	172	702	621	3	6	526	2292	0	1	77	63	3	18281	501	28	4.57
245	84	15	1	7.22	1.19	115	255	529	3	1	458	934	0	1	45	32	4	18228	482	28	4.56
255	84	10	5	7.27	1.15	117	259	365	3	2	454	878	0	1	39	31	3	14697	390	22	3.67
265	86	13	2	7.41	1.33	124	298	474	3	2	591	969	0	28	46	37	3	16012	483	29	4.00
275	92	7	1	7.48	1.02	114	237	365	3	1	416	796	0	1	37	28	3	14273	378	20	3.57
284	94	6	0	7.16	0.96	113	225	282	3	1	390	723	0	1	33	26	2	12428	338	15	3.11
Site: Pecan_Coarse																					
0	44	45	11	7.21	0.49	1	8	15	3	0	15	3	0	8	1	1	1	16541	472	46	4.14
10	53	40	7	7.16	0.41	3	34	121	16	0	121	16	0	34	8	4	3	16223	468	41	4.06
20	53	41	6	7.39	0.45	2	32	147	15	0	147	15	0	32	9	5	4	20463	596	57	5.12
30	50	39	11	7.28	0.60	9	84	263	29	1	263	29	1	84	17	9	4	8434	247	14	2.11
40	70	19	11	7.26	0.47	3	35	137	15	0	137	15	0	35	8	5	3	13683	359	28	3.42
50	71	26	3	7.35	0.82	19	149	318	40	1	318	40	1	149	24	12	4	11250	306	21	2.81
60	76	20	3	7.33	0.66	14	115	314	37	1	314	37	1	115	22	11	4	9851	283	18	2.46
70	86	6	8	7.01	0.32	4	64	150	18	1	150	18	1	64	11	6	3	7834	250	12	1.96
84	87	9	4	7.15	0.65	19	147	286	40	1	286	40	1	147	22	11	3	7037	256	10	1.76
90	92	5	2	6.94	0.51	10	82	141	18	1	141	18	1	82	12	6	2	7344	227	12	1.84
100	75	24	1	7.13	0.47	11	85	150	23	1	150	23	1	85	12	6	2	15106	447	36	3.78
110	64	9	28	7.27	1.13	36	162	423	49	2	423	49	2	162	31	16	5	16883	488	41	4.22

Depth	Sand	Silt	Clay	Water soluble fraction (EC in ds/m; concentrations in mg/kg soil; charge in meq/kg soil; SAR in mmole/$L^{0.5}$)														Acid leachable fraction (mg/kg soil)			$CaCO_3$*
(cm)	wt%	wt%	wt%	pH	EC	Mg^{2+}	Ca^{2+}	Na^{+}	K^{+}	Sr^{2+}	Cl^{-}	SO_4^{2-}	PO_4^{3-}	NO_3^{-}	Charge +	Charge -	SAR	Ca	Mg	Sr	wt%
120	67	10	23	7.58	2.78	180	647	1456	127	10	1456	127	10	647	114	54	8	12161	329	24	3.04
130	84	14	2	7.56	0.97	45	230	543	58	3	543	58	3	230	40	20	5	8389	246	16	2.10
140	87	11	2	7.31	0.85	34	187	419	41	2	419	41	2	187	31	16	4	4772	142	8	1.19
150	95	3	2	7.35	0.49	18	118	180	23	1	180	23	1	118	16	7	2	5029	136	8	1.26
160	97	3	0	7.06	0.34	9	65	152	19	1	152	19	1	65	11	6	3	4012	99	6	1.00
170	97	2	1	7.05	0.30	6	56	125	13	1	125	13	1	56	9	5	2	3841	87	6	0.96
180	97	1	1	6.98	0.36	6	50	177	12	0	177	12	0	50	11	6	4	4325	96	7	1.08
190	97	2	1	6.97	0.33	2	32	167	17	0	167	17	0	32	10	6	4	4520	96	7	1.13
200	97	1	2	7.28	0.37	2	35	211	21	0	211	21	0	35	12	7	5	5769	123	9	1.44
210	97	1	2	7.20	0.53	6	46	301	27	1	301	27	1	46	17	10	6	5788	164	8	1.45
220	91	7	2	7.06	0.63	7	51	253	20	1	253	20	1	51	15	8	5	6574	166	7	1.64
230	92	1	7	7.02	0.65	12	90	361	23	1	361	23	1	90	22	12	5	6033	160	6	1.51
240	96	0	4	6.99	0.53	7	70	274	22	1	274	22	1	70	17	9	5	5151	124	5	1.29
250	97	2	1	6.98	0.66	10	90	227	17	1	227	17	1	90	16	8	4				
Site: Alfalfa_Fine																					
0	38	56	6	7.09	0.59	14	68	75	42	1	75	91	5	191	9	7	1				
10	36	53	10	7.47	0.41	7	32	71	17	0	43	93	2	47	6	4	2				
20	35	57	8	7.43	0.38	6	25	74	14	0	40	84	2	15	5	3	2				
30	36	58	6	7.56	0.40	7	31	82	17	0	70	96	2	17	6	4	2				
40	41	46	13	7.81	0.40	7	30	106	8	0	115	160	3	28	7	7	3				
50	38	55	7	7.54	0.67	17	60	182	18	1	209	364	1	7	13	14	3				
60	68	30	2	7.97	0.43	7	22	110	11	0	101	210	0	2	7	7	3				
70	53	44	3	7.75	0.72	6	15	227	14	0	195	346	1	14	11	13	7				
80	38	59	2	7.00	0.76	4	10	289	10	0	240	409	1	5	14	15	11				
100	26	67	7	7.80	1.12	26	70	434	12	1	335	938	1	3	25	29	6				
120	48	48	4	7.85	0.68	16	57	210	18	1	219	463	0	2	14	16	4				
140	8	81	11	7.38	1.92	90	694	403	53	8	382	2404	0	6	61	61	2				
160	14	71	15	7.29	2.68	130	1416	388	76	15	241	4316	0	4	101	97	2				
180	9	80	11	7.27	2.73	149	1560	350	89	16	184	5101	0	4	108	112	1				
200	26	59	15	7.29	3.86	163	1511	471	214	19	397	4510	2	0	116	105	2				
220	20	72	8	7.46	2.43	93	1308	238	68	13	141	4202	0	65	86	93	1				
240	9	86	5	7.62	0.73	13	144	139	23	2	135	608	1	33	15	17	2				
260	3	67	31	7.75	0.73	8	115	136	17	1	130	518	1	12	13	15	2				
280	1	86	13	7.64	0.74	10	150	158	19	2	148	635	0	14	16	18	2				
Site: Alfalfa_Coarse																					
0	50	42	8	7.21	0.26	4	19	84	19	0	59	106	1	11	5	4	3				
20	51	43	7	7.26	0.33	5	23	111	16	0	85	156	1	7	7	6	3				
30	54	41	5	7.37	0.44	7	33	147	19	0	155	208	1	5	9	9	3				
40	67	28	5	7.30	0.60	12	50	197	23	1	201	403	1	3	13	14	4				
50	70	26	4	7.35	0.62	13	47	207	23	1	219	424	1	2	13	15	4				
60	55	42	4	7.53	0.77	15	56	276	25	1	256	563	0	1	17	19	5				
70	35	58	7	7.39	1.39	48	175	505	44	3	480	1166	0	2	36	38	5				
80	18	69	13	7.38	1.49	47	179	536	45	3	694	932	1	2	37	39	5				
90	8	76	16	7.48	1.09	28	123	314	26	2	580	421	0	2	23	25	4				

Depth	Sand	Silt	Clay	Water soluble fraction (EC in ds/m; concentrations in mg/kg soil; charge in meq/kg soil; SAR in mmole/L$^{0.5}$)														Acid leachable fraction (mg/kg soil)			$CaCO_3$*
(cm)	wt%	wt%	wt%	pH	EC	Mg^{2+}	Ca^{2+}	Na^{+}	K^{+}	Sr^{2+}	Cl^{-}	SO_4^{2-}	PO_4^{3-}	NO_3^{-}	Charge +	Charge -	SAR	Ca	Mg	Sr	wt%
100	47	48	5	7.51	0.37	4	19	92	10	0	85	98	1	2	6	4	3				
110	39	55	6	7.75	0.31	3	15	77	8	0	40	80	2	2	5	3	3				
120	25	66	9	7.79	0.33	3	14	85	8	0	41	86	2	2	5	3	3				
130	22	68	10	7.90	0.33	3	12	88	8	0	39	82	1	2	5	3	3				
140	71	26	3	7.95	0.20	2	6	54	5	0	17	31	1	1	3	1	3				
150	91	7	2	7.88	0.14	1	6	33	3	0	6	14	1	1	2	0	2				
160	91	7	2	7.84	0.15	2	9	33	4	0	14	43	0	1	2	1	2				
170	92	6	2	7.99	0.19	2	6	47	4	0	17	44	1	1	3	1	3				
190	86	11	3	7.49	0.22	2	9	64	5	0	27	75	1	1	4	2	3				
200	95	4	2	7.57	0.21	2	8	60	5	0	28	65	1	1	3	2	3				
210	96	3	1	7.49	0.11	1	5	25	2	0	6	16	2	1	1	1	2				
220	96	3	1	7.38	0.11	1	6	26	3	0	6	13	1	1	2	0	1				
230	94	4	2	7.69	0.13	1	6	34	3	0	9	23	1	1	2	1	2				
240	92	6	2	7.76	0.13	1	5	37	3	0	11	22	1	1	2	1	2				
250	94	4	1	7.57	0.12	1	5	33	3	0	11	20	2	1	2	1	2				
260	95	3	1	7.42	0.12	1	4	31	3	0	8	19	1	1	2	1	2				
270	96	3	1	7.71	0.11	1	5	29	3	0	8	18	1	1	2	1	2				
280	96	2	2	7.71	0.10	1	5	26	3	0	6	12	2	2	2	0	2				
290	96	2	2	7.74	0.09	1	5	25	2	0	6	13	2	2	1	0	2				
Alfalfa_Fine_D																					
0				7.21	0.26	10	12	156	37	1	43	62	3	28	9	3	5	45511	800	112	11.38
10				7.26	0.33	11	80	181	51	1	9	20		0	14	1	3	107345	2466	266	26.84
20				7.37	0.44	9	23	120	25	0	33	56	0	0	8	2	3	38691	584	95	9.67
30				7.30	0.60	6	36	116	21	0	24	36	0	0	8	1	3	59727	1048	149	14.93
40				7.35	0.62	12	16	277	19	1	61	128		1	14	4	7	63157	1066	179	15.79
50				7.53	0.77	5	51	138	14	0	26	47	1	0	9	2	3	32663	511	80	8.17
60				7.39	1.39	2	2	159	9	0	17	38	2	1	7	1	11	23119	411	46	5.78
The Natural Fabens site															0	0					
0	95	3	2	6.61	0.08	129	120	0	214	0	39	18		3	22	2	0	3970	134	11	0.99
20	80	13	7	8.31	0.76	219	232	218	233	1	215	194		6	45	10	1	28119	506	44	7.03
40	57	38	5	7.85	5.09	194	1116	2208	218	7	379	7234		20	174	162	9	27681	830	72	6.92
60	51	42	7	7.51	5.61	226	1541	2434	234	9	391	8980		18	208	198	9	21537	593	31	5.38
71	49	43	8	7.40	6.13	214	1364	2699	213	8	449	8922		23	209	199	10	23936	602	36	5.98
81	43	51	6	7.56	6.00	236	1519	2861	233	8	493	9426		28	226	211	10				
90	42	53	6	7.53	6.23	230	1466	3007	221	8	550	9503		19	229	214	11				
99	40	58	2	7.13	6.01	232	1453	2817	225	8	522	9236		22	220	207	10	24882	594	32	6.22

Table 2.2: Elemental loading of natural and agricultural soils through dry/wet depositions and agricultural soils

Sources	Ca g/m2/ yr	Mg g/m2/ yr	Sr g/m2/ yr	Na g/m2/ yr	K g/m2/ yr	Alk g/m2/yr	SO_4^{-2} g/m2/ yr	Cl g/m2/ yr	PO_4^{-3} g/m2/yr	NO_3^- g/m2/ yr
Irrigation										
IRW_RG	129	30	3	306	44	284	419	361	4	13
IRW_GW	356	56	4	568	45	329	883	638	4	100
Dust										
Fabens	0.1	0.0	0.1	0.3	0.1					
Pecan	0.2	0.0	0.1	0.5	0.4					
Soil Amendments										
K2CO3	0.000	0.000	0.000	-0.004	0.851		0.001	0.000		0.000
UREA	0.002	0.000	0.000	0.015	0.005		0.000	0.014	0.001	0.001
Rootex	0.019	0.001	0.000	0.000	0.000		0.036	0.001		0.000
H-85	0.019	0.001	0.000	0.000	0.000		0.002	0.001		0.000

Table 2.3: Elemental chemistry of water samples from the Pecan site.

Type	depth cm	Date	pH	EC dS/m	Alk meq/L	Na^+ ppm	Ca^{2+} ppm	Mg^{2+} ppm	K^+ ppm	Sr^{2+} ppm	Cl ppm	SO_4^{2-} ppm	PO_4^{3-} ppm	NO_3^- ppm	Charge + meq/L	Charge - meq/L	Charge difference	calcite SI	halite SI	gypsum SI
IRW_RG	0	4/3/14	7.64		4.7	530	145	50	64	3	578	740		2	36	36	0	0.3	-5.2	-0.6
IRW_RG	0	5/19/14	6.95	2.06	4.0	355	48	16	70	1					21	4				
IRW_RG	0	6/8/14	7.48	3.58	5.5	493	220	51	59	4	675	754		2	38	40	-3	0.5	-5.1	-0.7
IRW_RG	0	6/25/14			1.3	196	19	15	62	1					12	1				
IRW_RG	0	7/15/14	8.82	1.05	2.4	138	32	11	13	1	133	226		5	9	11	-10	0.8	-5.0	-0.6
IRW_RG	0	7/31/14	8.13	1.27	3.9	176	26	14	57	1	175	262		5	12	14	-11	0.2	-6.0	-1.4
IRW_RG	0	10/9/14	8.40	2.25	3.7	370	44	16	64	1	396	366	7	52	21	24	-5	0.7	-5.4	-1.5
IRW_RG	0	10/23/14	7.89		7.2	625	300	73	94	4					51	7				
IRW_RG	0	5/15/15	7.70	1.87	3.5	325	43	13	67	1	340	333	13	51	19	21	-5	0.0	-5.6	-1.5
IRW_RG	0	6/11/15	8.10	1.02	3.7	126	39	11	60	1	118	192	2	9	10	11	-7	0.5	-6.4	-1.6
IRW_RG	0	6/30/15	8.00	0.90	3.5	115	36	10	57	1	91	159	1	2	9	9	-2	0.3	-6.5	-1.7
IRW_RG	0	7/13/15				204	58	41	13	19	125	213		8	15	8				
IRW_RG	0	7/19/15	8.00	1.05	2.7	120	37	9	10	1	101	168	2	14	8	9	-7	0.2	-6.5	-1.7
IRW_RG	0	8/11/15	7.91	0.88	3.7	102	56	8	9	1	93	155	1	9	8	10	-9	0.3	-6.5	-1.6
IRW_RG	0	8/30/15	7.90	0.96	3.4	56	98	16	12	1	96	169		11	9	10	-4	0.4	-6.4	-1.5
IRW_RG	0	9/22/15				28	92	15	11	1	103	170		9	7	7				
IRW_RG	0	6/30/16	8.15	0.92	5.5	130	82	13	11	1	79	135	2	11	11	11	2	1.0	-6.5	-1.5
IRW_RG	0	9/12/16				126	75	10	11	1	116	154	2	18	10	7			-6.3	-1.4
IRW_RG	0	7/8/16				110	78	11	10	1										
IRW_GW	0	4/17/15	7.38			474	310	65	61	5	887	658		4	43	39	5	0.6	-5.0	-0.6
IRW_GW	0	4/17/15	7.25	4.26	6.8	597	266	60	57	4	741	1051		1	46	50	-4	0.4	-5.0	-0.5
IRW_GW	0	2/18/18				648	389	71	11	5										
IRW_GW	0	2/18/18				384	257	48	8	4										
SW	30	5/21/15	7.60	3.55		723	835	108	52	7	817	1621		635	84	67	11		-5.0	-0.1
SW	15	6/17/15	7.50	3.34		360	487	104	49	5	360	1057		226	50	36	16		-5.3	-0.3
SW	15	9/30/15	7.12	2.29		119	278	36	41	3	157	440	3	153	23	16	18		-5.9	-0.7
SW	15	7/18/16	7.74	3.98	1.2	473	559	70	50	5	366	1044	4	739	56	45	10	0.5	-5.5	-0.2
SW	15	9/19/16				170	170	20	29	1	148	354	2	6	18	12	22		-6.1	-0.9
SW*	15	9/19/16				115	165	20	25	2	129	282	3	12	16	10	23			
SW	30	7/3/14	6.95	5.54	4.2	715	443	71	115	6					62					
SW	30	9/1/14	7.83			381	215	19	81	3	363	855	1	22	31	28	4		-5.5	-0.6
SW	30	5/21/15				723	835	107	48	7	826	1613	2	0	83	57	19			
SW	30	6/17/15	7.31	3.77		441	534	66	59	5	507	1105		289	53	42	12		-5.1	-0.3
SW	30	9/30/15	7.29	2.32		218	259	36	36	3	185	513	2	42	26	17	23		-5.8	-0.8
SW	60	10/23/14	7.08		4.0	622	297	55	94	4	746	1213	1	209	49	54	-5	0.1	-5.0	-0.4
SW	60	6/17/15	7.35	5.81		992	943	154	75	9	1092	1810		224	105	72	19			
SW	60	7/10/15	7.25	4.72	6.4	949	498	112	59	6	1057	1497	3	101	77	69	5	0.4	-4.7	-0.4
SW	60	9/30/15	7.34	3.80		656	544	94	55	5	681	1151	6	20	65	44	20			
SW	60	7/19/16	7.07	4.76	3.5	720	548	99	56	6	709	1397	10	151	68	55	11	0.2	-4.8	-0.2
SW	120	7/19/16	7.20	6.83	10.2	1010	709	138	43	7	1844	2313		493	92	118	-13	0.8	-4.3	0.0
SW	120	6/27/16				1598	1106	244	72	12					147					
SW	120	7/19/16	7.20		10.2	1355	741	150	48	7	1070	1721	7	253	110	80	15	0.9	-4.5	-0.1

Type	depth cm	Date	pH	EC dS/m	Alk meq/L	Na^{+} ppm	Ca^{2+} ppm	Mg^{2+} ppm	K^{+} ppm	Sr^{2+} ppm	Cl^{-} ppm	SO_4^{2-} ppm	PO_4^{3-} ppm	NO_3^{-} ppm	Charge + meq/L	Charge - meq/L	Charge difference	calcite SI	halite SI	gypsum SI
SW*	120	9/19/16	7.73			367	281	44	40	3	1038	2440		368	35	86	-43			
SW	120	9/19/16				787	404	88	31	5	672	1205	2	85	63	45	16			
DRW	200	4/3/14	7.64	3.05	4.7															
DRW	200	5/19/14	8.35	4.29	6.4	710	185	19	60	4	929	744	2	9	43	48	-6	1.3	-4.8	-0.8
DRW	200	7/5/14	8.46	3.24	5.4	592	149	14	59	3	730	617		0	36	39	-4	1.2	-5.0	-0.6
DRW	200	7/28/14	7.56	3.89	3.9	654	158	17	59	3	838	702		1	39	42	-4	0.3	-4.9	-0.8
DRW	200	8/14/14	7.93	2.58	3.5	405	97	5	57	2	504	484		3	24	28	-7	0.3	-5.3	-0.8
DRW	200	9/1/14	7.80	3.75	3.4	621	81	16	61	3	746	645		0	34	38	-5	0.1	-5.0	-0.8
DRW	200	10/23/14	7.89	3.59	7.2	584	163	15	61	3	700	630	2	14	36	40	-5	0.9	-5.0	-0.8
DRW	200	5/1/15	7.90	3.87	5.4	846	328	49	12	5	1008	820	1	3	58	51	6	0.9	-4.8	-0.7
DRW	200	5/21/15	7.60	3.55		686	178	18	67	4	844	717	2	11	42	39	4			
DRW	200	6/17/15	7.31	2.43		372	291	33	16	3	486	424		4	34	23	20			
DRW	200	7/10/15	7.95	2.40	4.7	408	107	6	57	2	500	479		7	25	29	-7	-0.8	-5.3	-1.0
DRW	200	7/28/15	7.92	3.15	5.5						576	523		11		33				
DRW	200	8/19/15	8.05	2.67	5.1	420	342	39	12	3	563	547		1	39	32	9			
DRW	200	9/7/15	8.03	2.92	4.8	288	288	30	13	3	385	399		4	30	24	11			
DRW	200	9/28/15				579	232	37	12	3					40					
DRW	200	9/30/15	7.90	3.80		542	405	45	13	4	678	643	5	11	48	33	19			
DRW	200	5/21/16				759	288	44	15	4	845	729	2	12	51	39	13			

IRW_GW and IRW_RG=irrigation waters from ground water and Rio Grande respectively (placed at 0 cm depth); SW=soil waters from different soil depths; DRW=drainage water (placed at 200 cm).
* indicates that soil waters from Pecan_Coarse, and others from Pecan_Fine.


100 mi
New Mexico
El Paso
Texas
Mexico


Google Earth
200 m

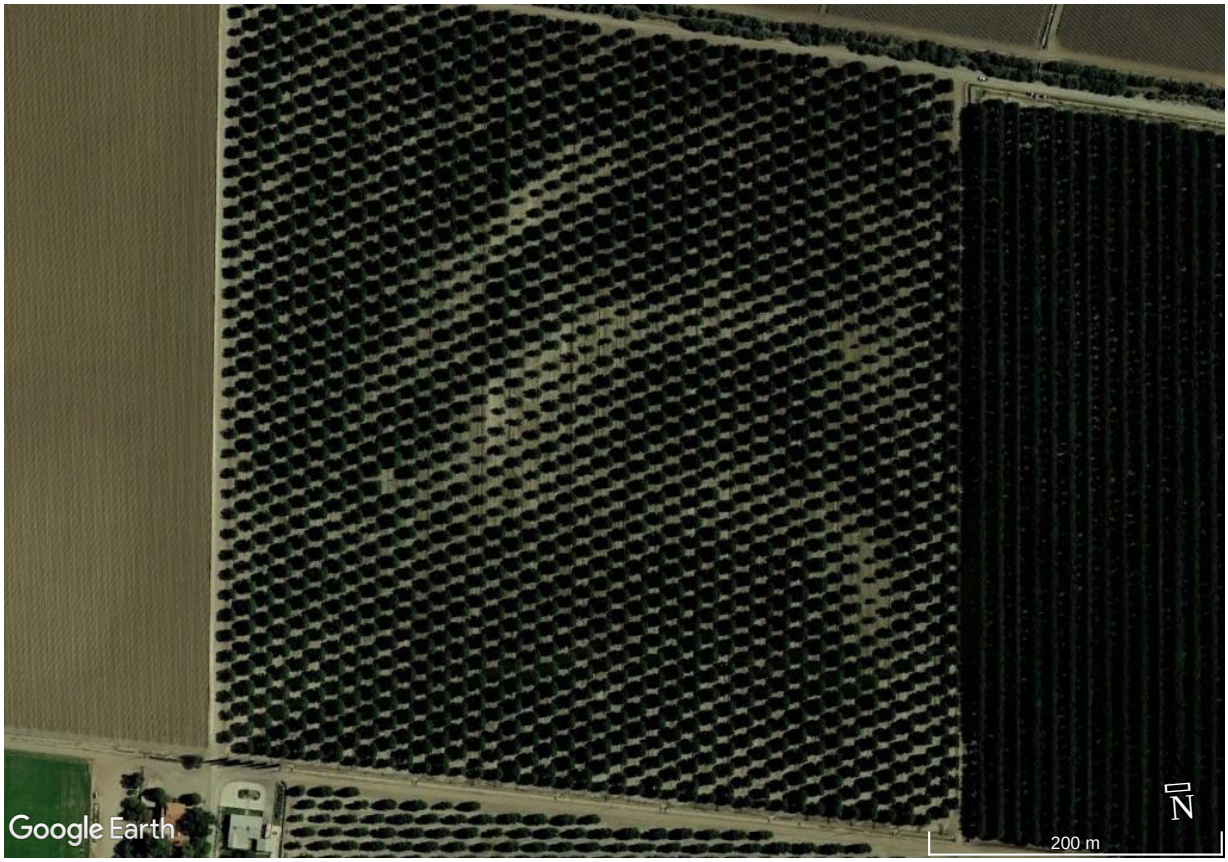
Google Earth
200 m
N

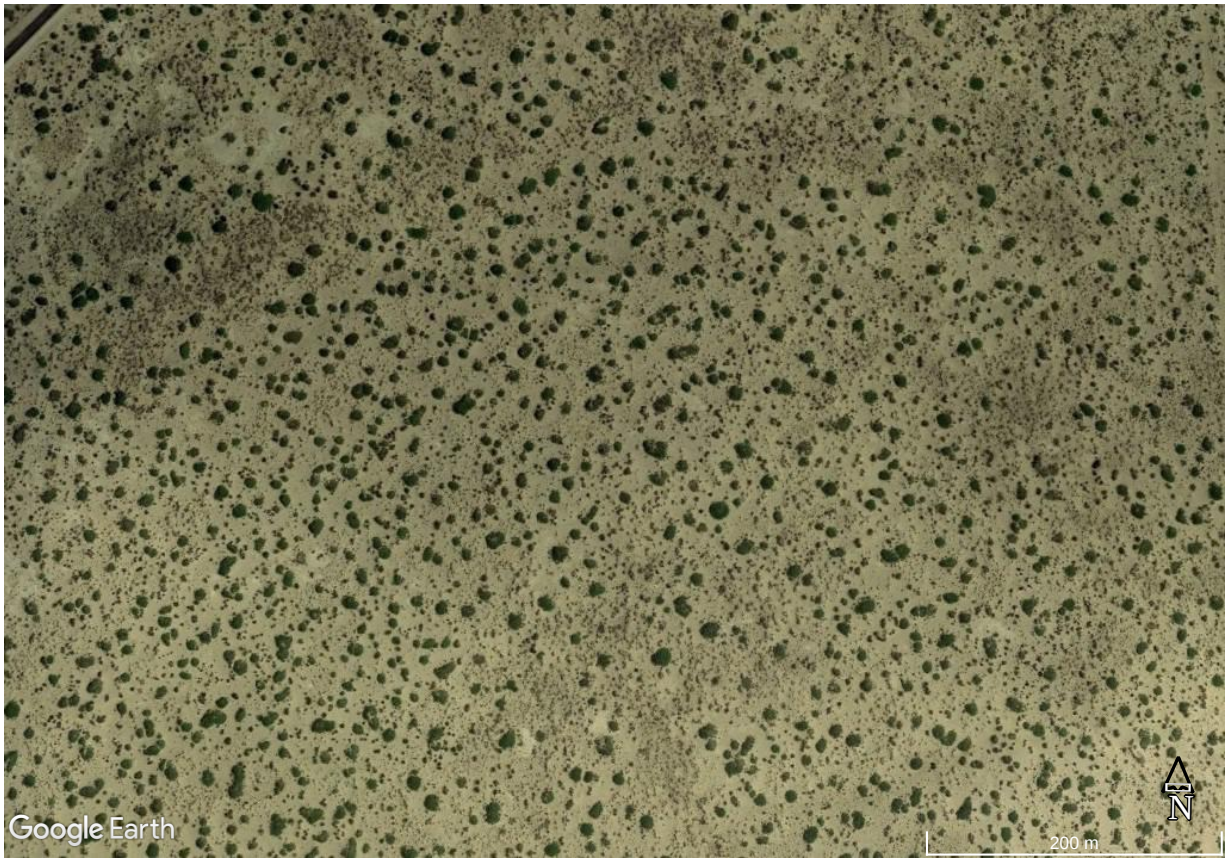

Figure **2.**1. Regional Map of research sites in the El Paso, TX region (A), including three study sites along the Rio Grande valley: two agricultural sites Alfalfa (B) and Pecan (C) and one natural sites at Fabens (D). In both agricultural sites, two soil profiles were chosen: Pecan_Fine and Pecan_Coarse (B) and Alfalfa_Fine and Alfalfa_Coarse (C).

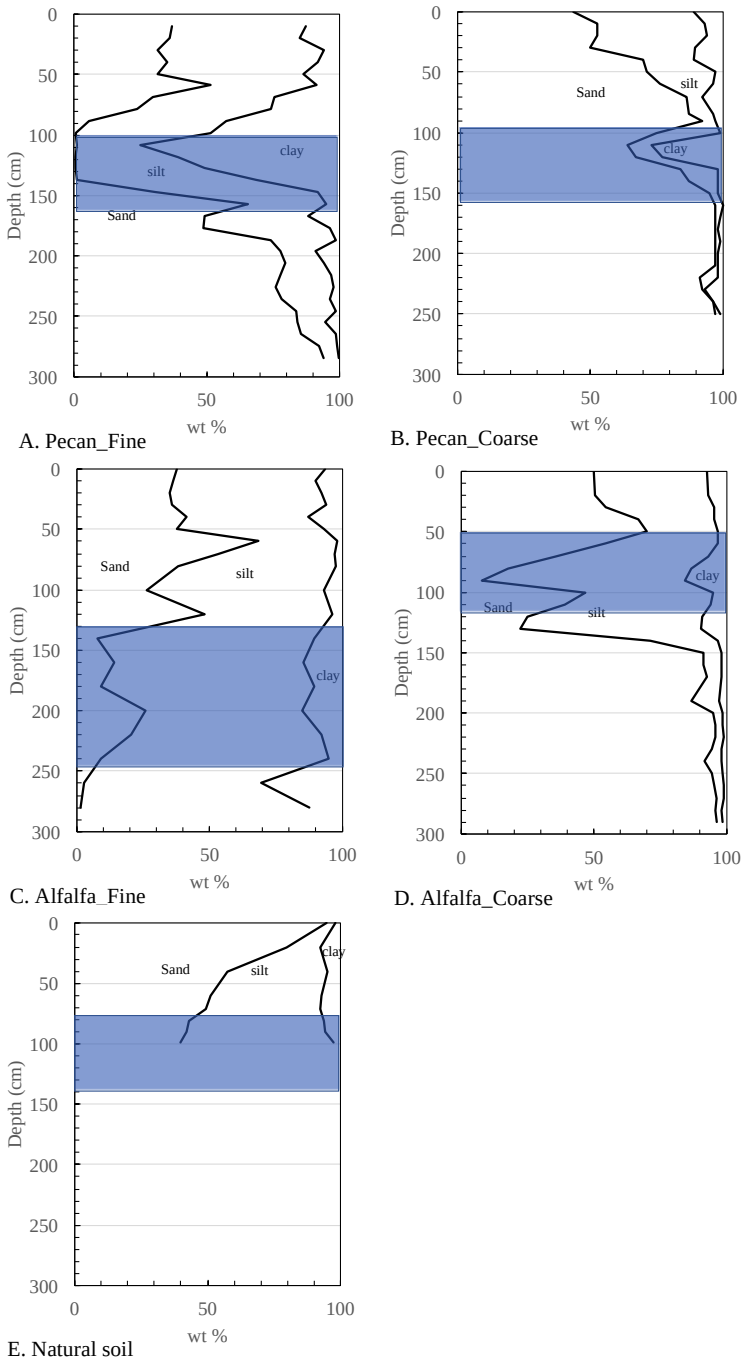

Figure 2.2. Soil texture for five soil profiles, Pecan_Fine (A), Pecan_Coarse (B), Alfalfa_Fine (C), Alfalfa_Coarse (D), and the natural site at Fabens (F). Shaded areas illustrate where salt accumulation peaked.

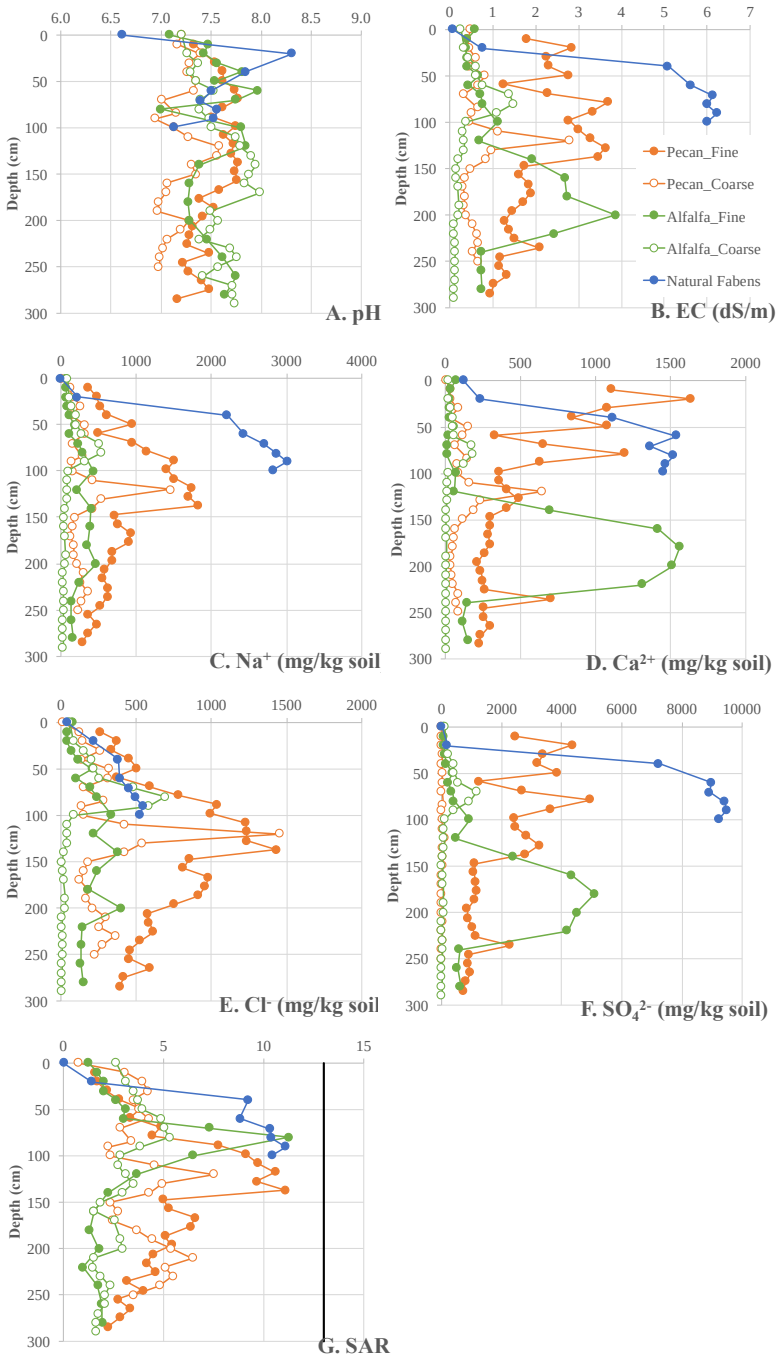

Figure 2.3. Depth profiles of pH (A), EC (B), Na^+ concentration (C), Ca^{2+} concentration (D), Cl^- concentration (E), SO_4^{2-} concentration (F), and sodium adsorption ratios (SAR, G), in the water-soluble fraction of soils from the pecan, alfalfa and natural sites.

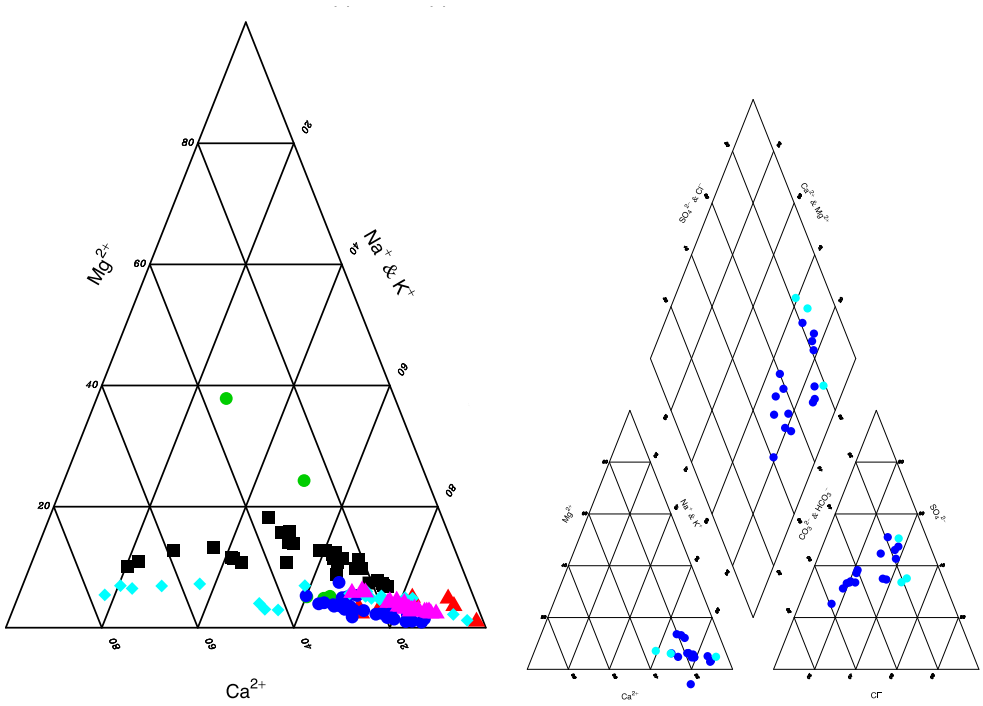

Figure 2.4. Piper-Hill diagrams for water-soluble fraction in Pecan_Fine (black squares), Pecan_Coarse (blue circles), Alfalfa_Coarse (pink triangles), Alfalfa_Fine (cyan diamonds), Alfalfa_FineD (red triangles) and Fabens, the natural site (green circles) (A), and for irrigation waters (ground water as cyan circles and river as blue circles) (B).

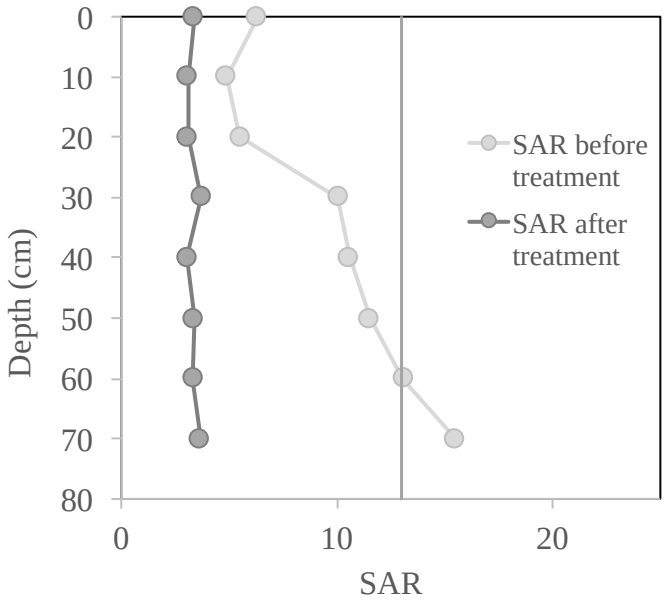

Figure 2.5. Sodium adsorption ratios (SAR) of soils at the Pecan_Fine site before and after treatment with gypsum. The threshold for sodic soil is 13, plotted as a vertical line for reference. SAR data before treatment was from Cox et al. (2018). SAR data after treatment were collected using the same method as Cox et al. (2018).

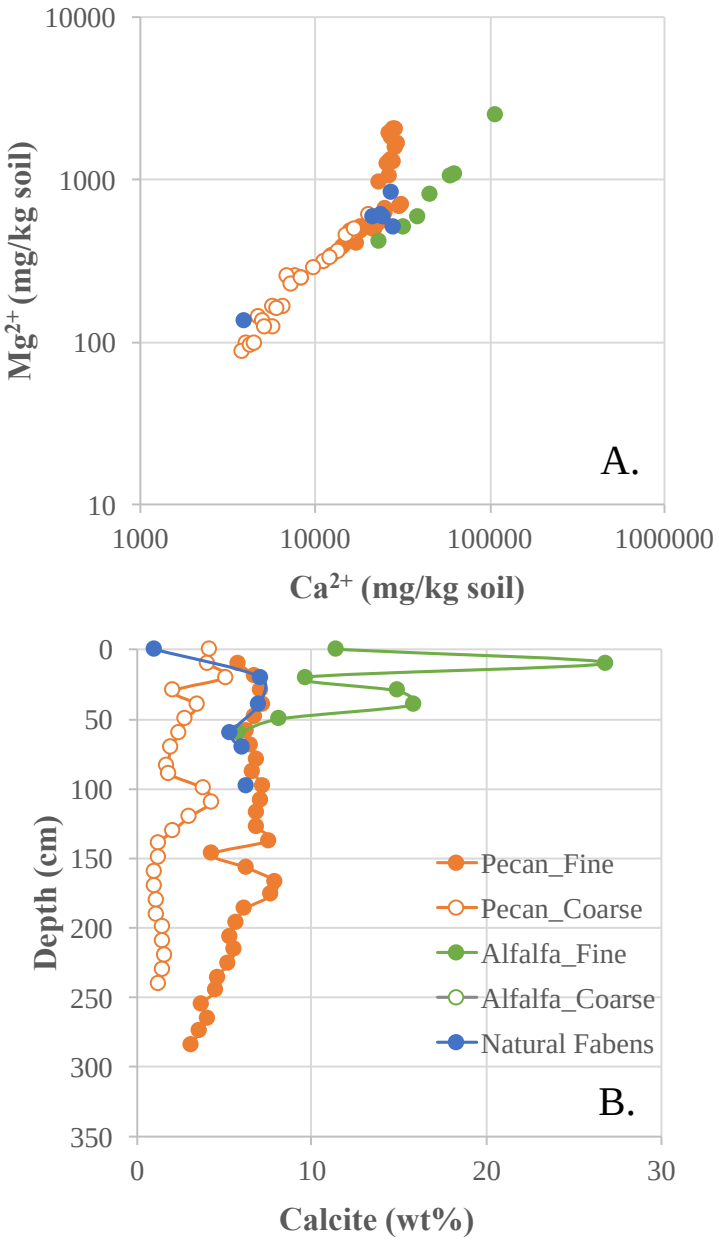

Figure 2.6. Acid leachable fraction of all soils is dominated by Mg^{2+} and Ca^{2+} (A), indicating presence of low-Mg calcite. The calcite weight % is plotted as a function of depth (B). Notice that data plotted as Alfalfa_Fine are collected from Alfalfa_Fine_D, a duplicate soil core near Alfalfa_Fine.

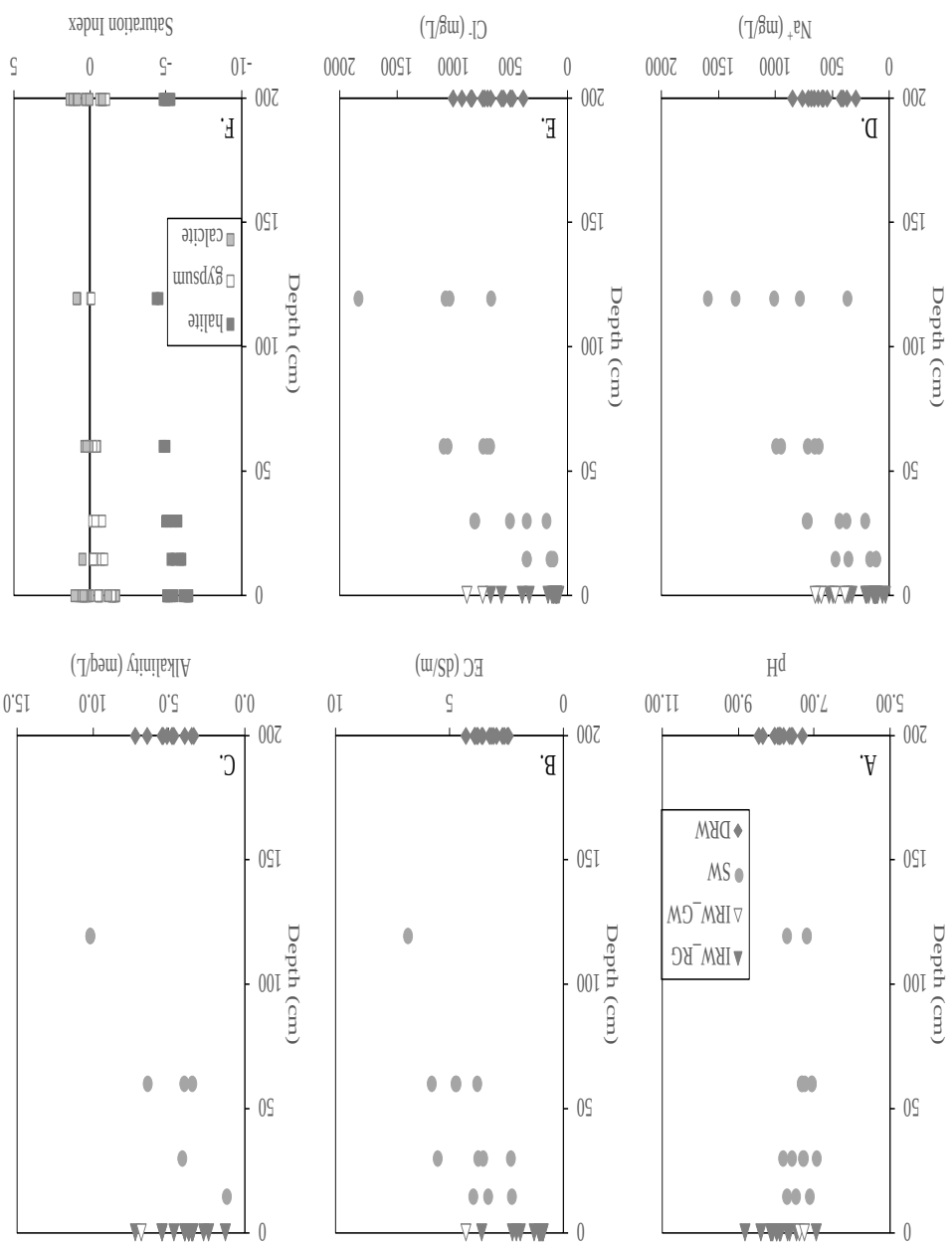

Figure 2.7. Major element chemistry of irrigation water (IRW, placed at 0 cm), soil water (SW) and drainage water (DRW, placed arbitrarily at 200 cm): pH (A), EC (B), alkalinity (C), Na^+ concentrations (D), Cl^- concentrations (E), and saturation indexes (SI) for halite, gypsum and calcite (F). IRW_RG and IRW_GW are irrigation waters from Rio Grande and groundwater, respectively.

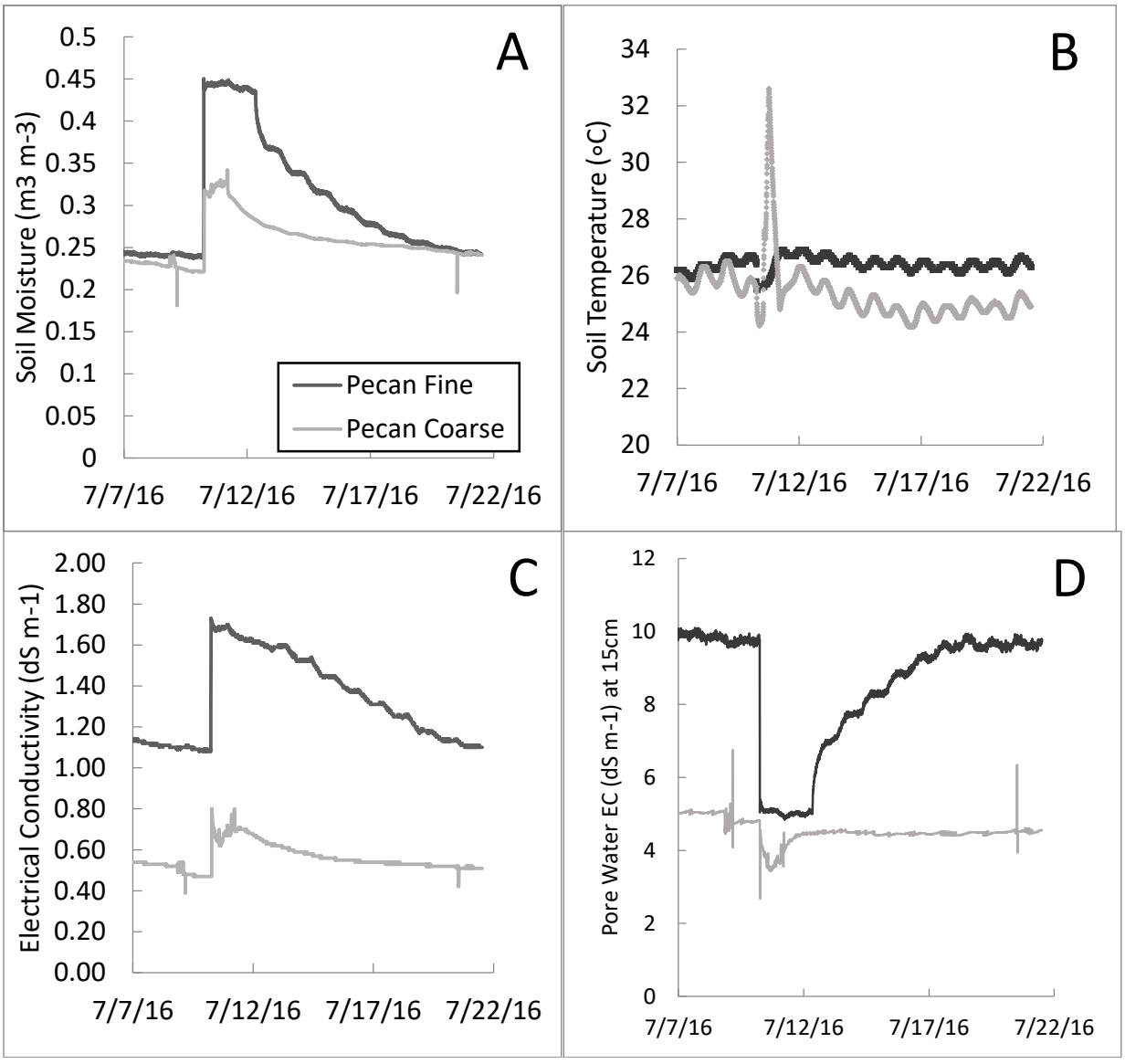

Figure 2.8. Evolution of soil moisture (A), soil temperature (B), bulk soil EC (C) and pore water EC (D) at 15 cm soil depths at the Pecan_Fine and Pecan_Coarse site for a flood-irrigation event on the whole pecan orchard. Pore water EC was calculated from bulk soil EC using equations (2)-(4) as discussed in the text.

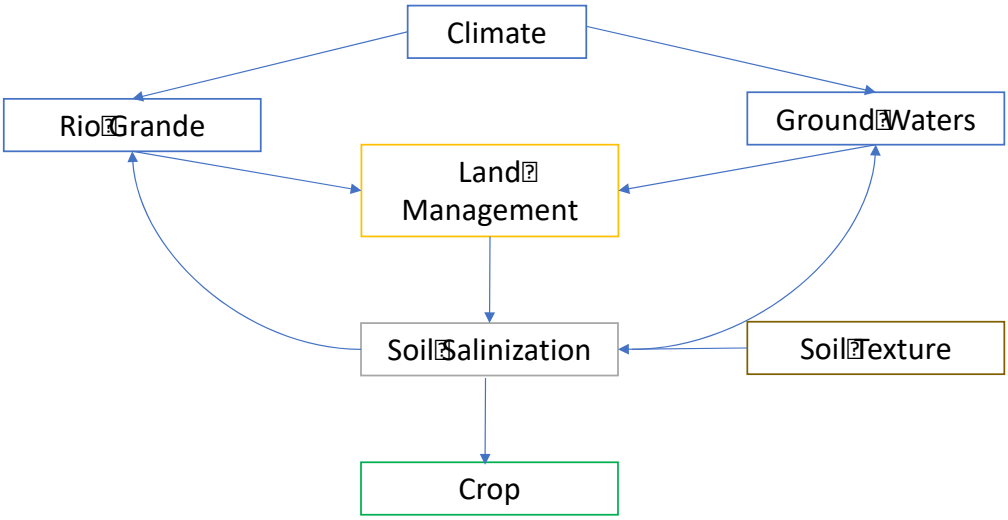

Figure 2.9. Conceptual model to illustrate the climate and management controls on soil salinization and crop production for our study sites.

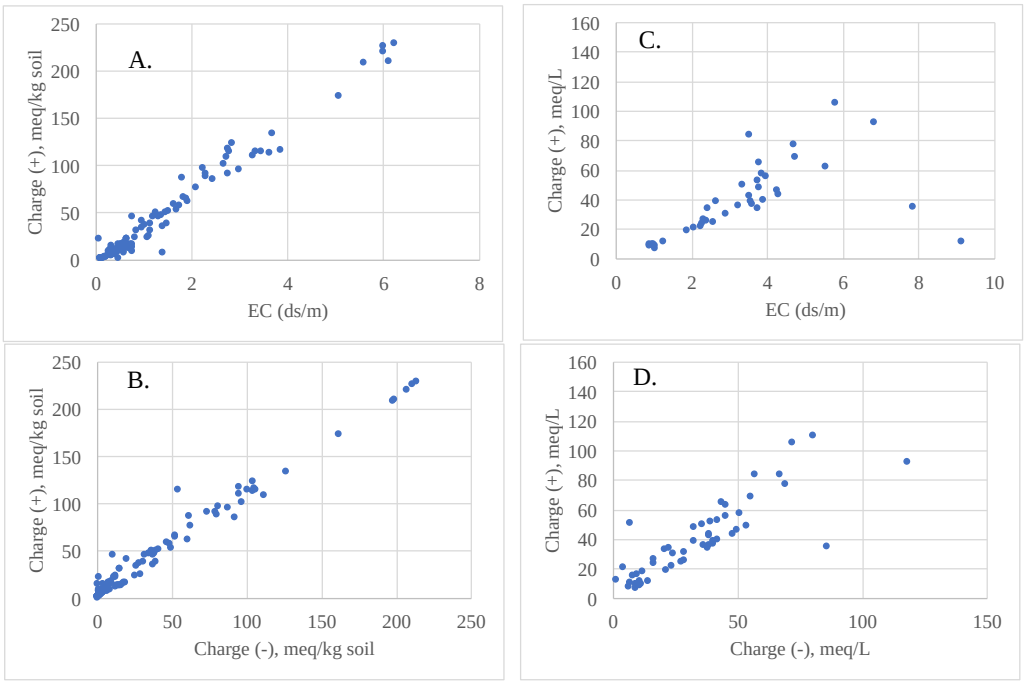

Appendix Figure 2.1. The total positive charge plotted as a function of electrical conductivity (EC) (A, C) and total negative charge (B, D) for water-soluble fraction of soils and water.

REFERENCES:

Amundson R, Richter DD, Humphreys GS, Jobbagy EG, and Gaillardet J. (2007) Coupling between biota and Earth materials in the Critical Zone. Elements 3: 327-332.

Ashworth J.B. (1990) Evaluation of Ground-Water Resources in El Paso County, Texas. Texas. Water Development Board Report 324.

Assouline S. et al (2015) Balancing water scarcity and quality for sustainable irrigated agriculture. AGU Publications Water Resources Research 10.1002/2015WR017071

Borrock, D.M., Engle, M.A. (2014) The role of climate in increasing salt loads in dryland rivers. Journal of Arid Environments 111, 7-13

Capo, R. C. and Chadwick, O. A. (1999). Sources of strontium and calcium in desert soil and calcrete. *Earth and Planetary Science Letters*, *170*(1), 61-72.

Cayan D.R. et al. (2013) The southwest climate of the future- projections of mean climate, In: Garfin, G., (Ed), Assessment of climate Change in the Southwest United States: A Report Prepared for the National Climate Assessment. NCA Regional Input Reports. Island Press, Washington, DC, p. 509

Chaganti V.N. and Crohn D.M. (2015) Evaluating the relative contribution of physiochemical and biological factors in ameliorating a saline-sodic soil amended with composts and biochar and leached with reclaimed water. Geoderma 259-260, 45-55.

Chorover J, Kretzschmar R, Garcia-Pichel F and Sparks DL. (2007) Soil biogeochemical processes within the Critical Zone. Elements 3: 321-326.

Choudhary, O.P. et al. (2004) Effect of sustained sodic and saline-sodic irrigation and application of gypsum and farmyard manure on yield and quality of sugarcane under semi-arid conditions. Field Crops Research 87, 103-116.

Cox C. et al. (2018) Soil quality changes due to flood irrigation in agricultural fields along the Rio Grande in western Texas. Applied Geochemistry 90, 87-100.

Crutzen PJ (2002) Geology of mankind. Nature 415: 23.

Daliakopoulos, I.N., Tsanis, I.K., Koutroulis, A., Kourgialas, N.N., Varouchakis, A.E. (2016) The threat of soil salinity: A European scale review. *Sci. Total Environ. 573* 727-739

Diaz-Hernandez, J.L. et al. (2018) Textural and isotopic evidence for Ca-Mg carbonate pedogenesis. Geochimica et Cosmochimica Acta 222, 485-507.

Doser D.I., Baker, M.R., Langford, R.P and Imana, E.M.C. (2007) Agricultural soils maps as a framework for conducting shallow subsurface investigations in the Rio Grande Valley near El Paso, Texas. Extended Abstract for the 20th EEGS Symposium on the Application of Geophysics to Engineering and Environmental Problems.

Drever J. I., 1997. The Geochemistry of Natural Waters: Surface and Groundwater Environments. (New Jersey: Upper Saddle River)

Elias E., Rango A., Steele C.M., et al. (2015) Assessing climate change impacts on water availability of snowmelt-dominated basins of the Upper Rio Grande Basin. *Journal of Hydrology: Regional Studies 3* 525-546.

Eshel G., Fine, P., and Singer, M. J. (2003) Total soil carbon and water quality: An implication for carbon sequestration. *Soil Society of America Journal 71,* 397-405.

Essington, M.E., (2003). Soil and Water Chemistry an Integrative Approach. CRC Press, Boca Raton, FL.

Falasca S.L., Ulberich A., Acevedo A., (2014) Identification of Argentinian saline drylands suitable for growing Salicornia bigelovii for bioenergy. *International Journal of Hydrogen Energy 39* 8682-8689

Floyd, K. W. and Gill, T. E. (2011). The association of land cover with aeolian sediment production at Jornada Basin, New Mexico, USA. *Aeolian Research 3*(1), 55-66.

Ganjegunte, G. K., Clark, J. A., Parajulee, M. N., Enciso, J., and Kumar, S. (2018) Salinity Management in Pima Cotton Fields Using Sulfur Burner. Agrosyst. Geosci. Environ., 1–10.

Ganjegunte, G.K., Sheng, Z. and Clark, J. (2012) Soil salinity and sodicity appraisal by electromagnetic induction in soils irrigated to grow cotton, Land Degradation and Development. DOI: 10.1002/ldr.1162.

Gile, L.H., Hawley, J.W., Grossman, R.B. (1981). Soils and geomorphology in the Basin and Range area of Southern New Mexico: Guidebook to the Desert Project. New Mexico Bureau of Mines and Mineral Resources., Socorro, NM, 222 .

Graham, R.C., and O'Green, A.T. (2010) Soil mineralogy trends in California landscapes. Geoderma 154, 418-437.

Gutzler, D.S. and Robbins, T.O. (2010) Climate variability and projected change in the western United States: Regional downscaling and drought statistics. Climate Dynamics, published online. doi:10.1007/s00382-010-0838-7.

Hall S. A. and Peterson J.A. (2013) Floodplain construction of the Rio Grande at El Paso, Texas, USA: response to Holocene climate change. Quaternary Science Reviews v 65 102-119.

Hillhorst M.A. (2000) A Pore-water Conductivity Sensor. Soil Sci. Soc. Am. J. 64: 192201925

Hogan J. et al (2007) Geologic origins of salinization in a semi-arid river: The role of sedimentary basin brines. Geology (35) 12:1063-1066.

Hu, Y., and Schmidhalter, U., (2002) Limitation of salt stress to plant growth. In Hock, B., Elstner, C. F. (Eds.) Plant Toxicology. Marcel Dekker Inc., New York, pp. 91-224

Jamil A., Riaz S., Ashraf M., Foolad M.R. (2011) Gene expression profiling of plants under salt stress. Crit. Rev. Plant Sci 30(5): 435-458.

Lal, R. (2007) Carbon management in agricultural soils. Mitigation and Adaptation Strategies for Global Change 12:303-322.

Marschner H. (1995) Mineral Nutrition of Higher Plants. 2nd ed., Academic Press, London.

Martinez-Beltran J, Manzur CL. (2005). Overview of salinity problems in the world and FAO strategies to address the problem. *Proceedings of the international salinity forum, Riverside, California*, April 2005, 311–313.

Mass, E.V., and S.R. Grattan. (1999). Crop yields as affected by salinity. In R.W. Skaggs and J. van Schilfgaarde, eds., Agricultural Drainage. Agron. Monograph 38. ASA, CSSA, SSSA, Madison, WI.

Miyamoto, S. (2010) Salt leaching in pecan orchards of the Southwest. Pecan South 28-36.

Monger, H. C. and Gallegos, R. A. (2000). Biotic and abiotic processes and rates of pedogenic carbonate accumulation in the southwestern United States—relationship to atmospheric CO_2 sequestration. Global climate change and pedogenic carbonates. CRC, Boca Raton, Fla, 273-289.

Nyachoti S., Jin L., Tweedie C.E., Ma L. (2017) Insight into factors controlling formation rates of pedogenic carbonates: A combined geochemical and isotopic approach in dryland soils of the US Southwest. *Chemical Geology* - in press

Ordoñez C., V.L. Lougheed, J.L.Gardea-Torresdey and L. J. Bain (2011) Impact of Metals on

Macroinvertebrate Assemblages in the Forgotten Stretch of the Rio Grande. Archives of Environmental Contamination and Toxicology. 60: 426-436.
Pannell D., and Ewing M, (2006) Managing secondary dryland salinity: Options and challenges. Agricultural Water Management v. 80 41-56.
Pascolini-Campbell M., Seager R., Pinson A., Cook B.I. (2017) Covariabilty of climate and streamflow in the Upper Rio Grande from interannual to interdecadal timescales. *Journal of Hydrology: Regional Studies 13*, 58-71.
Phillips, F. M., Emlen, Hall G. and Black, M. (2011) Reining in the Rio Grande: People, Land, and Water. University of New Mexico Press.
Phillips, F.M., Hogan, J., Mills, S. and Hendrickx, M.H. (2003) Environmental tracers applied to quantify causes of salinity in arid-region rivers: Preliminary results from the Rio Grande, southwestern USA. In Alsharha, A.S. and Wood, W.W. Eds., Water resources perspective: evaluation, management, and policy: Developments in water science, V50, Amsterdam, Elsevier Science, 327-334.
Picchioni, G.A., Karaca, H., Boyse, L.G., McCaslin, B.D., Herrera, E.A., (2000). Salinity, boron, and irrigated pecan productivity along New Mexico's Rio Grande basin. J. Environ. Qual. 29, 955–963.
Qadir M., et al. (2014) Economics of salt-induced land degradation and restoration. Natural Resources (38) 282-295.
Qi, Z. et al (2018) Spatial distribution and simulation of soil moisture and salinity under mulched drip irrigation combined with tillage in an arid saline irrigation district, northwest China. Agricultural Water Management v.201 219-231.
Reheis, M. C. and Urban, F. E. (2011). Regional and climatic controls on seasonal dust deposition in the southwestern US. *Aeolian Research 3*(1), 3-21.
Reheis, M.C. (2006). A 16-year record of eolian dust in southern Nevada and California, USA: controls on dust generation and accumulation. *Journal of Arid Environments* 67, 487–520.
Reynolds, J. F., Stafford Smith, D. M., Lambin, E. F., Turner, B. L., Mortimore, M., Batterbury, S. P. J., Downing, T. E., Dowlatabadi, H., Fernandez, R. J., Herrick, J. E., Huber-Sannwald, E., Jiang, H., Leemans, R., Lynam, T., Maestre, F. T., Ayarza, M., and Walker, B. (2007) Global desertification: building a science for dryland development, Science, 316, 847–851.
Richards L.A. (1954) Diagnosis and Improvement of Saline and Alkali Soils. Science 120 (3124): 800.
Rozema, J., and Flowers T. (2008) Crops for a Salinized World, Science v.322, 1478-1481.
Seager, R. and Vecchi, G.A. (2010) Greenhouse warming and the 21st century hydroclimate of southwestern North America. PNAS 107 (50), 21277–21282.
Shannak B., Corsmeier U., Kottmeier Ch., Al-azab T. (2014) Wind tunnel study of twelve dust samples by large particle size. Atmospheric Environment 98:442-453.
Sheng, Z. (2013) Impacts of groundwater pumping and climate variability on groundwater availability in the Rio Grande Basin. *Ecosphere* 4(1), 5. http://dx.doi.org/10.1890/ES12-00270.1
Shrivastava P., Kumar R. (2015) Soil salinity: A serious environmental issue and plant growth promoting bacteria as one of the tools for its alleviation. Saudi Journal of Biological Sciences (22)123-131.
Swetnam, T.W. and Betancourt, J.L. (1998) Mesoscale disturbance and ecological response to decadal climatic variability in the American Southwest. Journal of Climate 11: 3128–3147.

Szablocs, I. (1989) Salt affected soils, Boca Raton, CRC Press.
Szynkiewicz A., et al (2011) Anthropogenic sulfate loads in the Rio Grande, New Mexico (USA). Chemical Geology (283) 3-4:194-209.
Szynkiewicz A., et al. (2015) Isotopic studies of the Upper and Middle Rio Grande. Part 2- Salt loads and human impacts in south New Mexico and west Texas. Chemical Geology v.411, 336-350.
Wang X., Yang J., Liu G., et al. (2015) Impact of irrigation volume and water salinity on winter wheat productivity and soil salinity distribution. *Agricultural Water Management 149* 44-54.
White, W H., Nicole P. H., Krystyna, T., Sinan, Y., Randy, S. R., Thomas, E. G., Jin, L. (2015). Regional transport of a chemically distinctive dust: Gypsum from White Sands, New Mexico (USA). *Aeolian Research* 16, 1-10.
Williams A., Crossey L.J., Karlstrom K.E., et al., (2013) Hydrogeochemistry of the Middle Rio Grande aquifer system—Fluid mixing and salinization of the Rio Grande due to fault inputs. *Chemical Geology 351*, 281-298.
Wong V.N.L., et al. (2009) Carbon dynamics of sodic and saline soils following gypsum and organic material additions: A laboratory incubation. Applied Soil Ecology (41) 29-40
Woodhouse, C.A., Kunkel, K.E., Easterling,D.R., Cook, E.R. (2005) The twentieth-century pluvial in the western United States. *Geophysical Research Letters 32,* 7. http://dx.doi.org/10.1029/2005GL022413

Chapter 3: Relative proportion of natural versus irrigation-induced pedogenic carbonate in agricultural sites (Part 1): δ^{13}C isotopes

1. INTRODUCTION

The formation of pedogenic carbonates is favorable in arid to semi-arid climatic regions, that are typically characterized by low rainfall and high evaporation (e.g., Cerling and Quade, 1993). Pedogenic carbonates have been intensively studied, including morphology, deposition mechanisms and accumulation rates in natural environments worldwide (e.g., McFadden and Tinsley, 1985; Quade et al., 1995; Capo and Chadwick, 1999; Whipkey et al., 2000; Naiman et al., 2000; Van der Hoven and Quade, 2002; Dart et al., 2007; Tabor, 2007; Breecker et al., 2009; Violette et al., 2010). In the Southwestern United States, pedogenic carbonates are well documented through the Desert Soil-Geomorphic Project and other efforts in the Jornada basin, including sources, morphological stages development, and formation rates (Gile et al., 1966, 1981; Gile and Grossman 1979; Machete et al., 1985; Knuteson et al., 1989; Chiquet et al., 1999; Naiman et al., 2000). Pedogenic carbonates form when soil waters become supersaturated with calcite due to evapotranspiration, CO_2 degassing, and/or microbial activity (Reardon et al., 1980; Kempe et al., 1991; Cerling and Quade, 1993; Lorah and Herman, 1988; Ku, 2001; Szramek and Walter, 2004; Jin et al., 2008). Naturally, accumulation of pedogenic carbonate is limited by Ca supplies from the dissolution of primary Ca-bearing carbonate and silicate bedrocks and aeolian deposition (Zamanian et al., 2016), whereas abundant carbon originates commonly from soil CO_2, which can be sourced from soil organic matter, or atmospheric CO_2 (Cerling 1984).

$$Ca^{2+} + 2HCO_3^- = CaCO_3 + CO_2 + H_2O \qquad \text{Reaction 3.1}$$

According to Reaction (1), formation of pedogenic carbonate is intrinsically linked to

emission of CO_2. However, such release of CO_2 to the atmosphere has not been directly measured, partially because this is a small flux due to the slow accumulation rates of pedogenic carbonates (e.g., <0.01 to 1.3 gC m^{-2} yr^{-1} in southwest US; Monger and Gallegos, 2000) relative to soil respired CO_2 (Serna-Pérez et al., 2006). Indeed, the natural production of soil CO_2 has long been studied, where it is dominated by biotic sources including bacterial decomposition of organic matter, root respiration, and microryzeal activity, even in water-limited drylands (Trumbore et al., 1996; Davidson et al., 1998; Lal, 2004; Tang et al., 2005; Darrouzet-Nardi et al., 2015). In addition, CO_2 release during calcite precipitation may be episodic, driven by rainfall or snowmelt events, making it difficult to capture without automatic monitoring systems. The "FluxTower" or FLUXNET community identified "anomalous" abiotic CO_2 effluxes in several semiarid ecosystems, despite that it was concluded that contribution from calcite derived CO_2 was small (compiled by Serrano-Ortiz et al., 2010).

To meet the demand of the rapidly growing population, global food production has to greatly increase, putting extreme pressure on soil productivity. Natural ecosystems are converted to agricultural fields, and soils are intensively irrigated, leading to elevated soil salinity, sodicity and alkalinity in arid-lands (e.g., Sheta et al., 2000; Schoups et al., 2005; Jafari et al., 2012; Rath and Rousk, 2015). However, few studies have focused on calcite deposition in agricultural fields, even though irrigation loads supply significant amounts of Ca^{2+} and HCO_3^- to soils annually, and thus may dramatically alter carbon cycles (Suarez, 2000; Schlesinger, 2000; Sanderman, 2012; Nyachoti et al., 2017; Cox et al., 2018; Ortiz et al., 2018). Agricultural soils from an apple orchard in semi-arid British Columbia, Canada were shown to have elevated carbonate precipitation rates directly underneath the drip irrigation system, and their incubation experiments showed emission of CO_2 that was of inorganic carbon sources, highlighting the occurrence of secondary carbonate

precipitation as a direct result of irrigation (Hannam et al., 2016). One modeling effort estimated ~2.2 Tg C yr^{-1} (1Tg = 10^{12}g) are released to the atmosphere from ~16 million ha of irrigated fields in the western U.S. (Suarez, 2000). This is equivalent to an emission of abiotic CO_2 to the atmosphere and accumulation of pedogenic carbonate both at 14 g C m^{-2} yr^{-1}, one to two orders of magnitude higher than these rates in natural settings (e.g., Eghbal and Southard, 1993; Landi et al., 2003). If so, irrigation has the potential to significantly alter land-atmosphere CO_2 flux over a large area of the Earth's surface.

This work aims to quantify how much land-use change from natural arid environments to soil cultivated agriculture promotes pedogenic calcite accumulation and releases abiotic CO_2 to atmosphere and terrestrial carbon-climate feedbacks through Reaction 3.1. The implications of enhanced CO_2 production as a result of dryland agriculture would include an unexpected and otherwise, understudied source that would be widely impacting global carbon cycling, especially because dryland agriculture is so wide spread, and is expected to continue to grow with present climate model predictions. In this study, we focused on a well-studied pecan orchard near El Paso, Texas, and characterized soil, soil gas and water samples using combined geochemical and carbon isotopic tools. The specific goals are (1) to determine if majority of pedogenic carbonates observed in the soils accumulate during soil cultivation and (2) to evaluate if pedogenic carbonate accumulation in irrigated soils emits a substantial flux of CO_2 to the soil.

2. STUDY SITE

The managed soils along the U.S.-Mexico border in western Texas and southern New Mexico are typical and representative of the larger dryland areas in southwestern US and globally. These soils are developed on the Rio Grande floodplains in the late Holocene and have been intensively cultivated for the last 90 years. Previous work has investigated flood-irrigated soils

near El Paso, Texas and reported high salinity, alkalinity, and sodicity in almost all soils (Ganjegunte et al., 2012; Cox et al., 2018; Ortiz et al., 2018). The irrigation water, from Rio Grande river and local groundwaters, is at equilibrium with respect to calcite (Sznkiewicz et al., 2015; Ortiz et al., 2018); soil waters became oversaturated and high carbonate contents were observed, along with gypsum and minor halite, especially above the fine-grained soils where water penetration was slow (Cox et al., 2018; Ortiz et al., 2018). U-disequilibrium isotopes were studied in soils on alfalfa, one of the major crops in the area, and ages of pedogenic carbonate were determined to be much younger than those in the natural sites nearby (Nyachoti et al., 2017). Thus, it was suggested that younger pedogenic carbonate formed at faster rates, accelerated by dissolved Ca^{2+} and dissolved inorganic carbon loading through flood irrigation (Nyachoti et al., 2017).

Our study site is on a pecan orchard (*Carya illinoinensis*), near Tornillo, TX (Figure 1). Regionally, El Paso county is the 8th largest producer of pecans in the U.S. southwest. Pecan trees are flood irrigated every three weeks from April to October and over one meter of water is used per growing season. Typically, fields have standing water for a week and soils are saturated. With infiltration and continuous evapotranspiration, soils dry up, pushing the remaining soil water to become more concentrated and even saturated with respect to the most soluble evaporite salts such as halite and gypsum (Cox et al., 2018). Indeed, shallow soils were characterized and reported to have high salinity and sodicity due to elemental loading from such irrigation (Cox et al., 2018). To improve the soil sodicity, soil amendments including sulfuric acid, elemental S pellets, and gypsum are applied to the pecan orchard regularly. These chemicals either add easily soluble Ca directly or dissolve pedogenic carbonate in the soils to release Ca. Calcium will replace Na from soils, lowering the soil sodicity, allowing water infiltration, and thus leaching salts out.

The soil texture at the study site is quite variable, and it controls salt buildup and crop yield (Cox et al., 2018; Ortiz et al., 2018). Briefly, two soil profiles, approximately 40m apart in the same pecan field, were previously selected, Pecan_Coarse on sandy soils and Pecan_Fine on clayed soils (Figure 1), and the soil textural differences also account for significant differences in salt accumulation within the soils and primary productivity (Ortiz et al., 2018). The smaller trees were mainly observed on soils with clayey soils and thus much higher salinity; in contrast, the larger trees grow on sandy soils with significantly lower salinity (Cox et al., 2018; Ortiz et al., 2018).

3. METHOD

3.1. Soil sample collection and analyses

Archived soil samples from the Pecan_Coarse and Pecan_fine sites were used (Ortiz et al., 2018). Specifically, soils at each site were collected at about 10 cm interval until 300 cm deep by hand auguring. Soil pH, salinity and texture were characterized and reported previously (Ortiz et al., 2018).

Soil carbon (SC) and organic carbon (SOC) contents were quantified using a LECO 632C/S analyzer. About 0.2 g of ground bulk soil samples was weighed, mixed with combustion catalyst (Comcat), and combusted in the LECO furnace at 1950^{o}C. The moisture was then removed from the resultant gases and CO_2 was quantified by infrared detector for SC. Two standards of different carbon contents were used for calibration. Another aliquot of bulk soils was treated by 1:1 HCl to remove carbonate (also known as soil inorganic carbon; SIC) and then dried in the oven at 60 ^{o}C. The carbon content measured on these acid-leached soils was considered as SOC, and SIC was calculated as the difference between SC and SOC. Weight percent of calcite was then computed from SIC based on calcite stoichiometry ($CaCO_3$).

The C isotopes of organic matter ($\delta^{13}C_{SOC}$) and carbonate ($\delta^{13}C_{CaCO3}$) in the selected soil samples were analyzed on a continuous-flow isotope ratio mass spectrometer (IRMS; Finnigan Delta PlusXL). Precision for $\delta^{13}C_{SOC}$ was ±0.1‰ or better (1σ). In order to measure C isotope composition of the carbonate minerals ($\delta^{13}C_{CaCO3}$), soil samples were reacted with dehydrated H_3PO_4 under vacuum at 70°C. The released CO_2 was then measured by an IRMS (Finnigan MAT 252). For these measurements, precision is better than ±0.08‰ (1σ).

3.2. Soil gas sample collection and analyses

Two nests of soil gas tubes were installed at Pecan_Fine and Pecan_Coarse sites at four depths (15, 30, 60 and 120 cm) and sampled following a modified USGS protocol (Jin et al., 2014; Hasenmueller et al., 2015). Soil gas samples were collected using 60-mL gas-tight plastic syringes and needles after purging two tube volumes to clear the sampler tube. Gas samples were immediately transferred to pre-evacuated 15-mL LETCO® glass vials. Additional atmospheric gas samples for pCO_2 and $\delta^{13}C_{CO2}$ were taken as local atmospheric endmembers, as well as for quality control. Gas samples were collected prior to irrigation and also one week after each flooding event, when the pecan field was dry enough to be accessible for soil gas sampling.

Soil gas CO_2 concentrations (pCO_2) were measured by a LiCOR 7000 gas analyzer, calibrated with CO_2 standards with concentrations of 970 and 10300 ppmv. The isotopic composition of soil CO_2 was determined using a Europa 20-20 continuous flow Isotope Ratio Mass Spectrometer (IRMS) with an ANCA-TG preparation module for trace gas samples. Gas samples were flushed with He across two chemical traps that removed water and then trapped the CO_2. The carbon isotope ratios of soil gas samples were analyzed at the Jozef Stefan Institute in Slovenia. Precision in $\delta^{13}C_{CO2}$ is better than ± 0.1‰ (1σ), based on repeated internal standards.

3.3. Collection and analyses of irrigation waters

Irrigation water samples collected at the study sites included Rio Grande surface waters (IRW_RG), and local groundwaters (IRW_GW). The temperature, pH and EC values of the water samples were measured in the field. Concentrations of major cations and anions were measured with a Perkin Elmer inductively coupled plasma optical emission spectrometer (ICP-OES, DV5300) and Dionex-2100 ion chromatograph (IC), respectively at the Low-Temperature Geochemistry Laboratory of the University of Texas at El Paso (UTEP). The precision of ICP-OES and IC analyses was better than ± 3% for major elements and ± 10% for minor elements. Total alkalinity was determined on refrigerated water samples by weak hydrochloric acid titration using Mettler Toledo DL15 auto-titrator and data reanalyzed using the Gran alkalinity method (Gieskes and Rogers, 1973; Stumm and Morgan, 1996). The uncertainty for alkalinity titrations is ± 10% for most of samples. These water chemistry data including saturation indexes with respect to calcite were previously reported in Ortiz et al. (2018).

The C isotopes of dissolved inorganic carbon (with HCO_3^- as the dominant DIC species; $\delta^{13}C_{DIC}$) was measured at the Environmental Stable Isotope Laboratory at the University of Arizona through a contractual service. The precision in $\delta^{13}C_{DIC}$ is better than ± 0.1‰ (1σ).

4. RESULTS

The contents (SOC and SIC) and C isotope ratios ($\delta^{13}C_{SOC}$ and $\delta^{13}C_{CaCO3}$) of soil organic and inorganic carbon are reported in Table 3.1. The SOC contents at both sites are high in ground surface samples, at 1.4 to 1.6 wt%, and decreased with depth sharply (Figure 3.2A). The $\delta^{13}C_{SOC}$ values of soil organic matter were between -21.5 and -24.5 ‰ (Figure 3.2C), typical of C3 type vegetation such as the pecan trees. The SIC contents were higher in Pecan_Fine site (0.24 to 1.24 wt%) than in Pecan_Coarse site (0.07 to 0.66 wt%) (Figure 3.2B). Based on calcite stoichiometry,

the contents in the Pecan_Fine site are equivalent of 2 to 10 wt% pedogenic carbonate. The C isotope signatures of the calcite ($\delta^{13}C_{CaCO3}$) were very similar between the two soil profiles and narrow in range, around -3.7 to -6.0 ‰ (Figure 3.2D). Overall, the pCO_2 concentrations increased with depth for both sites, up to 74,000 ppm or almost 200 times of the atmospheric CO_2 level at 60 cm depth (Table 3.2; Figure3. 3A). The $\delta^{13}C_{CO2}$ values varied dramatically with depth and were much higher than the $\delta^{13}C_{SOC}$ values (Figure 3.3B). Several gas samples, from both shallow and deep soils, had extremely low pCO_2 but high $\delta^{13}C_{CO2}$, close to those of atmospheric CO_2.

The elemental data for all water samples had been reported by Ortiz et al. (2018) and included in Table 3.3, along with C isotope data ($\delta^{13}C_{DIC}$). All water samples were neutral with pH between 7.2 and 8.1, and dominated by Na^+, Cl^-, SO_4^{2-}, and Ca^{2+}. Relatively, the Rio Grande water samples used for irrigation had lower total dissolved solids (expressed as electrical conductivity EC, 0.9 to 1.9 dS/m) than two groundwaters (EC values at 3.8 and 4.3 dS/m (Table 3.3). The measured alkalinity values ranged from 3.4 to 3.7 meq/L in Rio Grande waters, and 5.3 to 6.8 meq/L in groundwaters; dissolved Ca^{2+} concentrations were lower in the Rio Grande waters (36-98 mg/L) than those in groundwaters (266-310 mg/L). The saturation indexes of these waters with respect to calcite were all positive, from 0.0 to 0.6. The $\delta^{13}C_{DIC}$ of Rio Grande samples used for irrigation waters ranged from -10.4 to -6.3‰, on average -7.3‰; the groundwaters used for irrigation exhibited more negative $\delta^{13}C_{DIC}$ ratios (give the range here), averaging at -11.3‰.

5. DISCUSSION

5.1. Conceptual model of $CaCO_3$ precipitation and inorganic CO_2 production

Soil and gas dynamics are sensitive to soil moisture conditions (Figure 3.4). Specifically, at the onset of each irrigation event, the field is flooded and the soil is saturated, pushing all soil gas bubbles including CO_2 to the atmosphere. The irrigation water is at equilibrium with calcite,

but unsaturated to other evaporite salts such as halite and gypsum (Cox et al., 2018). Existing salts that have accumulated from previous irrigation are dissolved, increasing concentrations of Ca^{2+}, Na^{+}, Cl^{-} and SO_4^{2-} in soil waters and leading to their oversaturation with respect to calcite. With continuous evaporation and transpiration, soil moisture content decreases and the soil waters become even more concentrated and oversaturated with respect to calcite. Thus, the calcite precipitates out in soils, accompanied by release of CO_2 according to Reaction (3.1). Gypsum and halite are more soluble than calcite, and they will precipitate out later under much lower moisture conditions (Ortiz et al., 2018).

Conversion of natural habitat to crop lands brings unusually wet conditions through irrigation in arid-lands, and allows the accumulation of soil organic matter. This leads to active soil respiration from plant roots and microbial community according to Reaction (3.2).

$CH_2O_{(OM)} + O_2 \rightarrow CO_2(g) + H_2O$ Reaction (3.2)

The soil respiration rate varies as a function of soil temperature and moisture (thus with irrigation schedule; Hursh et al., 2016). Nevertheless, soil cultivation leads to an elevated CO_2 efflux for arid-lands due to both biotic and abiotic processes, making soil pCO_2 much higher than atmospheric pCO_2 and moving CO_2 across the land- atmosphere interface. Below, we combined the carbon isotopic ratios of soils, soil waters and soil gases to determine if pedogenic carbonates in agricultural soils are young and formed in the last 90 years during soil cultivation, or old and formed predominantly naturally before human settlements and if the soil gas has detectable CO_2 that is from calcite precipitation according to Reaction (3.1). This study thus defines key linkages between flood irrigation, salt loading, and atmospheric CO_2 dynamics in agricultural soils typical of southwestern U.S. and many global drylands.

5.2. Controls on C isotope compositions of soil carbonates

Naturally, carbon in the pedogenic carbonates may be potentially sourced from atmospheric CO_2, soil respired CO_2 and primary carbonates from the bedrock (Sheldon and Tabor, 2009); C isotopic analysis ($\delta^{13}C$) can be used for such source identification (Vogel, 1993; Yang et al., 1996; Karim and Veizer, 2000; Singh et al., 2005; Jin et al., 2009). The C isotopic composition of soil respired CO_2 varies largely depending on the sources of soil organic matter and thus, biochemical pathways used for photosynthesis (Ehleringer et al., 1991; Vogel, 1993; Kraimer and Monger, 2009). The $\delta^{13}C_{SOC}$ values of soil organic matter were between -21.5 and -24.5 ‰ in the study site (Figure 2C), typical of C3 type vegetation such as the pecan trees (−30 to −24‰ for C3 plants; REF). Soil respired CO_2 is enriched in ^{13}C relative to its organic matter sources by a maximum of 4.4‰, due to fractionation from CO_2 diffusion, and mixing with atmosphere (Quade et al., 1989; Jin et al., 2009; Jin et al., 2014). Soil CO_2 is a large carbon reservoir and precipitation of calcite is slow, making soils an open system where pedogenic calcite formation occurs at isotopic equilibrium with soil water DIC and consequently, soil CO_2. Indeed, such a relationship has been commonly documented in modern vegetation, soil CO_2 and pedogenic calcite from arid to sub-humid environments (e.g., Amundson et al., 1988; 1989; Quade et al., 1995; Breecker et al., 2009). Even in soils developed on carbonate parent rocks in the southern Great Basin, carbon isotope compositions of pedogenic carbonates were observed to equilibrate with soil CO_2, with little influence from pre-existing limestone (Quade et al., 1989). Indeed, old pedogenic carbonates have been used as proxies to reconstruct changes in climate (mean annual temperature and precipitation), vegetation (relative proportions of C3 and C4) and historical atmospheric CO_2 levels (Amundson et al., 1988; Cerling et al., 1993; Quade et al., 1994; Rowe and Maher, 2000; Landi et al., 2003; Retallack, 2005; Sheldon and Tabor, 2009; Montanez, 2013).

Assuming chemical and isotope equilibrium conditions between soil CO_2 and calcite, we modeled the $\delta^{13}C_{CaCO3}$ for soils dominated by C3 and C4 vegetation, respectively (Figure 3.2D). The equilibrium fractionation factors between soil gas CO_2, dissolved inorganic carbon species, and calcite were calculated at 20 ^oC (Clark and Fritz, 1997), the mean annual air temperature for the region, based on available carbon isotope fractionation data. The pedogenic carbonates that were formed naturally with C3 plants and C4 plants would have $\delta^{13}C_{CaCO3}$ values around -12‰ and -5‰, respectively. The $\delta^{13}C$ value of atmospheric CO_2 is around−8.0‰ and becomes lighter with continuous release of CO_2 from fossil fuel combustion (e.g., Friedli et al., 1986). If pedogenic carbonate precipitates at equilibrium with atmospheric CO_2, the $\delta^{13}C_{CaCO3}$ values would be near 2‰. The soil carbonates in the pecan orchard had relatively uniform $\delta^{13}C_{CaCO3}$ values, overlapping with those formed under C4 vegetation (Figure 3.2D). However, such C4 vegetation landscape coverage has never been observed in the surrounding areas of this study (Monger et al., 2009; Weems and Monger, 2012).

Alternatively, carbon in calcite could be derived from DIC in irrigation water. The evolution of C isotope in precipitating calcite and CO_2 in Reaction (3.1) as a function of irrigation of $\delta^{13}C_{DIC}$ and extent of calcite precipitation (Figure 3.5). At Rayleigh fractionation, the fractionation factors between calcite and DIC (namely bicarbonate) and between CO_2 and DIC are constant at 20^oC, the continuous removal of calcite and CO_2 leads to higher $\delta^{13}C_{DIC}$ in the residual soil water. As a result, the solid and gas phases from each precipitation step (dashed lines) become more enriched in ^{13}C. Overall, the $\delta^{13}C_{CaCO3}$ of all calcite is estimated at -1.5‰ and $\delta^{13}C_{CO2}$ of all CO_2 was at -10.5‰ (Figure 53.). These findings agree with the shift towards enriched values of field $\delta^{13}C_{CaCO3}$ and $\delta^{13}C_{CO2}$.

This exercise revealed that naturally formed and irrigation-induced carbonate have distinct C isotope composition. In the two-component system (natural site, A=naturally occurring pedogenic carbonate, B=anthropogenic carbonate), the fraction of calcite in the bulk soil (mix) contributed by source A can be calculated by:

$$X_A = \frac{R_{mix} - R_B}{R_A - R_B} \qquad \text{Equation 3.1}$$

$R_A = \delta^{13}C_{CaCO3}$ = -12‰; $R_B = \delta^{13}C_{CaCO3}$ = -1.5‰; and $R_{mix} = \delta^{13}C_{CaCO3}$ (soil)= -4.5±0.6‰. Solving Equation 1, the secondary calcite derived from natural precipitation contributed 29% (X_A =22% to 34%) of total pedogenic carbonate. The uncertainty on X_A is large with just variables R_B constrained for limited irrigation samples. But still, this is consistent with previous conclusion that flood irrigation leads to elevated accumulation rates of pedogenic carbonates and 90 years of soil cultivation produced more pedogenic carbonates than several thousands of years of natural processes (Cox et al., 2018; Nyachoti et al., 2018; Ortiz et al., 2018).

5.3. Controls on C isotope compositions of soil gas CO_2

Soil pCO_2 measured in the agricultural field showed differences with depth, relatively low at surface and much higher at depths (Figure 3.3A). This is typical in natural systems, where soil respiration, root respiration and microbial activities release CO_2 at deeper soils (Reaction 3.2; Trumbore et al., 1996; Alling et al., 2012; Jin et al., 2014; Hasenmueller et al., 2015). Such diffusion profiles are observed in soils of all climatic conditions, although thicker soils and warmer/wetter climate tend to have higher pCO_2 levels, especially during the growing seasons (Jin et al., 2014). The ecosystems in drylands are typically limited by water; therefore, soil pCO_2 might be low in natural systems but the agricultural soils are more active due to water availability through irrigation (Figure 3). Indeed, soil pCO_2 as high as 70,000 ppm of were observed.

The Keeling plot revealed two clusters in all soil gas samples, one close to atmospheric CO_2 and the other next to the soil-respired CO_2 (Figure 3.6). However, the C isotopic ratios of soil gas samples were different from soil organic matter by more than 4.4‰, suggesting that soil CO_2 have more than two sources (air and soil respiration) or/and other processes fractionate C isotopes in soil gases. The inclusion of calcite-derived CO_2 ($\delta^{13}C_{CO2}$ = -10.5‰ according to the model) could explain the deviation of soil gas CO_2 from the atmosphere-soil respiration mixing curve. Thus, it is reasonable to conclude that soil CO_2 has a detectable contribution from the calcite precipitation as shown in Reaction 3.1.

The $\delta^{13}C_{SOC}$ values of soils in the pecan orchard were typical of C3 plants and no difference was observed between Pecan_Fine and Pecan_Coarse sites (Figure 3.2C). In comparison to those in the Pecan_Coarse site, soil gas samples from the Pecan_Fine site were closer to the calcite-derived CO_2 end-member (Figure 3.6). This suggested more contribution from calcite precipitation or/and lower contribution from soil respiration at the Pecan_Fine site. The latter was expected, given that pecan trees were much smaller in size at the Pecan_Fine site than those at the Pecan_Coarse site (Figure 3.1; Ortiz et al., 2018). This was due to the difference in soil texture: clayey soils at the Pecan_Fine site lowed the water infiltration rates and promoted more salt buildup; here the soil salinity exceeded tolerance levels of pecan, and stunted the growth. The former was also reasonable: salt buildup was more pronounced at the Pecan_Fine site, including secondary calcite (Figure 3.2B). If so, more CO_2 was expected to be released from calcite precipitation at the Pecan_Fine site.

5.4. Is pedogenic CO_2 efflux important to global C cycling?

Previous works on incubation of a calcareous soil from North-west Tunisia at different temperatures released CO_2 from both soil inorganic carbon and organic carbon sources (Chevallier et al., 2016). At the study site, loading of soil Ca^{2+} through irrigation has been calculated to be approximately 100 g m^{-2} yr^{-1} or 30 g C m^{-2} yr^{-1} (Cox et al., 2018; Ortiz et al., 2018). If this loading holds true in other drylands, calculations reveal that a potential total of *ca.* 30 g C m^{-2} yr^{-1} * 0.4 million km^2 = 12 Tg C yr^{-1} is released as CO_2 following irrigation. This value is 5 times the flux Suarez (2000) estimated for southwestern US alone. Assuming dryland irrigation has operated for 100 years, this released 1.2 Pg C of CO_2. Combined, these findings suggest dryland agriculture has the potential to significantly alter land-atmosphere CO_2 flux over a large area of the Earth's surface.

The soil CO_2 efflux, induced by calcite precipitation in irrigated fields, was sensitive to the chemistry of irrigation water, and hydrological conditions in Suarez (2000)'s models, thus efflux rates are likely to vary significantly among agricultural settings. With implications for similar regions worldwide, results will be scaled to determine the likely impact and significance in local to biome-wide carbon cycling. To date, representation of the potential shift in land-atmosphere CO_2 exchange associated with dryland agriculture has been poorly recognized and models forecasting the future state of the Earth System do not include such dynamics. More work is needed to collect CO_2 emission data from the agricultural sites in drylands and estimate its significance.

6. CONCLUSION

Drylands cover more than 40% of the terrestrial land surface and host more than two billion people, with most living in developing countries. The combined increase in population and food demand has converted natural dryland to irrigated agriculture coverage. Agriculture in drylands

along the Rio Grande valley, loading salts through irrigation, has also enhanced pedogenic carbonate development and produced CO_2 in soils for more land-atmosphere carbon exchange.

Natural accumulation of pedogenic carbonate has been well investigated but few studies have focused on calcite deposition in irrigated agricultural settings of arid-lands. More importantly, no previous studies have examined concomitant production of abiotic CO_2. Geochemical and carbon isotopic data were collected on two soil profiles of contrasting texture, in a well-studied pecan site to separate naturally formed "old" calcite and irrigation-induced "young" calcite and estimate the contribution of soil gas CO_2 from soil respiration, atmosphere and calcite precipitation. This study shows that loading of dissolved Ca and DIC facilitates the accumulation of pedogenic carbonate, especially in soils of finer texture. Irrigation-derived calcite and CO_2 were measurable in bulk soil carbonate and soil gases in these agricultural soils through carbon isotopes. This study clearly showed a great example how human activity is impacting C cycling in one of the largest biomes on Earth.

Table 3.1: Concentrations and C isotopic compositions of soil organic and inorganic carbon in two study soil profiles

Site	Depth (cm)	soil inorganic carbon wt %	soil organic carbon wt %	$d^{13}C_{CaCO3}$ ‰	$d^{13}C_{SOC}$ ‰	Site	Depth (cm)	soil inorganic carbon wt %	soil organic carbon wt %	$d^{13}C_{CaCO3}$ ‰	$d^{13}C_{SOC}$ ‰
Pecan_Fine						**Pecan_Coarse**					
P3_0_4	0	0.31	1.43	-4.3	-23.3	P4_0_10	0	0.41	1.56	-4.2	-24.5
P3_4_8	10	0.69	0.92	-4.6	-21.5	P4_10_20	10	0.52	0.63	-4.4	-22.8
P3_8_12	20	0.77	0.56	-4.8	-21.6	P4_20_30	20	0.43	0.37	-4.3	-22.8
P3_12_16	30	0.78	0.46	-4.7	-22.3	P4_30_40	30	0.40	0.29	-4.6	-22.4
P3_16_20	41	0.85	0.40	-5.1	-22.0	P4_40_50	40	0.22	0.19	-4.2	-22.6
P3_20-24	51	0.63	0.19	-4.6		P4_50_60	50	0.42	0.21	-5.2	
P3_24_28	61	0.73	0.43	-4.2		P4_60_70	60	0.38	0.15	-4.3	
P3_28_32	71	0.78	0.39	-4.1		P4_70_84	70	0.11	0.06	-4.2	
P3_32_36	81	0.69	0.54	-3.9		P4_84_90	84	0.20	0.13	-5.1	
P3_36_40	91	0.83	0.58	-3.6		P4_90_100	90	0.11	0.07	-4.5	
P3_40_44	102	0.80	0.62	-3.9		P4_100_110	100	0.11	0.10	-4.7	
P3_44_48	112	0.87	0.59	-3.6		P4_110_120	110	0.26	0.18	-5.5	
P3_48_52	122	0.84	0.65	-3.9		P4_120_130	120	0.66	0.34	-5.9	
P3_52_56	132	1.24	0.63	-5.0		P4_130_140	130	0.18	0.16	-5.6	
P3_56_60	142	1.05	0.22	-6.0		P4_140_150	140	0.25	0	-5.2	
P3_60_64	152	0.74	0.08	-5.0		P4_150_160	150	0.09	0	-4.6	
P3_64_68	163	0.97	0.13	-4.7		P4_160_170	160	0.12	0	-5.1	
P3_68_72	173	0.93	0.14	-4.7		P4_170_180	170	0.07	0	-4.1	
P3_72_76	183	0.66	0.19	-4.5		P4_180_190	180	0.09	0	-4.1	
P3_76_80	193	0.57	0.15	-3.9		P4_190_200	190	0.10	0	-4.3	
P3_80_84	203	0.55	0.08	-3.9		P4_200_210	200	0.07	0	-6.0	
P3_84_88	213	0.53	0.14	-3.7		P4_210_220	210	0.12	0	-4.5	
P3_88_92	224	0.33	0.49	-3.8		P4_220_230	220	0.17	0	-5.0	
P3_92_96	234	0.48	0.21	-3.7		P4_230_240	230	0.10	0	-4.7	
P3_96_100	244	0.48	0.12	-3.7		P4_240_250	240	0.10	0	-3.9	
P3_100_104	254	0.42	0.02	-3.7		P4_250_260	250	0.16	0	-4.9	
P3_104_108	264	0.39	0.12	-3.9							
P3_108_112	274	0.28	0	-4.0							
P3_112_116	284	0.24	0	-3.9							

Table 3.2: Concentrations and C isotopic compositions of soil gas CO_2 from two soil profiles.

Collection Date	Depth (cm)	pCO_2 (ppm)	$d^{13}C_{CO2}$ ‰	Collection Date	Depth (cm)	pCO_2 (ppm)	$d^{13}C_{CO2}$ ‰
Pecan_Fine				**Pecan_Coarse**			
5/2/14	15	3580	-18.7	5/1/15	15	506	-10.3
5/19/14	15	4323	-18.5	5/21/15	15	9924	-23.0
6/5/14	15	17775	-16.9	6/17/15	15	14571	-23.4
6/25/14	15	8358	-19.6	6/30/15	15	9259	-22.0
7/15/14	15	5983	-16.4	7/10/15	15	16770	-22.1
7/24/14	15	560		7/19/15	15	11096	-21.0
7/31/14	15	522		5/1/15	30	517	-10.1
8/14/14	15	494	-10.5	5/21/15	30	15743	-22.9
9/1/14	15	15552	-17.9	6/17/15	30	22812	-22.5
10/9/14	15	5711	-16.1	6/30/15	30	17917	-20.9
10/23/14	15	557		7/10/15	30	27746	-21.4
5/1/15	15	542		7/19/15	30	20332	-24.3
5/21/15	15	10948	-22.4	5/1/15	60	523	-10.7
6/17/15	15	23737	-20.0	5/21/15	60	34587	-20.0
6/30/15	15	7033	-17.7	6/17/15	60	44738	-20.5
7/10/15	15	23137	-19.8	6/30/15	60	498	-10.2
7/19/15	15	16165	-18.7	7/10/15	60	74073	-20.4
5/2/14	30	563		7/19/15	60	61453	-19.9
6/5/14	30	46091	-19.4	5/1/15	100	515	-10.4
6/25/14	30	20984	-18.3	6/30/15	100	481	-9.7
7/15/14	30	18248	-14.6				
7/24/14	30	19081	-19.8				
7/31/14	30	514	-11.6				
8/14/14	30	474	-10.4				
9/1/14	30	42744	-18.8				
10/9/14	30	15223	-18.8				
10/23/14	30	493	-10.6				
5/1/15	30	517	-10.3				
5/21/15	30	22147	-21.1				
6/17/15	30	38994	-21.1				
6/30/15	30	12255	-18.6				
7/10/15	30	1025					
7/19/15	30	26160	-18.4				
5/2/14	60	24851	-19.6				
5/19/14	60	35452					
6/5/14	60	4817	-19.4				
6/25/14	60	39093	-17.1				
7/15/14	60	2964	-18.2				
7/24/14	60	13484	-19.9				
7/31/14	60	488	-10.1				
8/14/14	60	488	-9.9				
9/1/14	60	62002	-18.5				
10/9/14	60	28464	-18.6				
10/23/14	60	507	-11.0				
5/1/15	60	501	-10.2				
5/21/15	60	30995	-19.4				
6/17/15	60	45312	-19.4				
6/30/15	60	515	-10.5				
7/10/15	60	50971	-19.0				
7/19/15	60	35512	-18.0				
5/1/15	100	496	-10.2				
5/21/15	100	26285	-20.4				
6/30/15	100	512	-12.0				
7/10/15	100	53279	-19.1				
7/19/15	100	57482	-18.2				

Table 3: Elemental and isotopic data for the water samples collected from this study

Type	Collection Date	Depth (cm)	$\delta^{13}C_{DIC}$ ‰	pH	EC (dS/m)	alkalinity (meq/L)	Na^{+} ppm	Ca^{2+} ppm	Mg^{2+} ppm	K^{+} ppm	Cl^{-} ppm	SO_4^{2-} ppm	calcite Saturation index
IRW_GW	4/17/15	WELL1	-10.5	7.38	3.77	5.3	474	310	65	61	887	658	0.6
IRW_GW	4/17/15	WELL2	-12.2	7.25	4.26	6.8	597	266	60	57	741	1051	0.4
IRW_RG	5/15/15		-10.4	7.70	1.87	3.5	325	43	13	67	340	333	0.0
IRW_RG	6/11/15		-6.6	8.10	1.02	3.7	126	39	11	60	118	192	0.5
IRW_RG	6/30/15		-6.3	8.00	0.90	3.5	115	36	10	57	91	159	0.3
IRW_RG	8/11/15		-6.5	7.91	0.88	3.7	102	56	8	9	93	155	0.3
IRW_RG	8/30/15		-7.2	7.90	0.96	3.4	56	98	16	12	96	169	0.4
IRW_RG	9/22/15		-6.8				28	92	15	11	103	170	

IRW_GW and IRW_RG: irrigation water, from groundwater and Rio Grande.

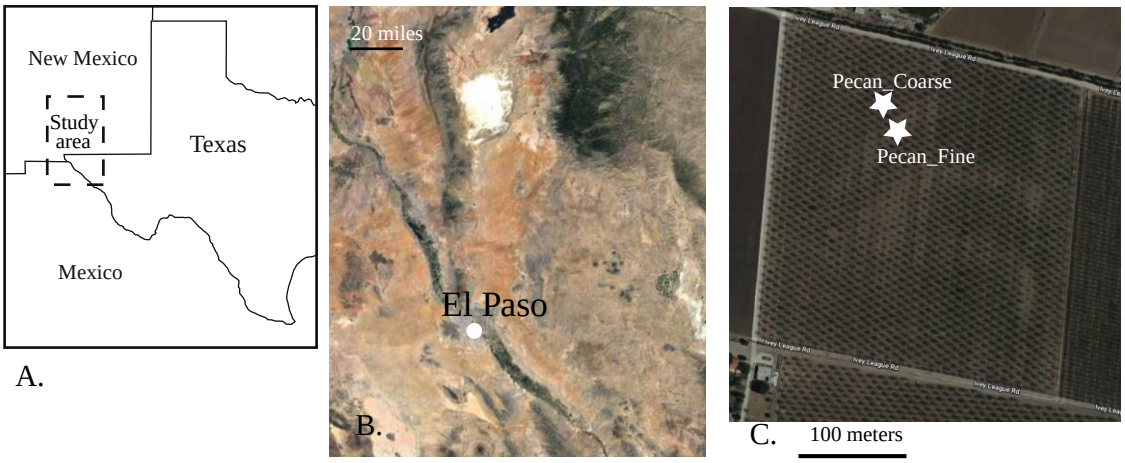

Figure 3.1. Location (A) and terrain (B) maps of study sites along the Rio Grande Valley. One agricultural site is selected on a pecan orchard near El Paso, TX. Within the pecan orchard, spatial heterogeneity in yield and canopy size is due to different soil texture and amount of salt buildup (C): sandy Pecan_Coarse and clayey Pecan_Fine.

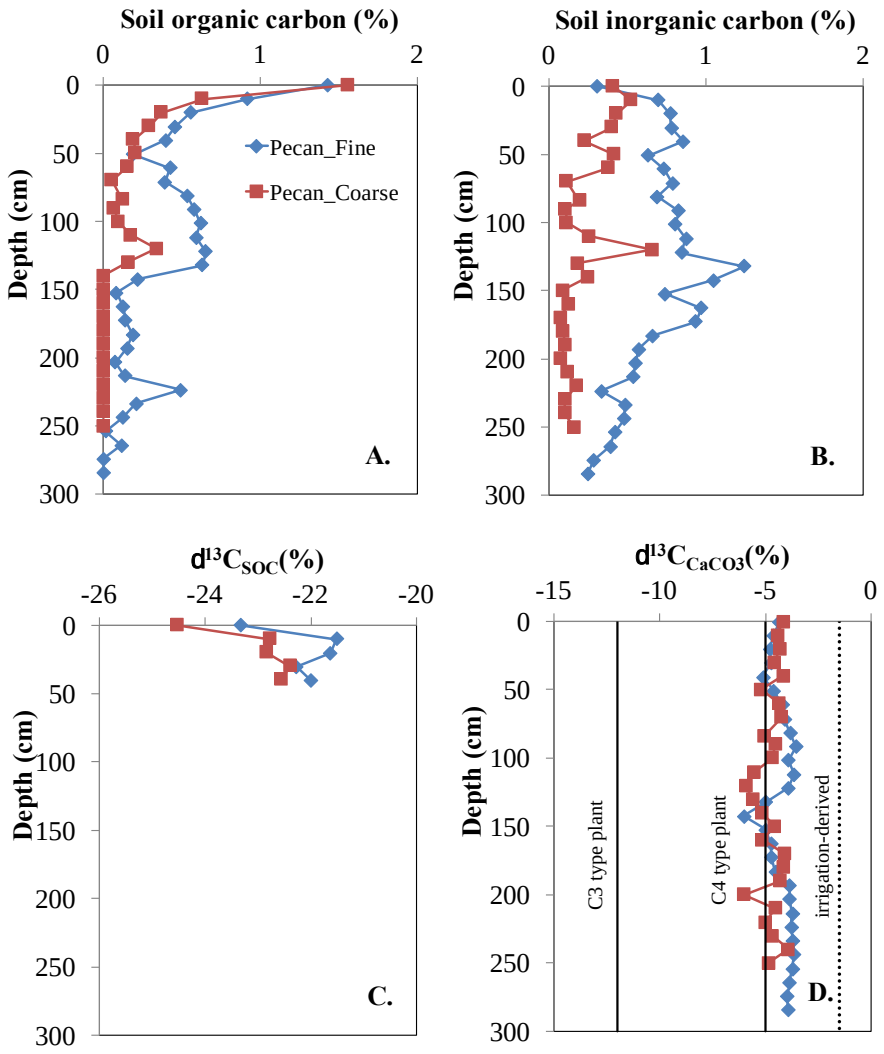

Figure 3.2. Depth profiles of soil organic carbon concentrations (A), soil inorganic carbon concentrations (B), and their C isotope compositions ($^{13}C_{SOC}$, C; $^{13}C_{CaCO3}$, D) at the Pecan_Fine and Pecan_Coarse sites. Vertical solid lines are $\delta^{13}C_{CaCO3}$ values at equilibrium with C3 vs. C4 types of vegetation, and dotted line is $\delta^{13}C_{CaCO3}$ of calcite at equilibrium with DIC in irrigation water. See text for details.

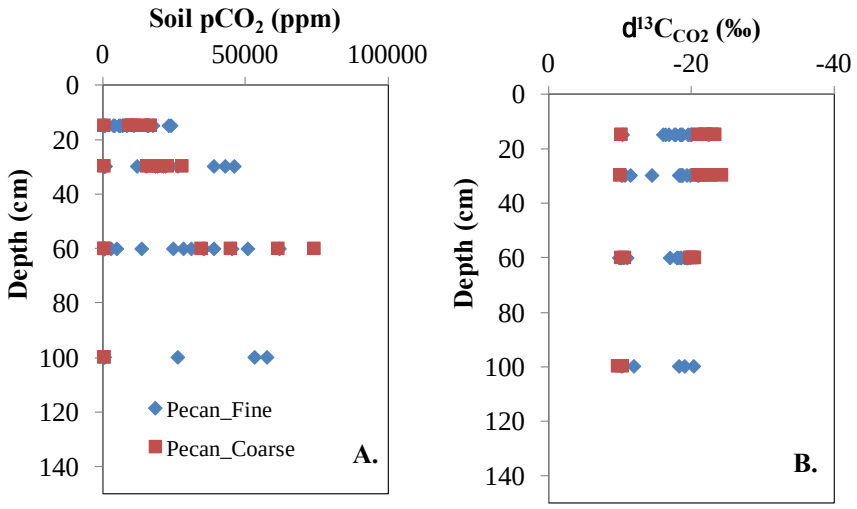

Figure 3.3: Depth profiles of soil pCO_2 concentrations (A) and isotopes ($^{13}C_{CO2}$, B) in soil gas samples from Pecan_Fine and Pecan_Coarse sites.

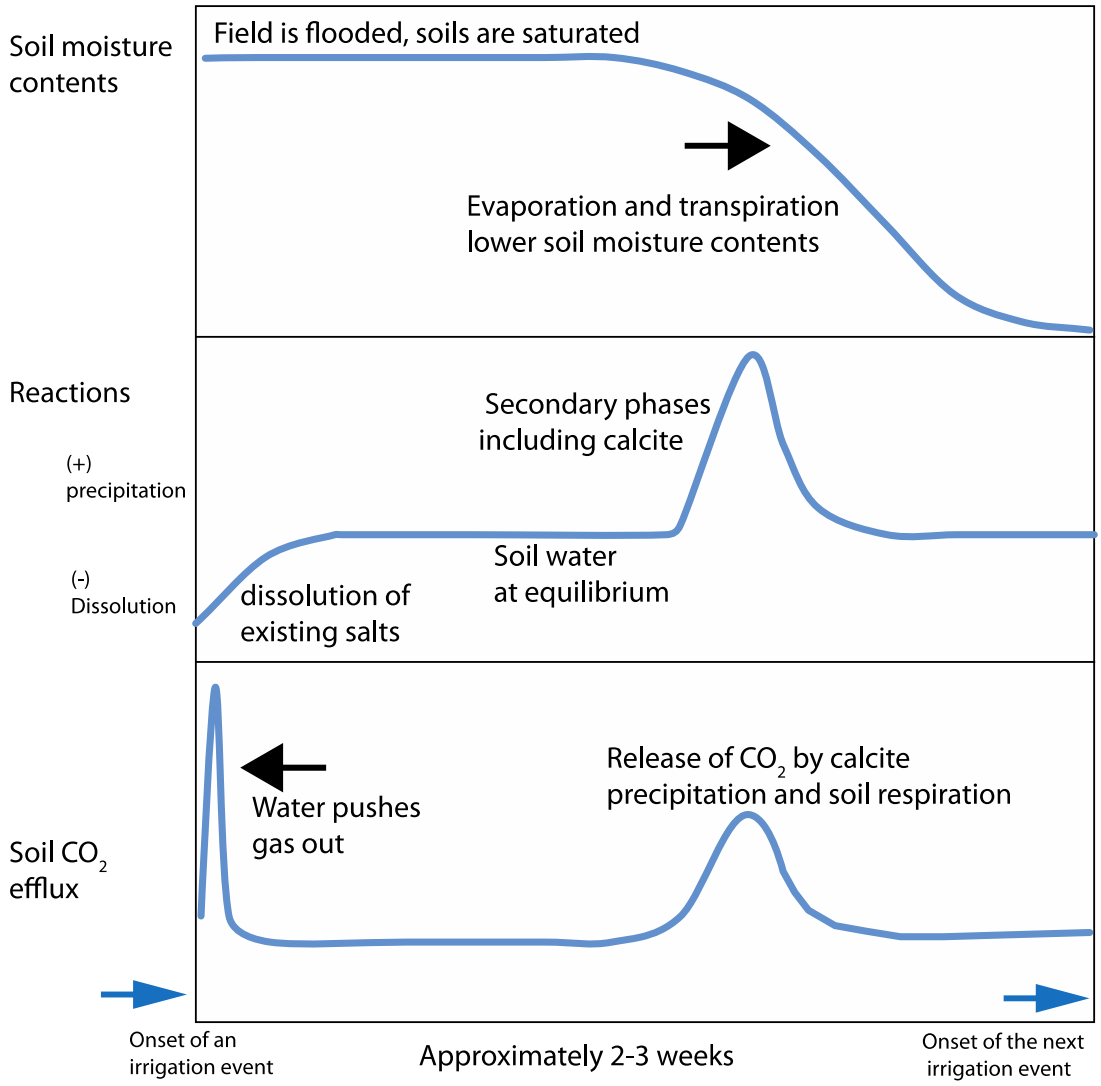

Figure 3.4: Conceptual models to illustrate the variation in soil moisture content induced by flood irrigation events in aridlands, and the accompanied chemical reactions and land-atmosphere gas exchange.

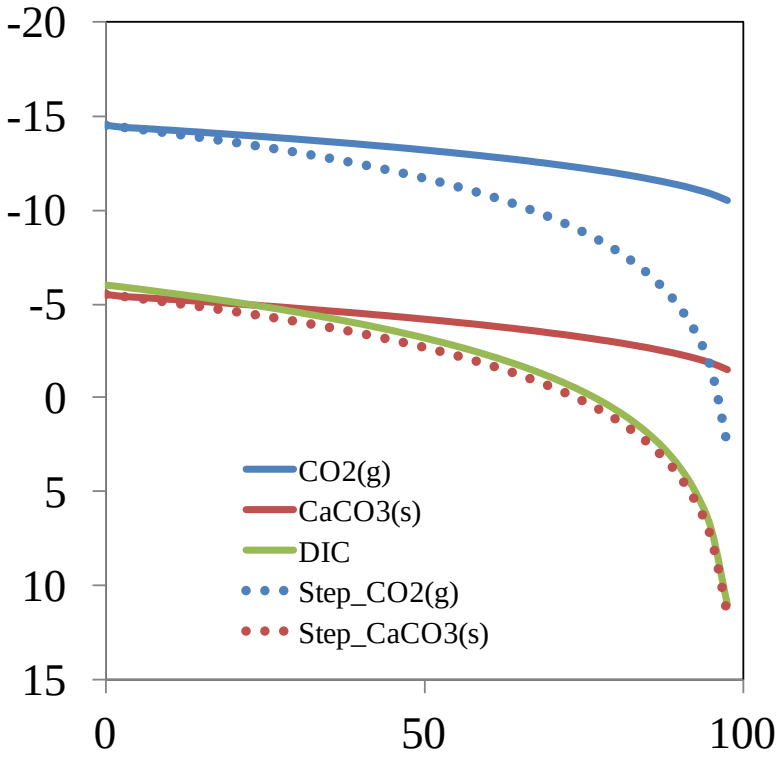

Figure 3.5. Evolution in $\delta^{13}C$ values of $CaCO_3$ and CO_2 as DIC and Ca^{2+} in an irrigation water slowly precipitates out according to Reaction 1, assuming Rayleigh fractionation. Isotopic composition for each species is plotted as dotted lines for each step or as solid lines accumulatively. Initial $\delta^{13}C_{CaCO3}$ is -6‰. When all DIC is converted to calcite and CO_2, the carbon isotopes of these endmembers are derived ($\delta^{13}C_{CaCO3}$ = -1.5‰; $\delta^{13}C_{CO2}$ = -10.5‰).

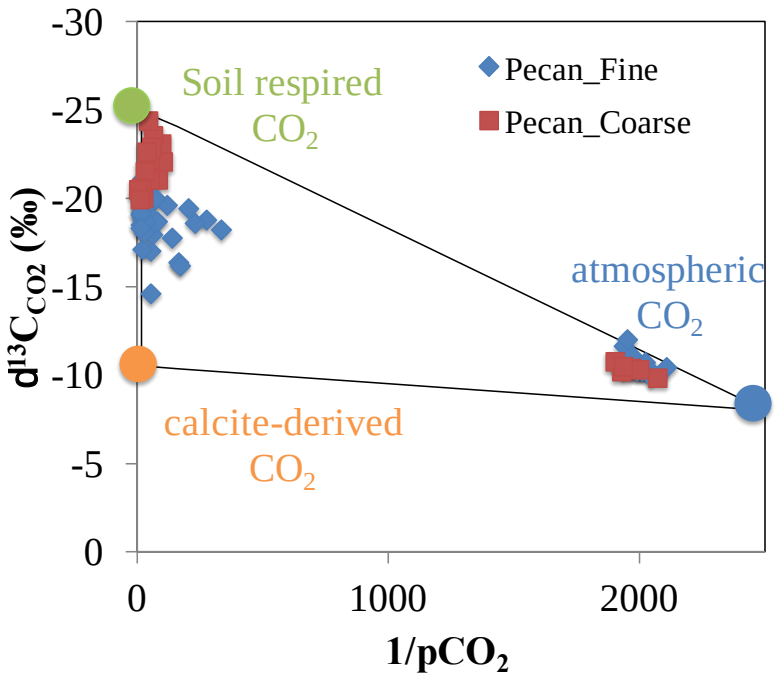

Figure 3.6. Keeling plot shows soil CO_2 is contributed by three end-member mixing (atmospheric, soil respired and calcite-derived) in two soil profiles. Pecan_Fine has finer soil texture and higher calcite content than Pecan_Coarse, and soil CO_2 in pecan_Fine receives more calcite-derived CO_2 contribution. Pecan_Corase soils support bigger trees and receive more soil respired CO_2.

REFERENCES:

Alling, V., Porcelli, D., Morth, C.-M. et al. (2012) Degradation of terrestrial organic carbon, primary production and out-gassing of CO_2 in Laptev and East Siberian Seas as inferred from $\delta^{13}C$ values of DIC. Geochimica et Cosmochimica Acta 95, 143-159.

Amundson, R.G., Chadwick, O.A., Sowers, J.M., and Doner, H.E. (1988) Relationship between climate and vegetation and the stable carbon isotope chemistry of soils in the eastern Mojave Desert, Nevada. *Quaternary Research* 29, 245-254.

Amundson, R.G., Chadwick, O.A., Sowers, J.M., and Doner, H.E. (1989) The stable isotope chemistry of pedogenic carbonates at Kyle Canyon, Nevada. *Soil Science Society of America Journal* 53, 201-210.

Breecker, D.O, Sharp, Z.D., McFadden, L.D. (2009) Seasonal bias in the formation and stable isotopic composition of pedogenic carbonate in modern soils from central New Mexico, USA. *Geological Society of America Bulletin* 121, 630-640.

Capo, R.C. and Chadwick, O.A. (1999) Sources of strontium and calcium in desert soil and calcrete. *Earth and Planetary Letters* 170, 61-72.

Cerling, T.E. (1984) The stable isotopic composition of modern soil carbonate and its relationship to climate. *Earth and Planetary Sciences Letters* 71, 229-240.

Cerling, T.E. and Quade, J. (1993) Stable carbon and oxygen isotopes in soil carbonates. In: Swart, P., Lohmann, K.C., McKenzie, J.A., Savin, S.M. (Eds.), Climate Change in Continental Isotopic Records. American Geophysical Union Geophysical Monograph,Washington, D.C., pp. 217–231.

Cerling, T.E., Wang, Y. and Quade, J. (1993) Expansion of C4 ecosystems as an indicator of global ecological change in the late Miocene. *Nature* 261, 344-345.

Chiquet, A., Michard, A., Nahon, D. and Hamelin, B. (1999) Atmospheric input vs in situ weathering in the genesis of calcretes: An Sr isotope study at Galvez (Central Spain). *Geochimica et Coscochimica Acta* 63, 311-323.

Clark, I. and Fritz, P. (1997) Environmental Isotopes in Hydrogeology. CRC Press.

Cox, C., Jin, L., Ganjegunte, G., Borrok, D., Lougheed, V., and Ma, L. (2018) Changes of soil quality due to flood irrigation in agricultural fields along the Rio Grande in western Texas. *Applied Geochemistry* 90, 87-100, doi.org/10.1016/j.apgeochem.2017.12.019.

Darrouzet-Nardi, A., Reed, S., Grote, E. and Belnap, J. (2015) Observations of net soil exchange of CO2 in a dryland show experimental warming increases carbon losses in biocrust soils. *Biogeochemistry* 1-16.

Dart, R.C., Barovich, K.M., Chittleborough, D.J., Hill, S.M. (2007) Calcium in regolith carbonates of central and southern Australia: Its srouce and implications for the global carbon cycle. *Palaeogeography, Palaeoclimatology, Palaeloecology*, 249, 322-334.

Davidson, E.A., Belk, E. and Boone, R.D. (1998) Soil water content and temperature as independent or confounded factors controlling soil respiration in a temperate mixed hardwood forest. *Glob. Change Biol.* 4(2), 217-227.

Eghbal, M.K. and Southard, R.J. (1993) Stratigraphy and genesis of Durorthids and Haplargids on dissected alluvial fans, western Mojave Desert, California. *Geoderma* 59, 151-174.

Ehleringer J.R., Sage R.F., Flanagan L.B. and Pearcy R.W. (1991) Climate change and the evolution of C4 photosynthesis. *Trends in Ecology and Evolution* 6, 95-99.

Friedli H., Lotscher H., Oeschger H., Siegenthaler U. and Stauffer B. (1986) Ice core record of the 13C/12C ratio of atmospheric CO_2 in the past two centuries. *Nature* 324, 237-238.

Ganjegunte, G.K., Sheng, Z. and Clark, J. (2012) Soil salinity and sodicity appraisal by electromagnetic induction in soils irrigated to grow cotton, Land Degradation and Development. DOI: 10.1002/ldr.1162.Gieskes and Rogers, 1973;

Gile, L.H. (1961). A classification of ca horizons in the soils of a desert region, Dona Ana County, New Mexico. *Soil Science Society of America Proceedings* 25, 52–61.

Gile, L.H. and Grossman, R.B. (1979) The Desert Project soil monograph: Soils and landscapes of a desert region astride the Rio Grande Valley near Las Cruces, New Mexico. Lincoln, NE: U.S. Department of Agriculture, Soil Conservation Service.

Gile, L.H., Hawley, J.W. and Grossman, R.B. (1981) Soils and geomorphology in the basin and range area of southern New Mexico— Guidebook to the Desert Project. Memoir 39. New Mexico Bur. Of Mines and Miner. Res., Socorro, NM.

Hannam, K.D., Kehila, D., Millard, Midwood, A.J., Neilsen, D., Neilsen, G.H., Forge, T.A., Nichol, C., and Jone, M.D. (2016) Bicarbonates in irrigation water contribute to carbonate formation and CO_2 production in orchard soils under drip irrigation. Geoderma 266, 120-126.

Hasenmueller, E.A., Jin, L., Stinchcomb, G.E., Lin, H., Brantley, S.L. and Kaye, J.P. (2015) Topographic controls on the depth distribution of soil CO_2 in a small temperate watershed. *Applied Geochemistry* 63, 58-69.

Hogan, F.M., Phillips, F.M., Mills, S.K., Hendrickx, J.M.H., Ruiz, J., Chesley, J.T., Asmerom, Y. (2007) Geologic origins of salinization in semi-arid river: the role of sedimentary basin brines. *Geology* 35, 1063–1066.

Jafari, H., Raeisi, E., Hoehn, E., Zare, M. (2012) Hydrochemical characteristics of irrigation return flow in semi-arid regions of Iran. *Hydrol. Sci. J.* 57, 173–185.

Jin, L., Williams, E., Szramek, K., Walter, L. M. and Hamilton, S. K. (2008) Silicate and carbonate mineral weathering in soil profiles developed on Pleistocene glacial drift (Michigan, USA): Mass balances based on soil water geochemistry. *Geochimica et Cosmochimica Acta* 72, 1027-1042.

Jin, L., Ogrinc, N., Yesavage, T., Hasenmueller, E.A., Ma, L., Sullivan, P.L., Kaye, J., Duffy, C., and Brantley, S.L. (2014) The CO_2 consumption potential during gray shale weathering: Insights from the evolution of carbon isotopes in the Susquehanna Shale Hills critical zone observatory. *Geochimica et Cosmochimica Acta* 142, 260-280.

Jin, L., Ogrinc, N., Hamilton, S.K., Szramek, K., Kanduc, T. and Walter, L.M. (2009) Inorganic carbon isotope systematics in soil profiles undergoing silicate and carbonate weathering (Southern Michigan, USA). *Chemical Geology* 264, 139-153.

Karim, A. and Veizer, J. (2000) Weathering processes in the Indus River Basin: implications from riverine carbon, sulfur, oxygen and strontium isotopes. *Chemical Geology* 170, 153-177.

Kempe, S., Pettine, M., and Cauwet, G. (1991) Biogeochemistry of European rivers. In Biogeochemistry of Major World Rivers (eds. S. Kempe, E. T. Degens, J. E. Richey). John Wiley & Sons, New York, SCOPE/UNEP 42, 169–211.

Knuteson, J.A., Richardson, J.L., Patterson, D.D. and Prunty, L. (1989) Pedogenic carbonates in a Calciaquoll associated with a recharge wetland. Soil Sci. Soc. Am. J. 53, 495-499.

Kraimer, R.A. and Monger, H.C. (2009) Carbon isotopic subsets of soil carbonate- A particle size comparison of limestone and igneous parent materials. *Geoderma* 150, 1-9.

Ku, T.C.W. (2001) Organic carbon–mineral interactions in near surface environments: implications for the global carbon cycles. Ph.D. Dissertation, University of Michigan, Ann Arbor, MI.

Lal, R. and Kimble, J.M. (2000) Pedogenic carbonates and the global carbon cycle. In: Lal, R., Kimble, J.M., Eswaran, H., Stewart, B.A. (eds.), Global Climate Change and Pedogenic Carbonates, 1-14.

Lal, R. (2004) Soil carbon sequestration to mitigate climate change. *Geoderma* 123 (1-2), 1-22.

Landi, A., Mermut, A.R., Anderson, D.W. (2003) Origin and rate of pedogenic carbonate accumulation in Saskatchewan soils, Canada. *Geoderma* 117, 143-156.

Lorah, M.M. and Herman, J.S. (1988) The chemical evolution of a travertine-depositing stream: geochemical processes and a mass transfer reaction. *Water Resources Research* 24, 1541–1552.

Machete, M.N. (1985) Calcic soils of the southwestern United States, in Weide, D., edit, Soils and Quaternary geology of the southwestern United States. *Geological Society of America Special Paper* **203**, 1-21.

McFadden, L.D. and Tinsley, J.C. (1985) Rate and depth of pedogenic carbonate accumulation in soils: formation and testing of a compartment model. In (Eds.Weide, D.L.) *Geological Society of America special paper* 203, 23-42.

Miyamoto, S. (2000) Soil Resources of El Paso: Characteristics, distribution and management guidelines. Texas Agricultural Experiment Station Bulletin.

Monger, H.C., Cole, D.R., Buck, B.J. and Gallegos, R.A. (2009) Scale and the isotopic record of C4 plants in pedogenic carbonate: from the biome to the rhizosphere." Ecology 90, 1498-1511.

Monger, H. C. and Gallegos, R. A. (2000) In: Global Climate Change and Pedogenic Carbonates (eds R. Lal, J. M. Kimble, H. Eswaran and B. A. Stewart). Lewis Publishers, Boca Raton, FL, 273–289.

Montanez, I.P. (2013) Modern soil system constraints on reconstructing deep-time atmospheric CO_2. *Geochim. Cosmochim. Acta* 101, 57-75.

Naiman, Z., Quade, J. and Patchett, P.J. (2000) Isotopic evidence for eolian recycling of pedogenic carbonate and variations in carbonate dust sources throughout the southwest United States. *Geochim. Cosmochim. Acta* 64, 3099–3109.

Nyachoti, S., Jin, L., Tweedie, C.E. and Ma, L. (2017) Formation of pedogenic carbonates in the semi-arid Rio Grande valley: insights from carbon, major elements, and U-series isotopes in natural and agricultural soils of southern New Mexico and western Texas. *Chemical Geology*, doi.org/10.1016/j.chemgeo.2017.10.014.

Ortiz, A. Ganjegunte, G.K. and Jin, L. (2018) Physical and chemical controls of salt movement and accumulation in natural versus irrigated drylands.

Quade, J., Cerling, T.E. and Bowman, J.R. (1989) Systematic variations in the carbon and oxygen isotopic composition of pedogenic carbonate along elevation transects in the southern Great Basin, United States. *Geological Society of America Bulletin* 101, 464-375.

Quade, J., Chivas, A.R., McCulloch, M.T. (1995) Stronsium and carbon isotope tracers and the origins of soil carbonate in southern Australia and Victoria. *Palaeogeography, Palaeloclimatology, Palaeloecology* 113, 103-117.

Quade, J., Solounias, N, Cerling, T.E. (1994) Stable isotopic evidence from paleosol carbonates and fossil teeth in Greece for forest or woodlands over the past 11 Ma. *Palaeogeography, Palaeloclimatology, Palaeloecology*, 108, 41-53.

Rath, K. and Rousk, J. (2015) Salt effects on the soil microbial decomposer community and their role in organic carbon cycling: a review. *Soil Biology and Biochemistry* 81, 108-123. http://dx.doi.org/10.1016/j.soilbio.2014.11.001

Reardon, E.J., Mozeto, A.A. and Fritz, P. (1980) Recharge in northern clime calcareous sandy soils: chemical and carbon-14 evolution. *Geochimica et Cosmochimica Acta* 44, 1723–1735.

Retallack, G.J. (2005) Pedogenic carbonate proxies for amount and seasonality of precipitation in paleosols. *Geology* 33, 333-336.

Rowe, P.J. and Maher, B.A. (2000) 'Cold' stage formation of calcrete nodules in the Chinese Loess Plateau: evidence from U-series dating and stable isotope analysis. *Palaeogeography, Palaeoclimatology, Palaeoecology*, 157, 109-125.

Sanderman, J. (2012) Can management induced changes in the carbonate system drive soil carbon sequestration? A review with particular focus on Australia. *Agriculture, Ecosystems and environment* 155, 70-77.

Schlesinger, W.H. (1982) Carbon storage in the caliche of arid soils: a case study from Arizona. *Soil Science* 133, 247-255.

Schlesinger, W.H. (2000) Carbon sequestration in soils: some cautions amidst optimism. *Agriculture, Ecosystems and Environment* 82, 121-127.

Schoups, G., Hopmans, J.W., Young, C.A., Vrugt, J.A., Wanllender, W.W. and Tanji, K.K. (2005) Sustainability of irrigated agriculture in the San Joaquin Valley, California. Proc.

Serna-Perez, A., Monger, H.C., Herrick, J.E., and Murray, L. (2006). Carbon dioxide emissions from exhumed petrocalcic horizons. *Soil Science Society of America Journal* 70, 795–805.

Serrano-Ortiz, P., Roland, M., Sanchez-Moral, S., JanssenS, I.A., Domingo, F., Goddéris, Y. and Kowalski, A.S. (2010), Hidden, abiotic CO_2 flows and gaseous reservoirs in the terrestrial carbon cycle: Review and perspectives. *Agricultural and Forest Meteorology* 150 (3), 321-329.

Sheldon, N.D. and Tabor, N.J. (2009) Quantitative paleoenvironmental and paleoclimatic reconstruction using paleosols. *Earth Science Reviews* 95, 1-52.

Sheta, A.S., Al-Sewailem, M.S., Sallam, A. Sh., Al-Mashhady, A.S. (2000) Nature and composition of newly formed precipitates in relationship to characteristics of groundwater in arid environment. *Arid Soil Res. Rehabil.* 14, 387–401.

Suarez, D. L. (2000) Impact of Agriculture on CO_2 as Affected by Changes in Inorganic Carbon', in Lal, R., Kimble, J. M., Eswaran, H., and Stewart, B. A. (eds.), Global Climate Change and Pedogenic Carbonates, CRC/Lewis Publishers, Boca Raton, FL, pp. 257–272.

Singh, S.K., Sarin, M.M. and France-Lanord, C. (2005) Chemical erosion in eastern Himalaya: Major ion composition of the Brahmaputra and $\delta^{13}C$ of dissolved inorganic carbon. *Geochimica et Cosmochimica Acta* 69, 3573-3588.

Szynkiewicz, A., Borrok, D., Ganjegunte, G., Skrzypek, G., Ma, L., Rearick, M., Perkins, G. (2015) Isotopic studies of the Upper and Middle Rio Grande. Part 2 -Salt loads and human impacts in south New Mexico and west Texas. To appear in Chemical Geology. *Chemical Geology* 411, 336-350.

Stumm, W., and Morgan, J.J. (1996) Aquatic Chemistry (3rd ed.). Wiley-Interscience, New York.

Szramek, K., McIntosh, J.C., Williams, E.L., Kanduc, T., Ogrinc, N., Walter, L.M. (2007) Relative weathering intensity of calcite vs. dolomite in carbonate-bearing temperate zone watersheds: carbonate geochemistry and fluxes from catchments within the St. Lawrence

and Danube River Basin. Geochemistry, Geophysics, and Geosystems 8, Q04002, doi: 10.1029/2006GC001337.

Tang, J., Misson, L., Gershenson, A., Cheng, W. and Goldstein, A.H. (2005) Continuous measurements of soil respiration with and without roots in a ponderosa pine plantation in the Sierra Nevada Mountains. *Agricultural and Forest Meteorology* 132, 212-227.

Tabor, N.J., 2007. Permo-Pennsylvanian palaeotemperatures from Fe-Oxide and phyllosilicate $\delta^{18}O$ values. *Earth Planetary Science Letters* 253, 159–171.

Trumbore, S.E., Chadwick, O.A. and Amundson, R. (1996) Rapid exchange between soil carbon and atmospheric carbon dioxide driven by temperature change. *Science* 272 (5260), 393-396.

Van der Hoven, S.J. and Quade, J. (2002) Tracing spatial and temporal variations in the sources of calcium in pedogenic carbonates in a semiarid environment. *Geoderma* 108, 259-276.

Violette, A., Riotte, J., Braun, J., Oliva, P., Marechal, J., Sekhar, M., Jeandel, C., Subramanian, S., Prunier, J., Barbiero, L. and Dupre, B. (2010) Formation and preservation of pedogenic carbonates in Southern Indian, links with paleo-monsoon and pedological conditions: Clues from Sr isotopes, U-Th series and REEs. *Geochimica et Cosmochimica Acta* 74, 7059-7085.

Vogel J.C. (1993) Variability of carbon isotope fractionation during photosynthesis. In: J.R. Ehleringer, A.E. Hall and G.D. Farquhar (eds.) Stable Isotopes and plant Carbon-Water Relations, Academic Press, San Diego, CA: 29-38.

Weems, S.L. and Monger, H.C. (2012) Banded vegetation-dune formation in the Medieval Warm Period and 20th Century, Chihuahuan Desert, New Mexico, USA. *Ecosphere* 3(3), Article 21 www.esajournals.org.

Whipkey, C.E., Capo, R.C., Chadwick, O.A., Stewart, B.W. (2000) The important of sea spray to the cation budget of a coastal Hawaiian soil: a strontium isotope approach. *Chemical Geology* 168, 37-48.

Yang C., Telmer K. and Veizer J. (1996) Chemical dynamic of the "St. Lawrence" riverine system: δD_{H2O}, $\delta^{18}O_{H2O}$, $\delta^{13}C_{DIC}$, $\delta^{34}S_{sulfate}$, and dissolved $^{87}Sr/^{86}Sr$. *Geochimica et Cosmochimica Acta* 60, 851-866.

Zamanian, K., Pustovoytov, K. and Kuzyakov, Y. (2016) Pedogenic carbonates: Forms and formation processes. *Earth-Science Reviews* 157, 1–17.

Chapter 4: Relative proportion of natural versus irrigation-induced pedogenic carbonate in agricultural soils along the Rio Grande valley, Southwestern US (Part 2): $^{87}Sr/^{86}Sr$ ratios as a Ca tracer

1. INTRODUCTION: NATURAL AND ANTHROPOGENIC CALCIUM SOURCES IN PEDOGENIC CARBONATES

Pedogenic carbonates, specifically calcite ($CaCO_3$), commonly form in hot drylands because of high evapotranspiration rates and its oversaturation in soil water (e.g., Van der Hoven and Quade 2002; Gocke et al., 2016; Zamanian et al., 2016). Pedogenic carbonates naturally form in regions of water scarcity, generally with less than 100 cm of annual rainfall and evapotranspiration exceeding rainfall (Jenney 1980; Birkeland 1984). The natural accumulation of pedogenic carbonates occurs when soil water becomes oversaturated in respect to calcite (e.g., Cerling and Quade 1993; Milliere et al., 2011):

$$Ca^{+2}_{(aq)} + 2HCO^{-}_{3(aq)} \leftrightarrow CaCO_{3(s)} + CO_{2(g)} + H_2O_{(l)} \quad \text{Reaction (4.1)}$$

Available Ca^{2+} for natural calcite precipitation includes endogenous mineral dissolution and surficial additions through wet and dry depositions (Capo & Chadwick, 1999; Hoven & Quade, 2002; Naiman, Quade, & Patchett, 2000). According to Van der Hoven and Quade (2002), in desert soils of New Mexico, USA, one of the common sources of Ca^{2+} in desert soil is atmospheric dust, with minor contribution from weathering of parent materials.

Agriculture has become increasingly popular in arid and semi-arid environments due to the increasing food demand and growing populations (Assouline et al., 2015; Battle-Aguilar et al., 2011). With limited rainfall and high evapotranspiration, irrigation becomes a critical practice, loading Ca and promoting precipitation of secondary calcite and other salts to soils (Cox et al., 2018; Falasca et al., 2014; Squires and Glenn, 2004). Eshel et al. (2007) observed that agriculture with treated effluent had higher Ca concentrations and significantly increased pedogenic carbonate

precipitation rates in comparison to irrigation with freshwaters. Typical changes to soils such as salinization are general as result of heavy cultivation that diminishes permeability, and osmotic potential among others (Cabot et al., 2014; Choudhary et al., 2004; Cox et al., 2018).

In this study, we aim to determine if agricultural practices have enhanced pedogenic carbonate precipitation by comparing and contrasting two cultivated arid-land soil sites and two natural soil sites in west Texas and south New Mexico. The focus is to identify whether the secondary calcites in soils are predominantly human-induced (Ca from irrigation and soil amendments) or naturally formed (Ca from dust, wet and dry deposition, or bedrock weathering). If the calcite in the system is human-induced, then the impacts of land-management practices such as flood-irrigation are substantial; further establishing that enhancement of secondary mineral precipitation is continuous and overshadows natural processes (Eshel et al 2007). Not only would the enhanced precipitation of calcite deteriorate soil quality and reduce water infiltration rates, as hardpan forms in natural arid-lands, but it could decrease the amount of soil organic carbon (SOC) (Rath and Rousk 2015; Seita et al. 2013; Wong et al 2009), while increasing the amount of inorganic-sourced CO_2 (Reaction 4.1).

Isotopic composition of Strontium ($^{87}Sr/^{86}Sr$) has been traditionally used to determine Ca sources, because Sr^{2+} can substitute Ca^{2+} in mineral structures (e.g., Capo et al., 1998; Capo and Chadwick 1999; Van der Hoven and Quade 2002). For example, Ca-minerals dissolve or precipitate with Sr and $^{87}Sr/^{86}Sr$ can be used to identify provenance of Sr and Ca in a system (Capo and Chadwick 1999). Sr isotope ratios have been applied to quantify the contribution of different Ca endmembers, such as dust and parent materials in soil formation (Li et al., 2016) or soil source lithology, groundwater flow paths and interactions with bedrock, mixing of stream waters, and plant-soil-water interactions (Saskia et al., 2018). Here, we used $^{87}Sr/^{86}Sr$ ratios to determine the

natural or agricultural proportion of Ca inputs into pedogenic carbonates in dryland soils of west Texas and south New Mexico.

2. Study Sites: Rio Grande Valley and Jornada Basin

The American southwest is considered arid-land. The far west Texas region of El Paso, is water deficient, with annual rainfall <25cm and annual potential evapotranspiration ~170-180cm (Scanlon et al., 2005). The Rio Grande in the U.S. southwest is a major source of irrigation water that makes agriculture possible along the Rio Grande valley as it flows from Colorado to New Mexico and Texas, which then become the international border between United States and Mexico. Agricultural areas in the middle Rio Grande Basin include Albuquerque, Hatch, and Las Cruces in New Mexico and El Paso, Canutillo, Fabens, and Tornillo in Texas. Rio Grande river is dammed at Elephant Butte in New Mexico, to regulate waters for irrigation use. Previous works have observed an increase in total dissolved solids (TDS) as the water flows downstream, due to natural geological upwelling and point-source additions from farmlands and from municipal wastewater-treatment plants (Phillips et al., 2003; Hogan et al., 2007; Williams et al 2013; Szynkiewicz et al., 2015).

Pecan (*Carya illinoinensis*), pima cotton (*Gossypium barbadense*) and alfalfa (*Medicago spp.*) are popular crops in the Rio Grande valley, as they are salt tolerant. Although high in TDS, the Rio Grande remains a major freshwater source of irrigation in the Rio Grande Basin. Typically, the agricultural fields are flooded multiple times during the growing season. Such flood irrigation is low in infrastructural cost, but it is demanding and inefficient in water usage (i.e. river and groundwaters) and leads to salt deposition (Ganjugante et al., 2015; Cox et al., 2018; Ortiz et al., 2019). Soil salinization has been documented broadly, both globally and locally, as a combination of poor land management, continuous irrigation, low water quality, and limited water drainage in

dryland agricultural sites as in U.S drylands (Falasca et al., 2014; Cox et al 2018; Ortiz et al., 2018; Qi et al., 2018).

Secondary calcite precipitation, according to Reaction 4.1, has been observed in previous work (Ortiz et al., 2018). The Rio Grande waters are oversaturated with respect to calcite, near saturation for gypsum and under-saturated with respect to halite (Szynkiewicz et al., 2015; Cox et al., 2018; Ortiz et al., 2018). Continuous evaporation and transpiration after irrigation drive calcite to oversaturation in the standing water on the fields, yielding calcite powders and nodules after drying (Nyachoti et al., 2017; Ortiz et al., 2018). Locally, anthropogenic sources of Ca^{2+} include the waters used for irrigation and soil amendments such as fertilizers. Previous work in the El Paso region along the Rio Grande, had reported higher calcite accumulation rates with younger calcite ages in agricultural sites than in the natural sites (Cox et al., 2018; Ortiz et al., 2019; Nyachoti et al., 2017). Although the agricultural sites reported by Nyachoti et al. (2017), Cox et al (2017) and in this study were only cultivated for approximately 90 years, U-series isotopic dating of these calcite samples ranges ~2.2 ± 1.7 ka and are presumably a mixture of older, natural calcite and much younger or modern calcite that formed at elevated rates with irrigation (Nyachoti et al., 2017; Eshel et al. (2007).

One natural regional aridland site that has been commonly studied was located in La Mesa geomorphic surface within Jornada Experimental Range (JER) near Las Cruces, New Mexico. This surface overlies fluvial sediments that were deposited between 5 and 0.8 Ma, when the ancestral Rio Grande ran through the Jornada Basin (Gile et al., 1981; Mack et al., 2006; 2012). Fluvial sediments underlying La Mesa surface belong to mainly the Camp Rice Formation consisting of materials ranging from conglomerate to mudstones derived from upstream (Mack et al., 1993). The La Mesa geomorphic surface occurs on an alluvial plain, which is heavily wind

eroded indicating deflation and depositional features oriented in the prevailing west-southwest wind direction (Monger et al., 2006). The geomorphic surface is estimated to be of late Pliocene to middle Pleistocene in age (Gile et al., 1981; Gile, 2002); its soils that contain stage-V pedogenic carbonates are estimated to be about 1.6 Ma (Mack et al., 1993; 1996). The Camp Rice Formation constitutes the parent material of soils at the La Mesa geomorphic surface (Mack et al., 1993). Similar to soil petrocalcic horizons on the Upper and Lower La Mesa geomorphic surface at the Mesilla Basin, these mature carbonates have been associated to wet and dry atmospheric deposition processes since fluvial Camp Rice Formation sediments contain minimal carbonates (<1% $CaCO_3$) (Gile et al., 1981; Capo and Chadwick, 1999).

3. METHODS

3.1. Soil collection

This study focused on two natural and two agricultural sites. Both agricultural sites are located in the far west El Paso County in Texas: a highly-managed pecan orchard in Tornillo, and one slightly less-managed alfalfa field in El Paso (Figure 4.1). These two sites have been previously studied for salt buildup and are introduced in great details in Ortiz et al. (2018). This pecan field has been cultivated for approximately 80 years, with pecan for the last 50 years and cotton for 30 years prior. The pecan orchard, is regularly fertilized, sprayed with pesticides and amended by sulfur and gypsum pellets among others (Ortiz et al., 2018a). At the pecan orchard, two soil cores of 250 cm and 300 cm had been collected at 10 cm increment resolution, with contrasting texture: Pecan_Fine and Pecan_Coarse (Figure 4.1). Pecan_Fine soils have a layer of clayey soils around 100-150 cm and have much higher soil salinity and sodicity than the sandy Pecan_Coarse soils (Ortiz et al., 2018a). These two soil profiles are less than 40 m apart and undergo the same soil amendments and irrigation schedule. However, the Pecan_Fine and

Pecan_Coarse soils are characterized by visually distinct pecan growth, mainly due to different amounts of salt buildup (Ortiz et al., 2018a). A 60-cm deep soil core was previously collected and characterized in an alfalfa field by Cox et al. (2018) (as Alfalfa) and Ortiz et al. (2018a) (as Alfalfa_Fine_D) in El Paso, Texas. These soils are silty clay loam alluvium of Harkey-age (NRCS Custom Soil Report). The alfalfa site is less managed: it undergoes fallow years when irrigation water is insufficient and has no history of soil amendments or fertilization. Both pecan and alfalfa soils are flood-irrigated with Rio Grande waters, whereas local groundwaters are used only for the pecan orchard.

Two natural sites of different soil ages are selected for comparison. A 110-cm core was augured at a Chihuahuan Desert scrub rangeland outside of Fabens, Texas and studied for soil salinity and dust deposition (Ortiz et al., 2018a). This natural site is dominated by honey mesquite (*Prosopis glandulosa)* and creosote bush (*Larrea tridentata),* localized sand dunes are also common to the area as a result of eolian deposits and its sediments are wind modified sandy alluvium, surrounded by Pleistocene-age soils (NRC Custom Soil Report). A soil profile in a pre-excavated trench was sampled at La Mesa geomorphic surface within the JER (Nychoti, 2016). The topsoil consists of unconsolidated sandy-loamy sediments, which are underlain by stage-V pedogenic carbonates (Robins et al., 2015). The boundary of the topsoil and petrocalcic layer is irregular. The sharp boundary is characterized by brittle to massively indurated, smooth micritic carbonate laminae (Robins et al., 2015). Previous studies have shown that the hard pan underlying the young alluvium in the JER show evidence of pedofeatures (e.g. ooids and pisoids), brecciation, dissolution pipes, and insignificant erosion (Robins et al., 2015). On a vertical profile, a soil sample (H1) was collected at ~40 cm depth below ground surface and two caliche samples were collected at depths of 60 cm (H2) and 200 cm (H3) respectively (Figure 4.1). In addition, approximately 3

m laterally away from the profile, soil-caliche boundary is shallower and a caliche sample (H4) was collected at 40cm at the boundary like H2 (Figure 4.1). Caliche hand samples H2 and H4 were saw-cut to expose a fresher surface then drilled along different laminae. The laminae are thought to have formed from infiltrating soil waters which are impaired from draining down the soil profile due to underlying plugged horizons (Gile et al., 1981). Three laminae in each caliche hand sample were sampled and labeled as A, B, and C. Where A is bottommost while C is the upper or outermost laminae. Assuming new growth of pedogenic carbonates on top of old units, lamina A is expected to have deposited earlier than lamina B which in turn is anticipated to be older than lamina C. Approximately 100 mg of the drilled samples along each lamina of all caliche samples were separately homogenized.

3.2. Dust Collection

Dust collection at both the pecan orchard site and the natural site were conducted using 150 cm passive dust traps above ground, as in Ganor (1975) and Shannak et al. (2014). Both dust traps were maintained for one year (2015-2016) and a single sample collected from each representing a composite of dry and wet deposition. The water leachable fraction of these two dust samples were reported in Ortiz et al. (2018a).

Additionally, archived dust samples from the JER were used for this study; details of dust collection were discussed by Bergametti and Gillette (2010) and Floyd and Gill (2011). Briefly, at least five Big Spring Number Eight (BSNE) dust samplers at 5, 10, 20, 50, and 100 cm above ground were placed on towers at various sites at the JER. Sample sites were chosen based on the dominant vegetation and the need to assess the effect of vegetation on dust mass fluxes (Bergametti and Gillette, 2010). Labels of dust samples therefore, were based on the dominant vegetation at the sampling spot (Bergametti and Gillette, 2010; Floyd and Gill, 2011). Based on proximity to La

Mesa soil profile, only dust samples from seven sites collected above the saltation zone (50 and 100 cm) were considered due to the likelihood of farther transport distance from 2005 and 2006. The dust-sized particles (≤50μm) would dissolve completely in strong acids; therefore, only visible organic materials (e.g. leaves) were removed before sample weighing.

3.3. Sequential extraction of soils and local dusts

The sequential extraction of water soluble and acid leachable fractions of the soils were conducted for the pecan, alfalfa, and natural Fabens soils as well as two dusts from Fabens and pecan fields and reported in Ortiz et al. (2018a). The water-soluble fraction is used to dissolve evaporite salts, such as $CaCl_2$, NaCl, $CaSO_4$ and Na_2SO_4. This fraction is directly linked to irrigation through soil salinity. For the water-soluble extraction, 10g of a soil sample and 1g of dust sample was weighed into a centrifuge tube, with 30 ml of de-ionized water (18.2 MΩ). The slurry was shaken for 15minutes on a shaker and centrifuged at 3500 rpm for ten minutes. The supernatant was passed through with a 0.45μm filter and weighed. Exchangeable cations were extracted from soils and dusts using the method explained in detail in Chapter 1 between water soluble and acid leachable fractions to remove cations adsorbed to clays. The acid leachable fraction dissolves carbonate minerals such as secondary calcite. 20mL of 1M or 2M acetic acid was added onto soil residue from the CEC fraction (not reported here), depending the soils total inorganic carbon concentrations. The mixture was shaken for 6 hours and centrifuged at 2500 rpm for 20 minutes and the supernatant filtered with 0.45μm paper filter. The soil residue was washed again with 3mL of 1M or 2M acetic acid. Two aliquots of acetic acid leachates were combined and dissolved in 2% HNO_3. Leachates from these sequential extractions were analyzed for major elements for evaluation of soil salinity and sodicity, and reported in Ortiz et al. (2018a). This study would focus on $^{87}Sr/^{86}Sr$ ratios (see procedure in Chapter 1).

3.4. Leaching of regional dust and caliche samples from JER

Approximately 50 mg of dust and 100 mg of powered soil and caliche samples were weighed, and leached with 1N acetic acid for 30 minutes. Then leachates were evaporated to dryness.

3.5. Collection of Rio Grande and soil waters

Nested lysimeters were placed at 15, 30, 60, and 120cm depths for both pecan sites, Pecan_Fine and Pecan_Coarse. Rio Grande and groundwater irrigation samples, as well as soil waters, were only collected from the pecan orchard. Lysimeter waters were collected and filtered using 0.45 µm membrane filters. The pH, EC, alkalinity, and concentrations of major ions were reported in Ortiz et al. (2018). Twenty-five milliliters of the full-strength filtered waters were dried in 30mL Teflon beakers, then dissolved in 0.5mL of 3.5N HNO_3^- before the Sr elution sequence for isotopic analysis.

3.6. $^{87}Sr/^{86}Sr$ Analysis

Soil leachates and water samples were analyzed for Sr isotope analysis. Strontium purification was conducted in a Class 100/1000 clean room-laminar air fume hood with Eichron Sr 100–150 µm resin in 1.5 mL Teflon columns. Two elution Sr purification sequences were conducted to attain an evaporable aliquot for analysis. Seven rinses with 3.5 N HNO_3 acid were performed in each sequence then an eighth rinse with 0.05N HNO_3 to yield the purified sample. All purified samples were then analyzed for $^{87}Sr/^{86}Sr$ isotopes on the multi-collector inductively coupled plasma mass spectrometry (MC-ICP-MS) using standard-sample bracketing method (Konter and Storm, 2014). The Sr isotope bracketing standard SRM 987 yielded average $^{87}Sr/^{86}Sr$ ratios of 0.710235± 0.000005 (2SE, n=32). For quality control purposes, USGS BCR2 rock standards were treated as bulk samples, with measured average $^{87}Sr/^{86}Sr$ ratios of 0.70502±0.00001 (2SE, n=9) that were within the values reported in literature (0.70502; Jweda et al., 2015). Sr

blanks were negligible pico-gram scales (~80 pg). For soil leachates, the uncertainty is typically within 0.0001 (2SE) except for several soils on the water-soluble fraction. For water samples, $^{87}Sr/^{86}Sr$ has a much lower uncertainty at 0.00002 (2SE). The Sr isotopes of regional dust and JER caliche in pedogenic carbonates were reported with 2SE less than 0.00001.

Non-parametric statistics to compare sequential extraction isotopic ratios such as the Wilcoxon Rank-Sum and Kruskal-Wallis Tests were computed using R version 3.3.2 (2016-10-31).

4. RESULTS

The major element chemistry in sequential leachates of soils and pecan/Fabens dust, and water samples have been reported by Ortiz et al. (2018a) and included here along with Sr isotopes in Table 4.1 and Table 4.2. The Sr isotopes of regional dust and JER caliche in pedogenic carbonates were reported in Table 4.3.

4.1. Sr isotopes and Ca/Sr ratios of the natural and agricultural soils

The $^{87}Sr/^{86}Sr$ ratios in the water-soluble fraction for the Pecan_Fine soils ranged between 0.7092 and 0.7104, and were more variable for Pecan_Coarse soils, ranging between 0.7080 and 0.7102, especially in shallow depths (Figures 4.2A, 4.2B). The water-soluble fraction in Alfalfa_Fine_D soils had a narrow range of values between 0.7101 and 0.7103 (Figure 4.2C), slightly radiogenic than that in pecan soils. The $^{87}Sr/^{86}Sr$ ratios in natural Fabens soils were also narrow in range, from 0.7090 to 0.7094 for water-soluble fraction (Figure 4.2D; Table 4.1). The $^{87}Sr/^{86}Sr$ ratios of pedogenic carbonates (from the acid leachable extraction) varied little among three agricultural sites, around 0.7097 to 0.7103, but different from that of natural Fabens (0.7092 to 0.7094) within the analytical uncertainty (Figure 4.2; Table 4.1). Both pecan profiles had slightly less radiogenic $^{87}Sr/^{86}Sr$ values towards the soil surface in the pedogenic carbonates, as

well as in the water-soluble fraction (Figure 2). Water-soluble fraction and acid leachable fraction for all soils were compared and they had similar $^{87}Sr/^{86}Sr$ ratios (Appendix Figure 4.1).

Ca/Sr (mass ratio) in the water-soluble fraction of agricultural soils varied little with depth in the pecan site (64-201) and ranged between 20 and 216 for Alfalfa_Fine_D. The acid-leachable carbonate fraction had higher ratios between 200 and 700 in the top meter, which decreased between 546 and 1000 at depth (Figure 4.3.). The natural Fabens soils had very different Ca/Sr ratios in its water-soluble salt fraction from agricultural soils, with higher ratio at the surface (1354) and remained constant the rest of the profile ~200, but similar Ca/Sr ratios in its carbonate fraction (Figure 4.3).

4.2. Ca/Sr and 87Sr/86Sr in irrigation waters, soil waters and soil amendments

The $^{87}Sr/^{86}Sr$ ranged narrowly between 0.7099 and 0.7105 in the Rio Grande waters used for irrigation at the pecan orchard, and the Ca/Sr mass ratios ranged from 25 to 98 with an outlier (Table 4.2; Figure 4.2). Two groundwaters used for irrigation gave $^{87}Sr/^{86}Sr$ values of 0.7096 and 0.7010 and Ca/Sr ratios of 67 to 74, overlapping with Rio Grande waters. Most soil waters collected during the growing season, from 2014-2016 were collected from the Pecan_Fine soils and they had similar $^{87}Sr/^{86}Sr$ values (0.7098 to 0.7102) and Ca/Sr ratios (67 to 116) as irrigation waters. Only one soil water was collected from Pecan_Coarse and its $^{87}Sr/^{86}Sr$ ratio was distinctively different at 0.7130. The Sr isotope ratio for one soil amendment sample was measured at 0.7106 (Table 4.1).

4.3. Sr isotopes of dusts and caliche profiles

Two dust samples from Fabens and pecan orchard (local dust), and archived dust samples from JER represent the modern dust samples in the region. The local dusts had $^{87}Sr/^{86}Sr$ values of 0.7091 and 0.7094, respectively in the water-soluble fraction, and Ca/Sr ratios of ~1. The acid leachable fraction of these dusts was more radiogenic in $^{87}Sr/^{86}Sr$ ratios at 0.7101 and 0.7109. The Ca/Sr ratios in carbonate fraction were at 465 and 415 respectively, much higher than those in water soluble fraction. The regional JER dust samples were only characterized for acid leachable fractions, and they showed almost constant $^{87}Sr/^{86}Sr$ ratios from 0.7086 to 0.7091 (Table 4.3).

The caliche samples showed distinct $^{87}Sr/^{86}Sr$ ratios with depth in the profile but homogeneous within each layer (Figure 4.2; Table 4.3). H3 samples from 200 cm below ground surface had $^{87}Sr/^{86}Sr$ ratios ~ 0.7112, much higher than H1, H2 and H4 samples. Interestingly, H1 and H4 were collected from the same depths (40 cm deep) but characterized by different $^{87}Sr/^{86}Sr$ ratios.

5. DISCUSSION

In agricultural settings of arid-lands, dissolved Ca is added through irrigation and soil amendments, enhancing accumulation of pedogenic carbonates, especially in fine texture soils (Cox et al., 2018; Ortiz et al., 2018a). Those studies have combined mass balance calculation, pedogenic carbonate dating methods and C isotopes and showed that pedogenic carbonate accumulations rates were higher in agricultural soils than those in natural soils with similar climate conditions along the Rio Grande valley and majority of the pedogenic carbonates in the soils were young and formed due to soil cultivation. These findings agree with previous work, where the use of fertilizers promoted pedogenic carbonate formation (Bughio et al., 2016).

This study focused on these well-constrained soils with contrasting land-uses and utilized Sr isotopes to identify different natural versus anthropogenic Ca end-members (rain and dust deposition, irrigation and soil amendments) and to quantify their relative contribution to the overall Ca in the pedogenic carbonates of young agricultural soils.

5.1. Temporal variation in Sr isotopes of natural Ca sources: rain and dust

Rain and dust have proven to be important sources of calcium for natural soils in arid-lands. Indeed, pedogenic carbonates have been well studied worldwide including those at Jornada Experimental Range (JER) through the Desert Project (e.g., McFadden and Tinsley, 1985; Quade et al., 1995; Whipkey et al., 2000; Van der Hoven and Quade, 2002; Dart et al., 2007; Monger et al., 2015). Here, Ca in natural pedogenic carbonates was sourced predominantly from dust, with little addition from local bedrock (Gile et al., 1981; Capo and Chadwick, 1999; Monger and Gallegos, 2000; Naiman et al., 2000; Reheis, 2006; Reheis and Urban, 2011). Since dust is a major source of Ca^{2+} in desert environments, we presume our JER caliche signatures to be representative of antecedent dust signatures that have been incorporated into pedogenic structures, as observed in Van der Hoven and Quade (2002) and Shalev et al. (2013). If so, two local dusts from the Fabens, pecan orchard and 14 regional dusts from Jornada Experimental Range (JER) can be used as representative modern dusts and caliche samples from JER, dated from 10 to 300 kyrs, can be used as records of historical dusts (Figure 4.4).

We observed an overlap of $^{87}Sr/^{86}Sr$ ratios in JER dust and shallow carbonates in soils and in caliche (H1 and H2; Figure 4.4): The $^{87}Sr/^{86}Sr$ ratios measured in acid soluble dust were around 0.7089; $^{87}Sr/^{86}Sr$ of shallow carbonates in soils and caliche were 0.7086 and 0.7089 respectively. This suggests that atmospherically derived Ca has contributed significantly to the formation of these young carbonates. Sr isotopic signatures for local dusts were slightly more radiogenic

(0.7091-0.7109) than those of JER dusts (0.7086-0.7091), probably reflecting some contribution from local soils.

The carbonates in older JER caliche samples (H3 and H4) have more radiogenic $^{87}Sr/^{86}Sr$ ratios (>0.7100) than those in shallow depths, and this might be associated with wetter conditions and enhanced weathering of silicate rocks (Capo et al., 1998) or a shift in wind direction and thus a different dust source, or rain water of different origins. The Camp Rice Formation and local soil silicates near Las Cruces have $^{87}Sr/^{86}Sr$ ratios between 0.7131 and 0.7173 (Capo and Chadwick, 1999). Probably a more radiogenic material must have supplied Sr during the formation of the carbonates at depth. Using Sr, C and O isotopes, Mark et al. (2012) suggested that secondary minerals opal and calcite in the Jornada Basin precipitated from a mixture of deep upwelling geothermal fluids and shallow meteoric groundwater. Such deep groundwater flowing through old granitic or clay-bearing formations is characteristic of radiogenic $^{87}Sr/^{86}Sr$ ratios. Another possible source of high $^{87}Sr/^{86}Sr$ ratios in these carbonates is the heterogeneous nature the basin fills (sediments), which is a wide combination of river and mountain alluvium. This implies that a more radiogenic $^{87}Sr/^{86}Sr$ ratios material could be locally or externally sourced through distant riverine alluvium or exogenic dust. The precise source of radiogenic Sr signature in carbonates at depth remains open for investigation.

5.2. Ca mass balance and Sr isotope signatures in agricultural soils

Inputs of Ca to natural and agricultural soils have been estimated, and despite of large uncertainties, the annual loading of soluble Ca through dust deposition is much smaller than that of agricultural-land management practices (Ortiz et al., 2018a). From two dust samples collected in Fabens and pecan orchard around El Paso, the estimated amount of Ca deposited from rain/dust is ~40-50g m^{-2} yr^{-1}, including ~0.1 g m^{-2} yr^{-1} as water soluble Ca^{2+}. The fertilizers and other

amendments are responsible for 0.04 g Ca^{2+} m^{-2} yr^{-1}, most of which are water soluble salts, whereas irrigation waters add ~120 g Ca^{2+} m^{-2} yr^{-1}.

The Rio Grande water and local groundwaters, both used for irrigation at the Pecan orchard has narrow and indistinguishable Sr isotopes (IRW_RG: 0.7099 to 0.7105; IRW_GW: 0.7096 to 0.7100; Table 4.2). Sr isotopic composition of Rio Grande water measured in this study falls into the typical range of Sr isotope ratios at other locations near El Paso during different seasons, ranging from 0.7089 to 0.7150, with an outlier of 0.7203 (Nyachoti, 2016). Consistent with Ca mass balance, the Sr isotope ratios of pecan and alfalfa soils in both water-soluble fraction and pedogenic carbonate fraction fall to the range in Sr isotope ratios defined by the irrigation waters, indicating that Ca addition to agricultural soils are predominantly from irrigation waters. However, the Fabens natural soils have distinctively different $^{87}Sr/^{86}Sr$ signatures.

The pecan soil leachates have slightly lighter values at the surface (~0.7095) for both water-soluble and acid leachable extractions (Figure 4.2); however, this trend is not observed at the alfalfa site and instead, relatively constant $^{87}Sr/^{86}Sr$ signatures are observed (~0.710). The difference in pecan and alfalfa soils are more likely due to soil amendments, as these two fields, only 25 miles apart, should receive similar amount and chemistry for dust deposition. However, this study has only isotopically characterized one of the soil treatments reported by Ortiz et al. (2018a). The $^{87}Sr/^{86}Sr$ ratio of urea is 0.7106, much higher than all soil leachates. Thus, other fertilizers and amendments that have not been analyzed in this study but with lighter $^{87}Sr/^{86}Sr$, must be important in contributing detectable Ca. Further analysis of all other soil fertilizers and amendments could elucidate the lasting impact-if any, on soils.

In addition, whether or not and where Sr signatures in soil amendments are observed, depend on several factors, including time and duration of their application, solubility and

dissolution kinetics after application etc. For example, 0.0023 g m^{-2} yr^{-1} of soluble and bioavailable Ca are added on the pecan orchard as urea, and may not precipitate out at the surface. Furthermore, urea is relatively acidic and can aid in the dissolution of existing pedogenic carbonates (Zamanian et al., 2016); calcite will re-precipitate at depth as a function of drying and wetting events (Knight, 1991; Marion et al., 1985; Sobecki and Wilding 1983; Zamanian et al., 2016). As such, application of might not be a significant contributor to top soil Ca, controlling soil $^{87}Sr/^{86}Sr$ ratios. In another case study, though Bughio et al. (2016) have found that mineral fertilizers facilitate pedogenic carbonate formation as it is an additional source of Ca^{2+} available for carbonate mineralization. Although the majority of the calcium in our agricultural systems is irrigation sourced, mineral fertilizer additions would further amplify its formation and needs detailed investigation on its fluxes and reactivity.

5.3. Ca/Sr as a conservative tracer

The WS fraction of agricultural soils among three sites has similar Ca/Sr ratios (Figure 4.3A), close to that of irrigation waters. However, the Ca/Sr ratios of the pedogenic carbonate fraction are very different from those in water-soluble fraction or irrigation waters, and they increase with depth (Figure 4.3B). Unless the biological uptake by pecan trees and alfalfa bushes fractionates Ca and Sr significantly as in works by Belanger et al. (2012), the difference in Ca/Sr ratios probably is due to shift in Rio Grande water chemistry. However, additional endmembers Ca/Sr characterization from the river would be needed.

The WS fraction is composed of mainly evaporite and extremely soluble salts such as gypsum and halite and existing salts which could be dissolving and re-precipitating after each irrigation event, as shown by pore-fluid EC data in Ortiz et al. (2018a). If so, Ca/Sr ratios in this fraction follow those of irrigation water, as observed in Figure 4.3A. However, research into

kinetics of dissolution and re-precipitation of such salts needs to be investigated further. In contrast, pedogenic carbonates remain at equilibrium or supersaturation in soils (positive SI values of soil waters with respect to calcite in Table 4.2). If so, Ca/Sr ratios in pedogenic carbonates are integrated over time. Moreover, texture controls water retention and location of calcite precipitation (Eshel et al. 2007; Lal, 2009; Zamanian et al., 2016; Cox et al., 2018). Calcite is likely to form above the clayey fine-textured layer as soil waters are supersaturated through evapotranspiration and forced to precipitate above the impermeable layer. With time, precipitation of salts and calcite lowers the permeability and may close the soils for further accumulation. Conceptually, calcite might be older with depth as observed in natural systems of arid-lands. If so, Ca/Sr ratios in irrigation waters must have been higher and decreased with time.

6. CONCLUSION

Nyachoti et al. (2017) used U-series isochron method, and dated pedogenic carbonates in Alfalfa field to be approximately 2.2±1.7 ka. Thus, in these agricultural soils, pedogenic carbonates are mixture of older calcite that has been formed naturally with new irrigation-sourced calcite. It is crucial to separate these two components. Through mass balance and C isotopes, previous chapters have clearly identified the pedogenic carbonates in agricultural soils along Rio Grande are overwhelmingly driven by soil cultivation, with dissolved inorganic carbon and dissolved calcium supplied by flood-irrigation and minor soil amendments. This study provides additional evidence using Sr isotopes.

Both water-soluble and peodgenic carbonates in agricultural soils along the Rio Grande valley have similar $^{87}Sr/^{86}Sr$ signatures as irrigation waters (Rio Grande and local groundwater), with some modification from soil amendments and additions. In contrast, different $^{87}Sr/^{86}Sr$ ratios were observed in natural soils of the same area. This is in agreement with a calculation of calcium

deposits from irrigation versus other endmember contributions. Because of the coupling between inorganic calcite production and CO_2 emissions, as in Reaction 4.1, we conclude that calcite derived CO_2 is important in agricultural soils and dryland cultivated agriculture can greatly impact regional and global carbon cycles. Projected changes in climate can only be expected to exacerbate these processes as river surface waters become more limited and saline, pushing farmers to use groundwater, that are brackish and even more oversaturated with respect to calcite.

Table 4.1: Ca concentrations, Ca/Sr mass ratio and 87Sr/86Sr isotopic ratios in the water soluble and acid leachable fractions of soil dust samples.

Depth cm	Ca (mg/kg soil)	Ca/Sr (g/g)	$^{87}Sr/^{86}Sr$	2SE	Ca (g/kg soil)	Ca/Sr (g/g)	$^{87}Sr/^{86}Sr$	2SE
	Water soluble fraction				Acid leachable fraction			
Pecan_Fine								
10	1103	118	0.70946	0.00005	24.0	362	0.7097	0.00002
20	1636	110	0.70960	0.00002	27.9	285	0.70975	0.00002
30	1075	98	0.70980	0.00010	29.6	332	0.70984	0.00001
39	843	92	0.71005	0.00004	29.8	261	0.71001	0.00002
49	1076	88	0.71008	0.00002	28.0	315	0.71002	0.00002
59	331	124	0.70922	0.00049	26.0	420	0.71008	0.00003
69	653	93	0.70955	0.00029	26.9	281	0.70998	0.00003
79	1194	88	0.71005	0.00095	28.6	290	0.70998	0.00002
88	627	89	0.71026	0.00002	27.5	226	0.70999	0.00002
98	355	105	0.71039	0.00008	30.1	220	0.71001	0.00002
108	358	107	0.71010	0.00013	29.4	216	0.71004	0.00006
118	410	102	0.71027	0.00010	28.4	220	0.71016	0.00002
128	487	102	0.71021	0.00002	28.4	209	0.71019	0.00002
137	412	98	0.71025	0.00002	31.3	227	0.71023	0.00002
147	296	132	0.71015	0.00002	17.9	353	0.71028	0.00002
157	301	134	0.71012	0.00002	26.1	462	0.71010	0.00002
167	285	126	0.71024	0.00002	32.8	380	0.71016	0.00002
177	297	137	0.71021	0.00002	32.0	427	0.71013	0.00002
186	260	151	0.71021	0.00002	25.7	553	0.71007	0.00002
196	211	201	0.71025	0.00001	23.6	592	0.71005	0.00002
206	236	191	0.71023	0.00002	22.3	633	0.71003	0.00003
216	251	172	0.71026	0.00001	23.2	591	0.71003	0.00003
226	264	154	0.71020	0.00002	21.9	623	0.70996	0.00004
235	702	115	0.70992	0.00001	19.0	681	0.71006	0.00002
245	255	182	0.71027	0.00002	18.9	685	0.70997	0.00003
255	259	166	0.71020	0.00002	15.3	698	0.70997	0.00002
265	298	138	0.71000	0.00002	16.6	568	0.70994	0.00002
275	237	174	0.71024	0.00002	14.8	735	0.70997	0.00002
284	225	183	0.71019	0.00002	12.9	861		
Pecan_Coarse								
0	8	93	0.70950	0.00033	11.3	370		
10	34	112	0.70800	0.00208	11.1	401	0.70979	0.00002
20	32	121	0.70932	0.00035	14.3	377	0.70987	0.00002

30	84	111	0.70901	0.00091	5.5	595		
40	35	115	0.70951	0.00045	9.2	486	0.70992	0.00002
50	149	109	0.71003	0.00009	7.5	533		
60	115	109	0.70988	0.00018	6.5	536	0.71000	0.00002
70	64	121	0.70972	0.00033	5.2	634		
84	147	106	0.71022	0.00022	4.6	664	0.71001	0.00003
90	82	110	0.70996	0.00011	4.8	589	0.71002	0.00002
100	85	101	0.71000	0.00014	10.2	421		
110	162	74	0.71014	0.00005	11.8	427	0.71007	0.00002
120	647	64	0.71019	0.00004	8.1	503		
130	230	83	0.70987	0.00023	5.5	532	0.71009	0.00002
140	187	87			3.1	595	0.70999	0.00006
150	118	97	0.71013	0.00011	3.3	617	0.71014	0.00002
160	65	103	0.70900	0.00065	2.6	670		
170	56	109	0.71020	0.00014	2.5	667		
180	50	115	0.70944	0.00053	2.8	647	0.71008	0.00002
190	32	129			2.9	652		
200	35	106	0.70983	0.00017	3.8	611	0.71016	0.00002
210	46	91			3.8	707	0.71020	0.00003
220	51	91	0.70993	0.00009	4.3	933		
230	90	95			3.9	954		
240	70	103	0.70990	0.00037	3.3	968		
250	90	95						
Alfalfa_Fine_D								
0	12	22	0.71031	0.00001	45.5	405	0.71011	0.00001
10	80	159	0.71030	0.00001	107.3	404	0.71011	0.00001
20	23	52	0.71033	0.00001	38.7	409	0.71012	0.00001
30	36	111	0.71031	0.00001	59.7	400	0.71011	0.00001
40	16	29	0.71028	0.00001	63.2	354	0.71011	0.00001
50	51	217	0.71013	0.00002	32.7	410	0.71008	0.00001
60	2	22	0.71025	0.00010	23.1	504	0.71005	0.00001
Natural_Fabens								
0	120	1354	0.70901	0.00019	4.0	362	0.70940	0.00010
20	232	311	0.70941	0.00007	28.1	644	0.70938	0.00002
40	1116	168	0.70928	0.00002	27.7	387	0.70940	0.00002
60	1541	177	0.70931	0.00004	21.5	695	0.70941	0.00002
71	1364	174	0.70933	0.00002	23.9	668	0.70940	0.00002
81	1519	187	0.70935	0.00009		51	0.70935	0.00008
90	1466	190	0.70934	0.00002		61	0.70941	0.00002

99	1453	193	0.70937	0.00002	24.9	773	0.70921	0.00010
Dust								
Fabens	3345	132	0.70914	0.00016	35	465	0.71012	0.00001
Pecan	2593	112	0.70937	0.00034	34	415	0.71088	0.00002
Soil Amendments								
urea			0.71057	0.00001				

Table 4.2. Major chemistry and Sr isotopes of water in the pecan orchard

Type	Depth (cm)	Date	pH	EC (dS/m)	Alk (meq /L)	Ca (ppm)	Sr (ppm)	Ca/Sr (g/g)	$^{87}Sr/^{86}Sr$	2SE
IRW_GW	0	4/17/15	7.38	3.8	5.3	428	6	74	0.70963	0.00001
IRW_GW	0	4/17/15	7.25	4.3	6.8	266	4	67	0.70995	0.00001
IRW_RG	0	4/3/14	7.64		4.7	145	3	46	0.70991	0.00001
IRW_RG	0	5/19/14	6.95	2.1	4.0	48	1	39	0.71015	0.00002
IRW_RG	0	6/25/14			1.3	19	1	25	0.71014	0.00001
IRW_RG	0	10/9/14	8.40	2.2	3.7	44	1	40	0.71006	0.00002
IRW_RG	0	5/15/15	7.70	1.9	3.5	43	1	38	0.71007	0.00001
IRW_RG	0	6/11/15	8.10	1.0	3.7	39	1	59	0.71047	0.00001
IRW_RG	0	6/30/15	8.00	0.9	3.5	36	1	65	0.71031	0.00002
IRW_RG	0	7/13/15				58	19	3	0.70985	0.00002
IRW_RG	0	7/19/15	8.00	1.0	2.7	37	1	66	0.71025	0.00001
IRW_RG	0	8/11/15	7.91	0.9	3.7	56	1	93	0.71048	0.00001
IRW_RG	0	9/22/15				92	1	98	0.71013	0.00001
IRW_RG	0	6/30/16	8.15	9.2	5.5	82	1	92	0.71010	0.00001
IRW_RG	0	9/12/16				75	1	97	0.71026	0.00001
SW	15	6/17/15	7.50	3.3		487	5	101	0.70982	0.00001
SW	15	7/18/16	7.74	4.0	1.2	559	5	116	0.71024	0.00001
SW	30	7/3/14	6.95	5.5	4.2	443	6	77	0.70993	0.00001
SW	30	5/21/15				835	7	119	0.70987	0.00002
SW	30	6/17/15	7.31	3.8		534	5	101	0.70979	0.00001
SW	30	9/30/15	7.29	2.3		259	3	100	0.70986	0.00001
SW	60	10/23/14	7.08		4.0	297	4	67	0.71005	0.00001
SW	60	6/17/15	7.35	5.8		943	9	101	0.71008	0.00001

SW	60	7/10/15	7.25	4.7	6.4	498	6	84	0.71012	0.00001
SW	60	9/30/15	7.34	3.8		544	5	101	0.71014	0.00001
SW	120	7/19/16	7.20	6.8	10.2	709	7	95	0.71002	0.00001
SW*	120	9/19/16	7.73	7.9		281	3	102	0.71296	0.00001
DRW	200	9/1/14	7.80	3.8	3.4	81	3	29	0.70984	0.00002
DRW	200	10/23/14	7.89	3.6	7.2	163	3	51	0.70982	0.00001
DRW	100	6/17/15	7.32			290	3	100	0.70986	0.00002
DRW	100	6/17/15	7.31	2.4		291	3	100	0.70985	0.00001
DRW	200	7/10/15	7.95	2.4	4.8	107	2	52	0.70986	0.00001
DRW	200	7/28/15	7.92	3.2	5.5				0.71243	0.00002
DRW	100	9/30/15	7.90	3.8		405	4	100	0.70984	0.00002

IRW_GW and IRW_RG are irrigation water samples from groundwaters and Rio Grande. SW=soil water. DRW= drainage water

Table 4.3. Sr isotope ratios of the acid soluble fraction in JER dust and caliche samples

Dust sample	$^{87}Sr/^{86}Sr$	Caliche Sample	Depth (cm)	$^{87}Sr/^{86}Sr$	Age (kyrs)*
M-Rabb	0.7087	H1	40	0.7086	
M-well	0.7091	H2C	60	0.7089	10-60
G-IBPE4	0.7087	H2B	60	0.7090	
P-Tobo	0.7088	H2A	60	0.7089	
P-Coli	0.7086	H3C	200	0.7111	200-280
T-TYL	0.7087	H3B	200	0.7112	
T-East	0.7088	H3A	200	0.7112	
M-Rabb	0.7088	H4C	40	0.7091	~120
M-well	0.709	H4B	40	0.7101	
G-IBPE4	0.7088	H4A	40	0.7102	
P-Tobo	0.7088				
P-Coli	0.7087				
T-TYL	0.7088				
T-East	0.7089				
min	0.7086			0.7086	
max	0.7091			0.7112	

*ages were estimated through U-disequilibrium methods; see details at Nyachoti (2016)

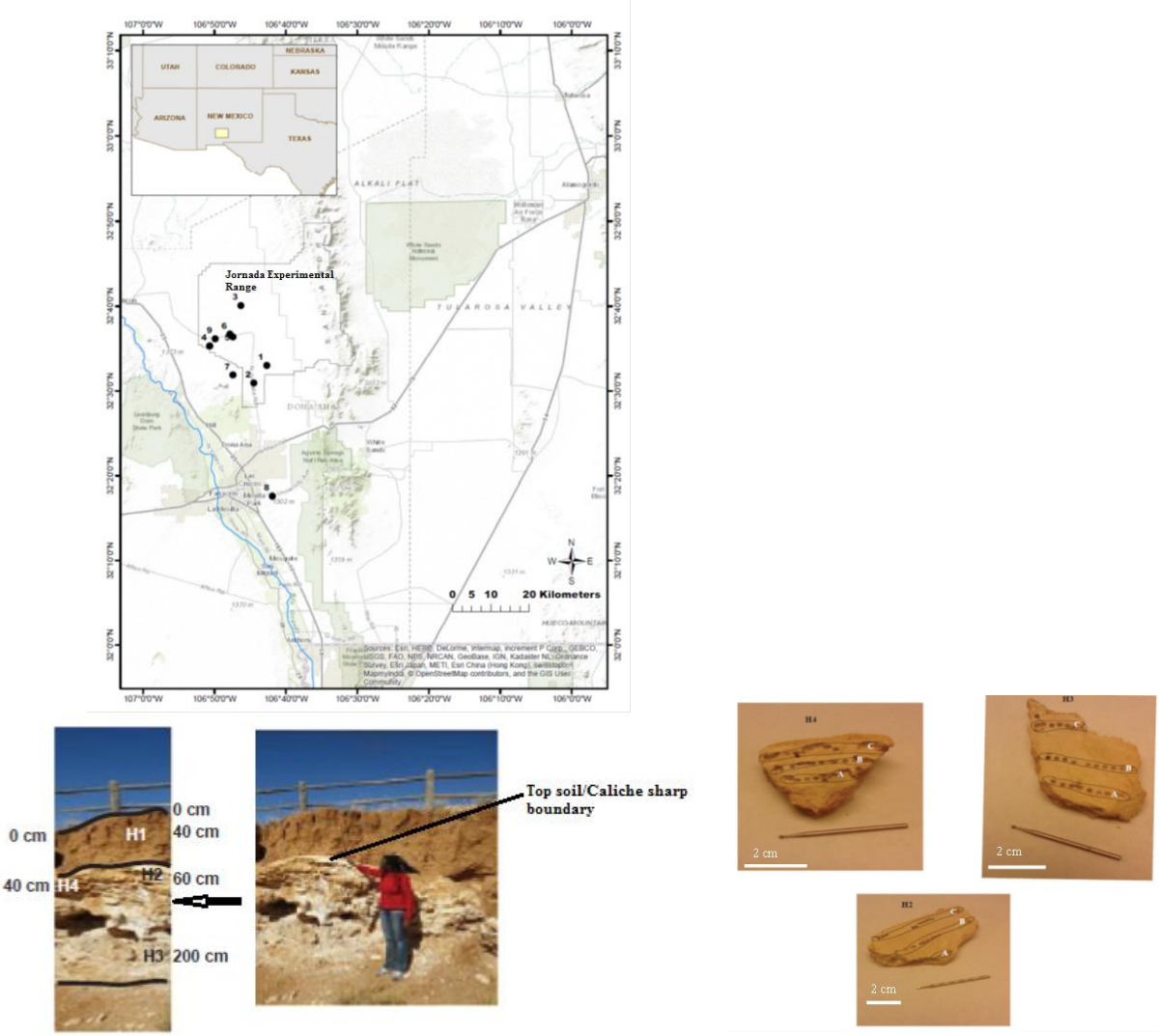

Figure 4.1: Location map showing a studied soil profile at Jornada Experimental Range (JER), as well as sites where modern dust (T-East (1), T-tyl (2), P_Tobo (3), G_IBPE (4), M-Well (5), M-Rabb (6), and P_Coli (7)) were sampled are also shown. An exposed trench at the La Mesa geomorphic surface within the Jornada Basin containing approximately 150 cm of thick horizon of stage V pedogenic carbonates/caliche. H1 is a soil sampled at 40cm from surface; H2 and H3 are caliche samples collected at 60 cm, 200cm respectively from surface. H4 is a caliche sample at 40cm from surface and 3m laterally away from H2 caliche. Saw-cut caliche samples of H4, H2 and H3 showing drilled lamina A, B, and C. A is the innermost lamina, B is the middle, and C is the outermost lamina.

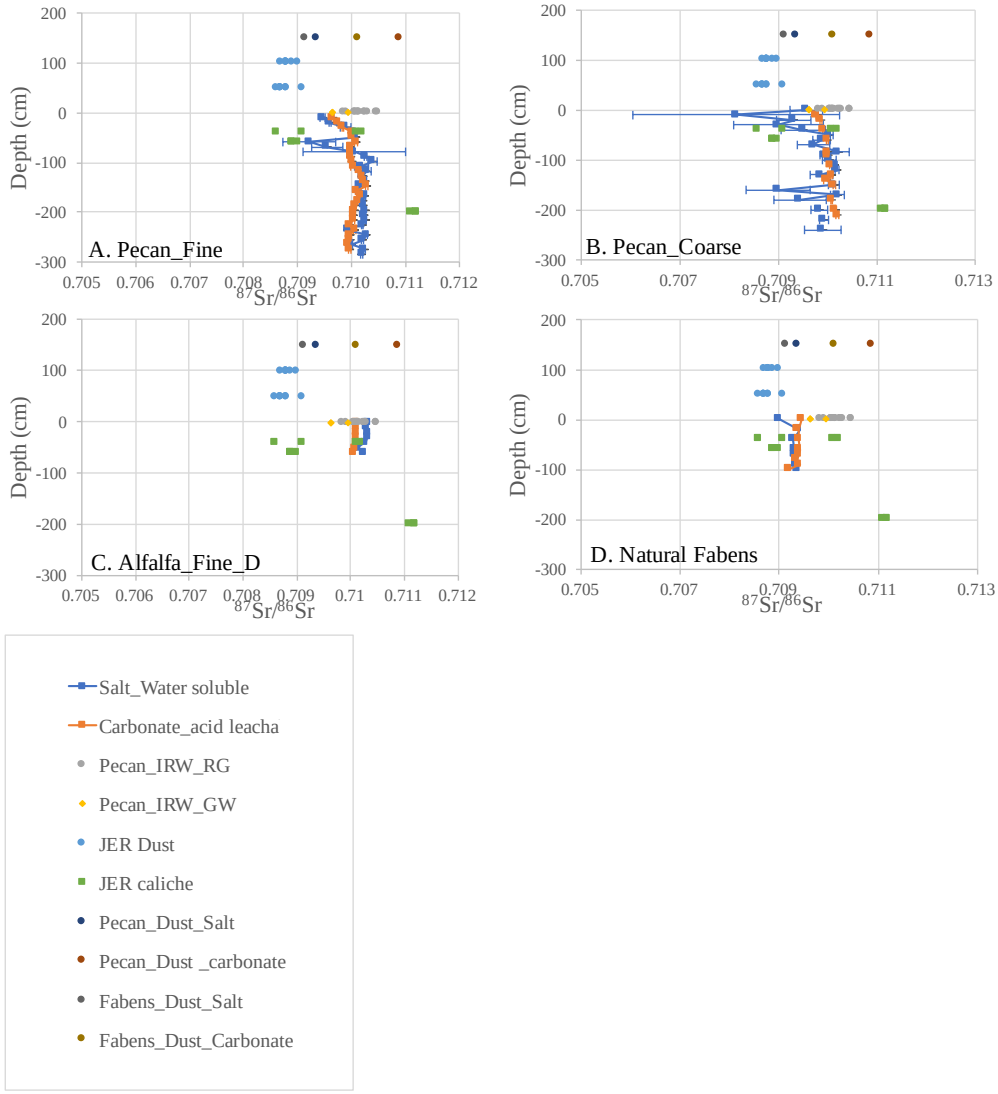

Figure 4.2. Depth profiles of Sr isotopes in Pecan_Fine (A), Pecan_Coarse (B), Alfalfa_Fine_D (C) and Natural Fabens (D), for both water soluble and acid leachable fractions. Also plotted are Sr isotope compositions of local and regional dust samples, as well as JER caliche samples.

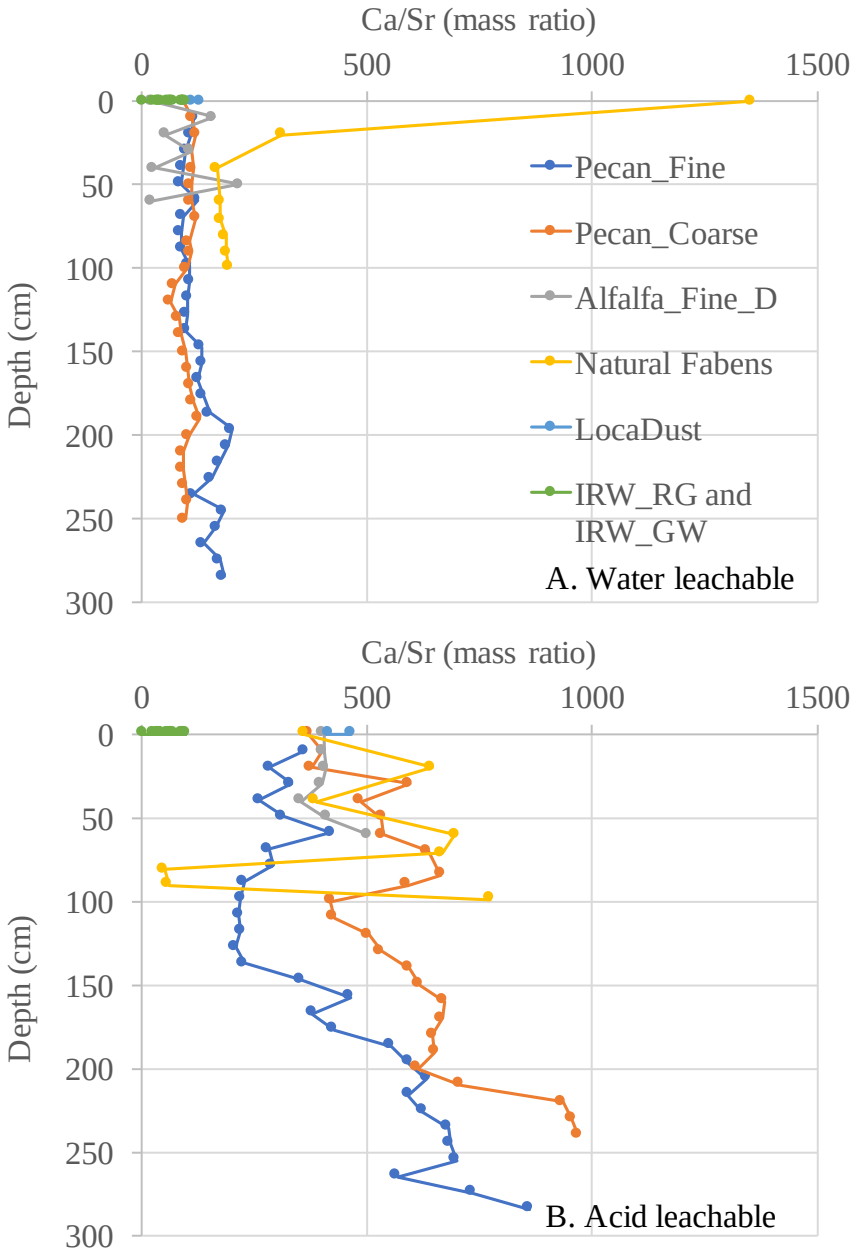

Figure 4.3. Depth profiles of Ca/Sr (mass ratio) in water leachable (A) and acid leachable (B) fractions of natural and agricultural soils. Also plotted are Ca/Sr ratios of irrigation waters and local dust samples.

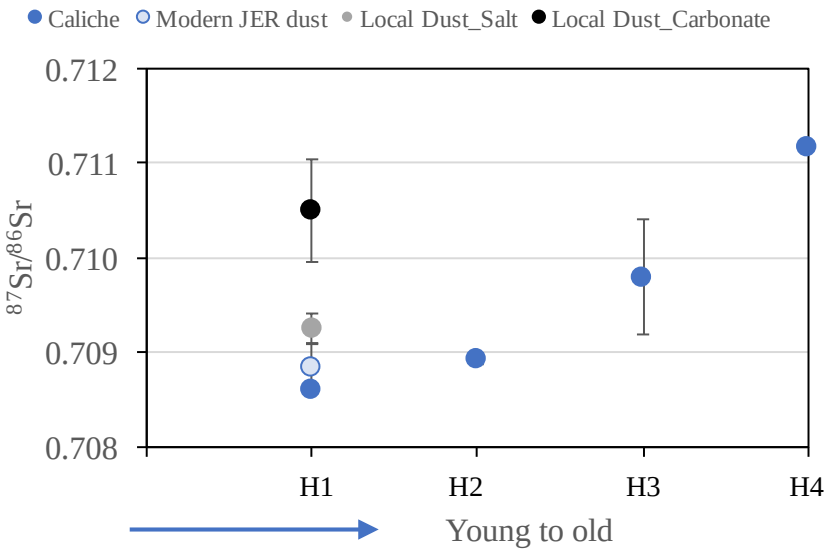

Figure 4.4. Sr isotope ratios of dust and caliche samples as a function of ages.

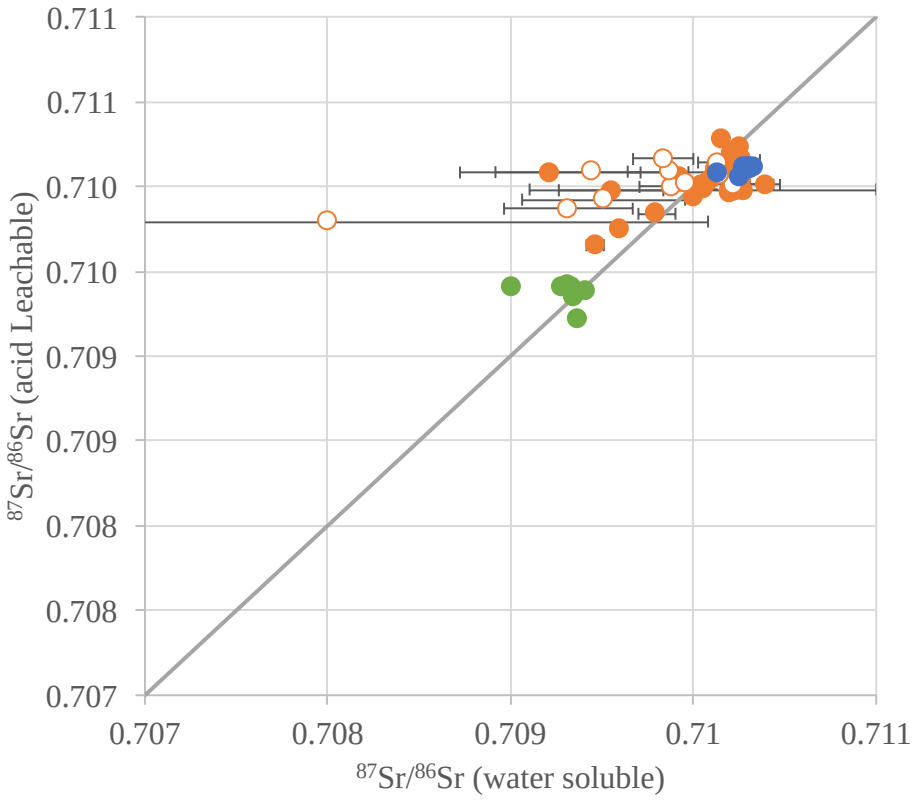

Appendix Figure 4.1: Sr isotopes of water soluble and acid leachable fractions are similar within uncertainties.

REFERENCES:

Assouline S., Russo D., Silber A., et al. (2015) Balancing water scarcity and quality for sustainable irrigated agriculture, *Water Resources Research*, 51. 9127-9140

Batlle-Aguilar B., Porporato D. B. (2011) Modelling soil carbon and nitrogen cycles during land use change. A review. Agronomy for Sustainable Development, Springer Verlag/EDP Sciences/*INRA* 31 (2) 251-274

Birkeland P.W. (1984) Soils and Geomorphology. Oxford University Press, New York, pp. 138-146

Borrok, D.M., Engle, M.A. (2014) The role of climate in increasing salt loads in dryland rivers. Journal of Arid Environments 111, 7-13

Bughio M.A., Wang P., Meng F., et al. (2016) Neoformation of pedogenic carbonates by irrigation and fertilization and their contribution to carbon sequestration in soil. *Geoderma 262, 12-19*

Cabot C., Sibole J.V., Barcelo J., Poschenrieder C. (2014) Lessons from crop plants struggling with salinity. *Plant Science 226*, 2-13

Capo, R.C. and Chadwick, O.A. (1999) Sources of strontium and calcium in desert soil and calcrete. Earth and Planetary Letters 170, 61-72.

Capo R., Stewart B.W, Chadwick O.A. (1998) Strontium isotopes as tracers of ecosystem processes: theory and methods. *Geoderma*, 82, 197-225

Cerling T.E., and Quade J. (1993) Stable Carbon and Oxygen Isotopes in Soil Carbonates. *Geophysical Monograph Series.* https://doi.org/10.1029/GM078p0217

Choudhary O.P, Josan A.S., Bajwa M.S., Kapur M.L. (2004) Effect of sustained sodic and saline-sodic irrigation and application of gypsum and farmyard manure on yeild and quality of sugarcane under semi-arid conditions. *Field Corps Research 87*, 103-116

Cox C., et al. (2017) Soil quality change due to flood irrigation in agricultural fields along the Rio Grande in western Texas, *Applied Geochemistry*, 90, 87-100, doi:10.1016/j.apgeochem.2018.01.007

Dart, R.C., Barovich, K.M., Chittleborough, D.J., Hill, S.M. (2007) Calcium in regolith carbonates of central and southern Australia: its source and implications for the global carbon cycle. Palaeogeography, Palaeloclimatology, Palaeloecology 249, 322-334.

Eshel G., and Fine, P., (2007) Total soil carbon and water quality: An implication for carbon sequestration, *Soil Sci. Soc. Am. J.*, 71:397-405 doi:10.2136/sssaj2006.0061

Falasca S.L., Ulberich A., and Acevedo A. (2014) Identification of Argentinian saline drylands suitable for growing *Salicornia bigelovii* for bioenergy, *International Journal of Hydrogen Energy* 39, 8692-8689

Floyd K.W. and. Gill, T.E. (2011) The association of land cover with aeolian sediment production at Jornada Basin, New Mexico, USA. *Aeolian Research 3*, 55-66

Ganjegunte, G.K., Ulery, A., Niu, G., Wu, Y. (2017) Effects of treated municipal wastewater irrigation on soil properties, switchgrass biomass production and quality under arid climate. Ind. Crop. Prod. 99, 60–69.

Ganor, E., 1975. Atmospheric Dust in Israel. Sedimentological and Meteorological Analysis of Dust Deposition (Ph.D. thesis). Hebrew University of Jerusalem.

Gile, L.H., Hawley, J.W. and Grossman, R.B. (1981) Soils and geomorphology in the basin and range area of southern New Mexico— Guidebook to the Desert Project. Memoir 39. New Mexico Bur. Of Mines and Miner. Res., Socorro, NM.

Gile, L. H. (2002). Lake Jornada, an early-middle Pleistocene lake in the Jornada del Muerto Basin, southern New Mexico. *New Mexico Geology24*(1), 3-14.

Gocke M., Pustovoytov K., Kuzyakov Y. (2012) Pedogenic carbonate formation: Recrystallization versus migration-Process rates and periods assessed by 14C labeling. *Global Biogeochemical Cycles 26*, GB1018, doi1029/2010GB003871

Harrison E., and Dorn R. (2014) Introducing a terrestrial carbon pool in warm desert bedrock mountains, southwestern USA, *Global biogeochemical Cycles*, AGU Publication 10.1002/2013/GB004568

Hogan J.F., et al. (2007) Geologic origins of salinization in a semi-arid river: The role of sedimentary basin brines. *Geology*, (35) 12:1063-1066

Jenny, H. (1980). The Soil Resource: Origin and Behaviour, Ecological Studies 37. Springer Verlag.

Knight, W.G. 1991. Chemistry of arid region soils. Ch. 4. In J. Skujins (ed.) Semiarid lands and deserts: Soil resource and reclamation. Marcel Dekker, New York.

Lal, R. and Kimble, J.M. (2000) Pedogenic carbonates and the global carbon cycle. In: Lal, R., Kimble, J.M., Eswaran, H., Stewart, B.A. (eds.), Global Climate Change and Pedogenic Carbonates, 1-14.

Lal, R. (2009) Sequestering carbon in soils of arid ecosystems *Land Degradation and Development 20 https://doi.org/10/1002/ldr.934*

Li, J., et al. (2016) Sr-Nd elements and isotopes as tracers of dust input in a tropical soil chronosequence, *Geoderma*, 262, 227-234

Lippmann, F. 1973. Sedimentary carbonate minerals. Minerals, Rocks and Inorg. Mater. Ser. 4. Springer-Verlag, Berlin.

Mack, G.H., Salyards, S.L., James, W.C. (1993). Magnetostratigraphy of the Plio-Pleistocene Camp Rice and Palomas Formations in the Rio Grande rift of southern New Mexico. *American Journal of Science 293*, 49-77.

Mack, G. H., McIntosh, W. C., Leeder, M. R., Monger, H. C. (1996). Plio-Pleistocene pumice floods in the ancestral Rio Grande, southern Rio Grande rift, USA. *Sedimentary Geology 103*(1), 1-8.

Mack, G. H., Seager, W. R., Leeder, M. R., Perez-Arlucea, M., Salyards, S. L. (2006). Pliocene and Quaternary history of the Rio Grande, the axial river of the southern Rio Grande rift, New Mexico, USA. *Earth-Science Reviews 79*(1), 141-162.

Mack, G. H., Jones, M. C., Tabor, N. J., Ramos, F. C., Scott, S. R., Witcher, J. C. (2012). Mixed Geothermal and Shallow Meteoric Origin of Opal and Calcite Beds In Pliocene–Lower Pleistocene Axial–Fluvial Strata, Southern Rio Grande Rift, Rincon Hills, New Mexico, USA. *Journal of Sedimentary Research82*(8), 616-631.

Marion GM, Schlesinger WH, Fonteyn PJ. 1985. CALDEP: A regional model for soil CaCO3 (caliche) deposition in southwestern deserts. Soil Science 139: 468–481.

McFadden, L.D. and Tinsley, J.C. (1985) Rate and depth of pedogenic carbonate accumulation in soils: formation and testing of a compartment model. In (Eds.Weide, D.L.) Geological Society of America special paper 203, 23-42.

Milliere, Hasinger O., Bindschedler S., Cailleau G., Spangenber J.E., and Verrechia E.P. (2011) Stable carbon and oxygen isotope signatures of pedogenic needle fibre calcite. *Geoderma (161)* 74-87.

Monger, H. C. and Gallegos, R. A. (2000) In: Global Climate Change and Pedogenic Carbonates (eds R. Lal, J. M. Kimble, H. Eswaran and B. A. Stewart). Lewis Publishers, Boca Raton, FL, 273–289.

Monger, H.C., Kraimer, R.A., Khresat, S., Cole, D.R., Wang, W. and Wang, J. (2015) Sequestration of inorganic carbon in soil and groundwater. Geology 43 (5), 375-378. https://doi.org/10.1130/G36449.1

Naiman Z., Quade J., Patchett J. (2000) Isotopic evidence for eolian recycling of pedogenic carbonate and variations in carbonate dust sources throughout the southwest United States, *Geochemimicia et Cosmochimica Acta*, 64,18:3099-3109

Nigro A., et al. (2017) Strontium isotope as traces of groundwater contamination, *Procedia Earth and Planetary Science*, 27, 352-355

Nyachoti, S., Jin, L., Tweedie, C.E. and Ma, L. (2017) Formation of pedogenic carbonates in the semi-arid Rio Grande valley: insights from carbon, major elements, and U-series isotopes in natural and agricultural soils of southern New Mexico and western Texas. Chemical Geology, doi.org/10.1016/j.chemgeo.2017.10.014.

Ortiz, A. and Jin, L. (2018a) Physical and chemical controls of salt movement and accumulation in natural versus irrigated drylands. To be submitted.

Phillips F., Mills S., Hendrickx M., Hogan J. (2003) Environmental tracers applied to quantifying causes of salinity in arid-region rivers: Results from the Rio Grande Basin, Southwestern USA, *Development in Water Science*, 50; 327-334

Qi Z., Feng, H., Zhao Y., Zhang T., Yang A., Zhang Z. (2018) Spatial distribution and simulation of soil moisture and salinity under mulched drip irrigation combined with tillage in an arid saline irrigation district, northwest China. *Agricultural Water Management 201, 219-231*

Quade, J., Chivas, A.R., McCulloch, M.T. (1995) Stronsium and carbon isotope tracers and the origins of soil carbonate in southern Australia and Victoria. Palaeogeography, Palaeloclimatology, Palaeloecology 113, 103-117.

Rath, K. and Rousk, J. (2015) Salt effects on the soil microbial decomposer community and their role in organic carbon cycling: a review. Soil Biology and Biochemistry 81, 108-123. http://dx.doi.org/10.1016/j.soilbio.2014.11.001

Reheis, M.C. and Hihl, R. (1995) Dust deposition in southern Nevada and California, 1984-1989: Relations to climate, sources area, and source lithology. J. Geophys. Res. 100, 8893-8918.

Reheis, M. C. and Urban, F. E. (2011). Regional and climatic controls on seasonal dust deposition in the southwestern US. *Aeolian Research3*(1), 3-21.

Reheis, M.C. (2006). A 16-year record of eolian dust in southern Nevada and California, USA: controls on dust generation and accumulation. *Journal of Arid Environments*67, 487–520

Robbins, C.W., 1985. The CaCO3–CO2–H2O system in soils. J. Agron. Educ. 14.

Saskia R.E., Snoeck C., Crowley Q.G., Babechuck M.G. (2018) 87Sr/86Sr and trace element mapping of geosphere-hydrosphere-biosphere interactions: A case study in Ireland *Applied Geochemistry*, doi:10.1016/j/apgeochem.2018.01.007.

Scanlon B. et al (2005) Evapotranspiration estimates with emphasis on groundwater evapotranspiration in Texas, *Water Resources.*

Seita R., Gottschalk P., Smith P., et al. (2013) Soil salinity decreases global soil organic carbon stocks. *Science of the Total Environments 465* 267-272

Shalev N., Lazar B., Halicz L., Stein M.m Gavrieli I., Sandler A., Segal I. (2013) Strontium isotope fractionation in soils and pedogenic processes *Procedia Earth and Planetary Science (7)* 790-793

Shannak B., Corsmeier U., Kottmeier Ch., Al-azab, T. (2014). Wind tunnel study of twelve dust samples by large particle size. *Atmospheric Environment 98,* 442-453

Sobecki TM, Wilding LP. 1983. Formation of calcic and argillic horizons in selected soils of the Texas coastal prairies. Soil Science Society of America Journal 47: 707–715.

Squires V.R., and Glenn E.P. (2004) Salinization, Desertification and Soil Erosion. V.R Squires (Ed.), The Role of Food, Agriculture, Forestry and Fisheries in Human Nutrition, UNESCO, EOLSS Publishers, Oxford UK

Szynkiewicz A., et al. (2015) Isotopic studies of the Upper and Middle Rio Grande. Part 2- Salt loads and human impacts in south New Mexico and west Texas, *Chemical Geology*, 411, 336-35

Van der Hoven S.J. and Quade, J (2002) Tracing spatial and temporal variations in the sources of calcium in pedogenic carbonates in semiarid environment, *Geoderma*, 108, 259-276

Whipkey, C.E., Capo, R.C., Chadwick, O.A., Stewart, B.W. (2000) The important of sea spray to the cation budget of a coastal Hawaiian soil: a strontium isotope approach. Chemical Geology 168, 37-48.

Williams A. J., et al. (2013) Hydrogeochemistry of the Middle Rio Grande aquifer system – Fluid mixing and salinization of the Rio Grande due to fault inputs, *Chemical Geology*, 351, 281-298

Wong V. N.L., Dalal R.C., Greene, R.S.B. (2009) Carbon dynamics of sodic and saline soils following gypsum and organic material additions: A laboratory incubation. *Applied Soil Ecology 41* 29-40

Zamanian K., et al., (2016) Pedogenic carbonates: Forms and formation processes, *Earth-Science Reviews 157*, 1-17

Chapter 5: Using flow-through column experiments to study dynamics of CO_2 emissions and calcite accumulation in flood-irrigated sediments

1. INTRODUCTION

Exploding global populations have increased the demand of food production and arid-land agriculture is one of the major land-use changes in the world to accommodate a 70-100% increase in food demand (World Bank, 2008; Evans, 2009; Kearney, 2010, Gregory and George, 2011; Tilman et al., 2011). Arid-lands usually are characterized by high temperature and evapotranspiration rates, but low annual rainfall, and are challenged by salt buildup when employed for cultivation of salt-tolerant crops. Previous works have identified soil salinization as a global problem threatening sustainable food production and regional economy (Falasca, et al., 2014; Shrivastava & Kumar, 2015; Wang, et al., 2015). Arid-land agricultural practices in far-west Texas have led to soil salinization as a result of continuous flood irrigation using water of high total dissolved solids (TDS) and poor soil drainage (Cox et al., 2018; Ortiz et al., 2019a). Increased soil salinity diminishes crop production and is also thought to decrease microbial soil respiration and microbial community structures (Rath & Rousk, 2015; Wong et al. 2009).

The continuous flooding with irrigation waters contain elevated TDS leading to calcite precipitation in hot arid-land soils (Cox et al., 2018; Ortiz et al., 2018). Indeed, high evapotranspiration, driven by high temperature and dry air, concentrates irrigation waters, and leads to salt formation, especially calcite. Pedogenic carbonate, or secondary calcite ($CaCO_3$), is one of the most common minerals that precipitates in soils, following to Reaction 5.1. Stoichiometrically, one mole of CO_2 is produced and released into the soil for every mole of calcite precipitated. Thus, flood irrigation has been observed to be a major anthropogenic contributor to the modification of calcium and carbon cycles in west Texas and may also be important in global arid-land cultivation (Ortiz et al., 2018).

Reaction 5.1: $Ca^{+2}{}_{(aq)} + 2HCO^{-}_{3(aq)} \leftrightarrow CaCO_{3(s)} + CO_{2(g)} + H_2O_{(l)}$

Soils have been established to be important CO_2 reservoirs and emission of CO_2 from soils to the atmosphere is considered to be a major global C flux (Schlesinger and Andrews, 2000; Serrano-Ortiz et al. 2010; Bourges et al., 2012; Fernandez-Cortes et al., 2015). Multiple sources of soil-produced CO_2 include biogenic sources, such as root respiration, microbial basal respiration, respiration by autotrophs and heterotrophs (Kuzyakov, 2006). However, abiotic production of CO_2 can be accomplished through Reaction 1, and can be a dominating process in arid lands, which have lower organic matter and would also have lower biogenic CO_2 production. Because CO_2 is a ubiquitous green-house gas, the quantification of CO_2 emission through Reaction 1 is fundamental to determine the effect that arid-land agriculture can have on global or regional CO_2 production. Ortiz et al. (2018b) showed that calcite-sourced CO_2 in flood-irrigated fields was detectable by C isotopes during the growing season in pecan orchards near El Paso, Texas. The quantitative separation of biogenically respired versus calcite-sourced CO_2, however, proves difficult, as both biogenic soil respiration and calcite precipitation rates vary with time during an irrigation event, as functions of soil temperature and moisture content (Zamanian et al., 2016).

Many major variables control the magnitude of salt accumulation, including quantity and quality of water used for irrigation and soil texture-related permeability. Indeed, agriculture near the Rio Grande occurs in soils that form on abundant interfingerings of floodplain sediments (Hall and Peterson, 2013). Depth and thickness of fine textured sediments impact water drainage and flow, and thus depth and magnitude of salt accumulation. Therefore, soil texture is an important factor controlling the calcite formation (Ortiz et al 2018 a,b). In the southwestern U.S., the Rio Grande is the major desert river that provides freshwaters for agricultural use. Multiple natural and anthropogenic sources, including upwelling of basin brines, municipal wastewater and agricultural

runoff, increase the salinity of the river as it flows through its expanse (e.g., Williams et al 2013; Synkiewcz et al. 2015). Synkiewcz et al. (2015) has shown that the river waters near the El Paso, Texas region are already over-saturated with respect to calcite and near saturation for gypsum ($CaSO_4*2H_2O$). Projected climate variability including increased temperatures and reduced headwater snowmelt threaten the quantity and quality of Rio Grande waters (Borrok and Engle, 2014). The prolonged use of groundwater for agriculture will likely increase if there is diminished surface water availability in the Rio Grande valley (Sheng, 2014). However, groundwaters of the Middle-Rio Grande tend to have higher TDS and even become brackish with more pumping (Sheng, 2014; Nyachoti, 2016; Ortiz et al., 2019a). Therefore, a shift in irrigation sources from surface water to groundwater in response to drought will accelerate salt accumulation rates and can potentially have catastrophic effects on regional and local economies and soil ecology (Ortiz et al., 2019a). As an area of high crop-production in the southwestern United States, it is vital to determine the possible impacts that perceived changes in surface water chemistries or increased use of saline groundwaters for irrigation can have on calcite precipitation and CO_2 production. Furthermore, projected increases in temperature should increase the rate of evapotranspiration, soil solution concentration and salt precipitation.

With the threat of increased temperatures, decreased surface water availability, surface water salinity and soil salinization, it is important to examine the individual contributions that such future scenarios have on calcite precipitation and CO_2 production. To assess the complex and dynamic system of flood irrigation and inorganic carbon, while eliminating the biological processes that release soil respired CO_2, we ran a series of column experiments, free of organic matter and microbial activities, to simulate 1-dimensional (1-D) flow of irrigation water and its interaction with sediments and compared these to field measurements. To mimic agricultural fields

of varying soil textures, porosities and gas diffusivities, we focused on two contrasting and simple soil texture types (sand and clay). Furthermore, because flood irrigation is a widely-used irrigation method, we initiated flooding events of different levels of water salinity in flow-through column experiments to assess rates and magnitude of calcite precipitation and CO_2 production as a function of water chemistry dynamics. Our experiments were designed to explore the parameterization of calcite-induced production of soil CO_2 as a result of flooding with water of varying salinity. This is important as salinity is expected to increase as a result of groundwater usage or/and changes in climate.

2. METHODS

2.1. Experiment setup

A set of flow-through columns (80cm in height and 20cm in diameter) were prepared using industrial PVC pipe. Two Sand+Clay columns were packed using three layers of dry sediments: two layers of laboratory-grade quartz sand and one layer of clay in between (Figure 5.1). Both the top-sand and the middle-clay layers were 20 cm thick, while the bottom sand layer was 40 cm thick. The clay was granular bentonite clay, consisting of primarily montmorillonite with 90-100% purity and pH between 6 and 9. The weight of sediment for each layer was recorded and used to calculate bulk density and porosity (Table 5.1). A nest of sensors was placed into each column to record soil gas concentrations, moisture, temperature and electrical conductivity (EC) (Figure 5.1). In each column, one Apogee SO-110 Response Thermistor Reference Oxygen Sensor was placed at 30 cm depth. Two Vaisala GMT220 Carbon Dioxide probes and two Decagon 5TE sensors (for EC, moisture and temperature) were inserted at 15 cm and 30 cm, respectively. All sensors were sealed into the column with water-proof silicone glue. Both O_2 and CO_2 sensors were connected to a CR-1000 Campbell Scientific data logger, with a datum collection resolution per minute.

Campbell Scientific user-interface software Loggernet 4.5 was used to record and download datasets for O_2 and CO_2 sensors. Soil moisture, temperature and EC were logged in Decagon data loggers with datum collection resolution per minute. Data for the Decagon 5TE sensors was downloaded using the ECH2O software. Data analysis was conducted using R version 3.3.2 (2016-10-31).

An additional column was packed with 80 cm thick sand only (Figure 5.1). In the sand column, two Vaisala GMT220 Carbon Dioxide probes at 15 and 60 cm, plus three Decagon 5TE sensors (for EC, moisture and temperature) were inserted at 15, 30, and 60 cm.

After packing the porous media and sensors, all columns were allowed to equilibrate with the atmosphere for 2-3 days prior to the simulated flooding events. Three experimental treatments were defined by irrigation water composition (Table 5.1): de-ionized water (DI) in the sand column, and simulated river water of different chemistry (1RGW and 2RGW) in either of the Sand+Clay columns (Chemistry data in Table 5.1). Simulated river water was made by dissolving $CaCl_2$ and $NaHCO_3$ salts. Irrigation water in 2RGW column was twice as concentrated as that of 1RGW. Both were slightly oversaturated with respect to calcite (Table 5.1). Five liters of water was used for flood irrigation, and based on the dimension of the columns, this would be similar to the amount of water used for the field during each irrigation.

The DI-Sand experiment was run on a green-roof at the University of Texas at El Paso between August and October in 2016. Daily air temperatures in the green roof ranged from 35 to 45ºC. Local daily temperatures and air pressures were downloaded from the El Paso Airport weather station open source database available at www.wunderground.com. The DI-Sand experiment was run for 14 days after irrigation.

The 1RGW-Sand+Clay and 2RGW-Sand+Clay experiments were run in a non-climate controlled green-house at the Texas A&M Agrilife Extension in El Paso, Texas in summer 2018. Green-house temperature ranged between 22 and 68 ºC. Air pressures from the KTXELPAS108 weather station were used and downloaded from the same open source (www.wunderground.com). The 1RGW and 2RGW experiments were run for 90 days until the columns reached steady state and no observable changes in CO_2 flux were recorded.

Drainage water samples were only collected for the DI experiment, as it was the only experiment with water outflow from the bottom of the column. Time series of pH, EC and major cations were captured *in-situ* with sensors calibrated with 1413 µS cm^{-1} and 12.9 mS cm^{-1} standards (for EC) and pH 4 and pH 7 buffer solutions (for pH). CO_2 efflux from the columns was recorded daily ±1 hour from 12:00 P.M. with a Li-820 CO_2 gas analyzer with an opaque chamber, secured with duct-tape to ensure a closed system during measurements.

2.2 CO_2 flux calculation in the column

CO_2 flux (F_{CO2}) were calculated for flow-through column experiments with the CO_2 concentrations measured at 15cm and 30cm and using Fick's law of diffusion:

$$F_{CO2} = -D_s \frac{dC}{dz} \qquad \text{Equation 5.1}$$

Where D_s (m^2/s) and *dC/dz* are the gas diffusion coefficient and CO_2 concentration gradients, where *dC* is in mole and *dz* in m. The gas diffusion coefficient (D_s) was estimated according to Millington and Quirk (1961) and Xiao (2015):

$$D_s = (D_a) \frac{\varepsilon^{10/3}}{\Phi^2} \left(\frac{273.15+T}{295.15}\right)^{1.75} \qquad \text{Equation 5.2}$$

$$\Phi = 1 - \frac{\rho_b}{\rho_s} \qquad \text{Equation 5.3}$$

where D_a is the diffusion coefficient of free air ($16 \times 10^{-6} m^2 s^{-1}$); T is the soil temperature; total porosity, Φ, was calculated from the measured soil bulk density for each layer (ρ_b) and assumed particle density (ρ_s) for of 2.56 g cm^{-3} according to Equation 3. Air-filled pore space (ε), was calculated by the difference between total porosity (Φ) and volumetric water content (θ) from the 5TE soil moisture sensors:

$$\varepsilon = \Phi - \theta \qquad \text{Equation 5.4}$$

The CO_2 diffusion calculation will be validated by comparing to limited surface CO_2 efflux measurements collected by a LiCOR Li-820 infrared gas analyzer.

2.3. Converting bulk soil EC to pore-fluid EC

Change in fluid chemistry due to evaporation, dissolution and precipitation of secondary salts can be better understood by real-time variation in pore-fluid EC, which can be computed by bulk EC from the 5TE sensors (Hilhorst, 2000):

$$\sigma_p = \frac{\varepsilon'_{p} * \sigma_b}{\varepsilon'_b - \varepsilon'_{\sigma b=0}} \qquad \text{Equation 5.5}$$

Where, σ_p is the pore-water EC (dS m^{-1}); ε'_p is the unitless real portion of the dielectric permittivity of the soil pore-water; σ_b is the bulk EC (dS m^{-1}); ε_b is the real portion of the bulk soil dielectric permittivity, unitless; $\varepsilon'_{\sigma b=0}$ is the real portion of the dielectric permittivity of the dry soil. ε'_p can be calculated from the soil temperature by:

$$\varepsilon_p = 80.3 - 0.37 * (T_{soil} - 20) \qquad \text{Equation 5.6}$$

where T_{soil} is the soil temperature (^{o}C) at a given depth (either 15 or 30cm) and is also real-time data collected from the 5TE sensors. Furthermore, ε'_b is calculated using the raw VWC counts and converting these to bulk dielectric with a calibration:

$$\varepsilon'_b = \frac{\varepsilon_{Raw}}{50} \qquad \text{Equation 5.7}$$

$\varepsilon'_{\sigma b=0}$ is an offset term to represent the dielectric permittivity of dry soils, a generic offset of 4.1 is used.

2.4. Field Measurements

Our field site is located in the pecan farm of Rio Bravo Farms, Tornillo, Texas. Eight plots were selected, four of which were placed on soils where trees had visually stunted growth, referred to as Pecan_Fine and the other four in soils where trees were broad and lush, referred to as Pecan_Coarse. Each set of plots were set in a gradient of distance from their individual pecan tree trunks (Figure 5.2). Ortiz et al. (2019a) identified different textures between these two sets of plots and thus different amounts of salt buildup, including calcite contents. Ortiz et al. (2018b) analyzed soil gas samples from Pecan_Fine and Pecan_Coarse for C isotopes and pCO_2, and clearly identified calcite-derived CO_2 signature using keeling plot. Thus, these are well-characterized and constrained sites.

Dark chamber measurements were conducted using Li820, ten days after flooding, once the fields were dry enough for measurements for each of the eight plots in 2016. Daily measurements until the continuing flooding event occurred, approximately every 20 days and were taken approximately ±1 hour from 12:00 P.M. Furthermore, the soil near each tree was equipped with Decagon 5TE soil moisture, EC and temperature sensors at 15, 30, 60 and 120 cm.

3. RESULTS

3.1. DI-Sand experiment-the baseline control

Although all columns were open to drain at the bottom, only the sand-filled column had detectable water outflow and no ponding at the sand surface. Right after the irrigation, the pH was slightly higher than the inflow (5.8 to 7.6) as the waters flowed out of the column. Then, pH slowly declined and stabilized at 7.4. Electrical conductivity of the outflow water increased substantially

from 2.1 to 146 µS cm^{-1} at the measurement of the first outflow sample, then proceeded to ~90 µS cm^{-1} (Figure 5.3A).

3.2. Data from the sand-clay columns and pecan orchard

A leak in the 1RGW column at the 15cm depth sensor aperture led to the loss of ~2.54L in the 1RGW column during flooding. A leak in the 2RGW, at the same 15cm sensor aperture also occurred but was quickly stopped, losing 1.15L. After adding 3L out of a total of 5L of water, ponding began to occur in both columns. Total ponded water was found by calculating the volume of a cylinder, whereby we used the height of the water and multiplying it by pi and the radius squared. For, 1RGW treatment, only 0.86L was standing above the sediments, and then infiltrated over the course of 24 hours. For the 2RGW treatment, the water was ponded for approximately six days, with a maximum of 2.35L water on the first day. The pH and EC of this ponded water increased after 6 days, as evaporation concentrated pond-water chemistry (Figure 5.3B).

Soil Water

Volumetric water content (VWC) increased immediately after flood irrigation both in the field and in all column experiments (Figure 5.4). The infiltration of soil water diminishes the gas-filled pore space in the top-sand and soil layers for all column and field measurements. For the sand column, water drained quickly, and VWC remained relatively constant at each depth; soil moisture only decreased slowly with time at the shallow depth of 15 cm (Figure 5.4A). The VWC behaved similarly in the sandy layer of the Sand+Clay columns (1RGW and 2RGW) and in the top-soil of the pecan orchard; however, pecan soils reached field-capacity sooner than the column experiments (~10 days after flooding in pecan fields versus ~30 days after flooding for 1RGW and 2RGW) (Figures 5.4B and 5.4C). This is probably due to combination of different factors, including amounts of water used for irrigation, water lateral flow, texture, and also the transpiration

in the pecan orchard that uses up water quickly. The VWC for clay layers in the 1RGW and 2RGW columns increased slowly over time and reached maximum values approximately 20 days after flooding (Figure5. 4B). At the 2RGW column, the clay layer might even have reached saturation, as the highest VWC was over 0.5 m^3/m^3, close to total porosity estimated using bulk and particle densities (Table 5.1; Figure 5.4B).

The amount of water that infiltrated into each sand and clay layer for every column was quantified using VWC and dimension of the sediment layers. At the end of the experiments, all water remained in the column (2.46 L for the 1RGW irrigation scenario and 3.85L in 2RGW irrigation scenario) (Figure 5.4D). Not surprisingly, within each column, almost all water was in the clay layer (1.28 L in 1RGW and 3.08 L in 2RGW) instead of sand layer (0.14 L in both 1RGW and 2RGW). This exercise indicates that 52% was held in the clay layer, and 1% in sand for 1RGW column, and thus 1.18 L was evaporated (or 47%), mostly from the surface sand layer. In the 2RGW column, 80% of total water added to the column remained in the clay, losing only 0.77L by evaporation, or 20%.

Pore-Fluid EC

Bulk EC for the sand column with DI irrigation was less than 0.01 ds/m, falling below the detection limit of the EC sensors. The pore-fluid EC for sediments in the Sand+Clay columns (1RGW, 2RGW) and the shallow soils in the pecan orchard (15 cm at Pecan_Fine and Pecan_Coarse sites) were calculated from bulk soil EC according to Equations (5.5) through (5.7). The pore-fluid EC followed similar trends in the Sand+Clay columns between two irrigation scenarios (Figure 5.5A). The pore fluid EC increased sharply at the top-sand layers, reaching a maximum of 73 dS/m for 2RGW and 10 dS/m for 1RGW. After the recorded peaks, pore-fluid EC decreased to negative values in the sand layer, which were not realistic. So, we assumed that a

threshold moisture level was reached and the constants in equations (5.5) to (5.7) were not reasonable. Pore-water EC at the clay layers behaved similarly between 1RGW and 2RGW columns, and had a slow increase with time. Pore-fluid EC increased linearly for both clay layers, reaching 3 dS/m at the end of the experiment. The pore-fluid EC calculated at the beginning of the irrigation agreed reasonable well with the EC values measured on the irrigation water used in 1RGW and 2RGW columns (Figure 5A; Table 5.1).

In the pecan orchard, pore-fluid EC showed inverse trend as soil VWC: a decrease in EC upon flooding, followed by an increase after water drying up (Figure 5.5B). Although from the same depth (15 cm), the pore fluid at the Pecan_Fine site had much higher EC values than that at the Pecan_Coarse site. As discussed in Cox et al. (2018) and Ortiz et al. (2018), this was due to initial dissolution of evaporite salts, such as gypsum, halite and calcite that have been previously accumulated; then afterwards, salt precipitated out, keeping the pore fluid EC relatively constant.

CO_2 concentrations in the column experiments

The pCO_2 concentrations, daily noon averages, were reported for Sand+Clay columns for two depths (15 cm, sand layer, and 30 cm, clay) in Figure 6. With irrigation, pCO_2 at the 15-cm increased sharply in both 1RGW and 2RGW experiments, dropped to background levels after 20 days, and then increased slowly over time after that. The pCO_2 at the 30 cm also increased in response to irrigation, but did not drop to the background levels until the end of the experiments.

Calculated and measured CO_2 efflux for the column experiments

Calculated CO_2 efflux (F_{CO2}) data for the Sand and Sand+Clay columns were calculated using Equations (5.1) through (5.4) and presented in Figure 5.7. In the Sand experiment, CO_2 diffused from shallow soils (15cm) to atmosphere upon flooding and F_{CO2} exhibited a large peak and then stabilized at ~40 mol/m2/min (Figure 5.7A). The F_{CO2} from 60 cm to 15 cm was much

higher and also increased with time to reach ~300 mol/m2/min towards the end of the experiment (Figure 5.7A). For the Sand+Clay column with 2RGW irrigation, CO_2 was concentrated from 15 cm (sand) to 30 cm (clay) during initial flooding, when water was ponded, as observed by a negative F_{CO2} peak (Figure 5.7C). Following that, CO_2 slowly moved back from clay layer to the sand layer but positive F_{CO2} decreased over time. This negative peak in F_{CO2}; however, was not observed in 1RGW scenario, probably because of the leak. But still, water infiltration to clay was shown to push the gas CO_2 out to the sand layer above. This F_{CO2} decreased too, like 2RGW (Figure 5.7C). The CO_2 emission from sand layer to atmosphere showed a large peak in the 2RGW scenario, as water pushed gas out of the column (Figure 5.7B). After that F_{CO2} decreased to almost zero, and then showed two small peaks. In the 1RGW scenario, no large peak was observed; instead, F_{CO2} gradually increased with time and stabilized at ~20 mol/m^2/min.

F_{CO2} efflux was measured for the Sand and Sand+Clay columns and in the pecan field using chambers around noon (Figure 5.8). The measured and calculated F_{CO2} showed the same trend: Bi-directional movement from soil to atmosphere and also from atmosphere to soil; however, they were different by one order of magnitude (Figure 5.8A). F_{CO2} from Sand+Clay columns to atmosphere showed similar trends for 1RGW and 2RGW scenarios, much higher than calculated F_{CO2} (Figure 5.8B). Approximately 14 days after the simulated flooding, both 1RGW and 2RGW columns had large peaks in CO_2 efflux (~600 mol/m^2/min) that lasted seven days of the experiment. Cumulative curves of the FCO_2 efflux showed that the 1RGW column emitted more CO_2 than the 2RGW column at the end of the experiments (Figure 5.9).

If soil respiration is the dominant contributor of soil CO_2, then we expected that CO_2 efflux was higher at the Pecan_Coarse site and also near the tree at each site, where pecan trees are more productive. However, the maximum CO_2 efflux varied among eight sites in 2015 (Figure 5.8D):

highest observed at the Pecan_Fine site and lowest at the Pecan_Coarse site. At each site, the highest efflux was not detected near the pecan tree; instead it was between trees. These observations suggested that soil respired CO_2 might not be the dominant source of 1D CO_2 efflux and pedogenic CO_2 is as important. Horizontal transport of CO_2 should further be explored to determine controlling sources (biotic or abiotoc) of soil CO_2.

For year 2016, F_{CO2} data were collected from three irrigation events (Figure 8E) and four measurements at each site was also averaged (Figure 8C). For the first two irrigation events, F_{CO2} showed large peaks, but for the last irrigation even, F_{CO2} decreased sharply, although the overall fluxes were similar in size and all data collection was carried out one week after each irrigation (Figure 8C).

4. DISCUSSION

Sand and bentonite clay were selected due to their difference in characteristic water and gas transport. Sand facilitates gas diffusion and water and infiltration, but clay tends to be relatively impermeable layer over which, water retains and evaporates, calcite precipitates and CO_2 is released. Over time, calcite buildup lowers permeability and forms caliche hardpan in natural drylands. In the column experiments, contrasting properties of sand and clay play a significant role in controlling the CO_2 production and transport. Indeed, we will focus on three processes that govern CO_2 emission from soils to atmosphere, regardless in the columns or in the flood-irrigated pecan field: 1) water-atmosphere gas exchange during initial irrigation and ponding, 2) the release of trapped soil CO_2 when the water-seal dries and 3) calcite-induced CO_2 emission. The effective time-line for both columns can be clearly observed in the cumulative curves for 1RGW and 2RGW efflux measurements (Figure 9), as discussed below. All of these physical or chemical processes

are dynamic, controlled by the moisture conditions. Even soil respiration in the pecan orchard is known to be much higher in optimum soil moisture contents.

4.1. Physical controls on CO_2 movement

As water infiltrates each column after irrigation, we observed upward and downward gas movement. Upon flooding, simultaneous pushing towards the atmosphere occurs as water infiltrate the sand and displace pore-gas. Downward movement follows as soil CO_2 is pushed from the top sand layer into deeper pores in the clay layer. This thrust effectively traps the gas in the column. (Figure 5.7). As a consequence, pCO_2 in both sand and clay layers increase sharply, especially in 2RGW column (Figure 5.6), typically accompanied by decrease in pH of DI+Sand outflow, where outflowing water pushed CO_2 downward, while also allowing higher CO_2 to dissolve into the DI water (Figure 5.3A). After this, pCO_2 at 15 cm quickly returns to background level while pCO_2 at 30 cm remains high (Figure 5.6). The physical draining of surface water and evaporation of highly permeable sands, allows these to equilibrate with the atmosphere sooner as pore-gas connectivity with the atmosphere increases. This agrees with what Xiao et al. (2015) and Hashimoto and Komatsu (2006) have observed higher pore-gas connectivity with the atmosphere at surface soils than in deeper soils.

Ponding was not observed in the sand column due to its high porosity. As DI water quickly drained, soil moisture content decreased and stabilized at both 15 and 60 cm depths and gas-filled pores were abundant (Figure5. 10). Moisture was almost constant at 60 cm, but decreased slowly at 15 cm depth in sand due to evaporation for the sand column. Furthermore, temperature, air pressure (not plotted), and moisture show diurnal cycles, impacted by atmosphere conditions as this experiment was carried out on a roof. Consistently, higher F_{CO2} efflux is observed at Sand experiment, possibly as a result of the unimpeded atmospheric pressure pumping (Figure 5.7A).

Whereby, diurnal changes in barometric pressure physically displace CO_2 in and out of the sediment profiles.

This recorded water-atmosphere exchange could be the result of $HCO_3^{-}{}_{(aq)}$ actively degassing into CO_2 gases (both 1RGW and 2RGW waters were saturated with respect to $CaCO_3$ and had pH>5) (Liss, 1973). An additional source of water-atmosphere exchange could be pore-CO_2 bubbling up as infiltrating waters displace stored gases. The 1D fluid flow in the columns is certainly different from field gas and water movement, where lateral transport can also occur and requires further investigation

High pH can represent increased water salinity from calcite precipitation and NaCl*(aq)* concentration. This can mean decreased water pCO_2 of waters and increased CO_2 flux (Garcia-Luque et al., 2005). We observed increase pond-water pH before complete evaporation and infiltration (Figure 5.3A), which would help explain our efflux measurements from 1RGW and 2RGW pond waters.

Field efflux measurements were not taken immediately after flooding; therefore, we cannot confirm the gas-exchange of the water-atmosphere interphase or that initial displacement of soil CO_2 into the atmosphere occurs as water fills pore-spaces, but expect similar trends to have occurred. It is also possible that when the pecan orchard is flooded, ponded water acts as a carbon sink during the day and as a source of CO_2 at night if sufficient opportunistic algae or macrophytes are present. Bolpagni et al (2007) observed that estuarine waters became CO_2 sinks during daylight hours, as macrophytes take up atmospheric CO_2 for photosynthesis and turn to CO_2 sources at night, as they respired.

4.2. Drying of the water seal

Without transpiration in the columns, evaporation becomes dominant in removing water from the system. In the Sand+Clay experiments, it was roughly estimated that at least 20% of water was lost after 2 months of experiments, through the top sand layer. If so, pore spaces previously sealed with waters open up, allowing CO_2 to escape from sand to atmosphere. As observed by Gaumont-Guay et al. (2006), Guntinas et al. (2009), Hashimoto and Komatsu (2006), Pla et al (2017), and Yu et al., (2017), high volume of pore-waters diminishes pore-gas movement, particularly if soil water is greater than the field-capacity of soils. It is only after soils reach field capacity, and lose the water seal, that trapped CO_2 can be released. At this time step, pCO_2 quickly dropped to atmospheric level in the sand layer (15 cm; Figure 5.6), sending a large flux of CO_2 to atmosphere (Figure 5.7B; Figure 5.8B). Indeed, approximately 10 days after flooding CO_2 efflux measurements show peaks of the same magnitude (38-731 mol m^{-2} min^{-1}; 6/19/18 to 7/3/18) in both Sand+Clay columns even with different irrigation chemistry (1RGW and 2RGW). Cumulative measurements of CO_2 efflux show approximately 7800 mol/m^2/min emitted for 1RGW and approximately 6500 mol/m2/min for the 2RGW experiments (Figure 5.9). In addition, the infiltration of water from sand to clay layer continues to release air, including CO_2, from clay to sand. Bentonite is an expansive clay and can shrink and swell depending upon moisture conditions. With wetting, pore-water may physically trap CO_2, adding another physical control on gas movement.

4.3. Calcite precipitation and CO_2 emission

The irrigation waters used in both Sand+Clay experiments are slightly oversaturated with respect to calcite (Table 5.1; SI=0.4 for 1RGW and SI=1.8 for 2RGW). With continuous evaporation, pore-fluid EC at 15 cm in the sand layer begins to increase, driving calcite to precipitate and CO_2 to form according to Reaction 1 (Figure 5.5A). This is confirmed by calculated

and measured F_{CO2} (Figure 5.7B; Figure 5.8B; Figure 5.9). Indeed, FCO_2 is positively correlated with pore fluid EC at 15 cm of both Sand+Clay columns (Figure 5.11A), as calcite precipitation is driven by oversaturation of pore fluid and accompanied by CO_2 emission. Such a correlation is not strong and even negative in 30 cm or the clay layer (Figure 5.11B), suggesting that water infiltration is the dominant factor to move CO_2 instead of calcite precipitation. This is reasonable as evaporation drives water loss primarily out of the surface sand instead of the deep clay layer.

Data from 1RGW and 2RGW experiments however show two separate clusters in Figure 11A. This difference could be due to (1) the amount of water that is leaked, (2) the chemistry of irrigation water and (3) amount of evaporation that is lost. Due to leakage, the Sand+Clay column with 1RGW received less water than that with 2RGW; irrigation water with 1RGW is also half concentrated than that with 2RGW. Furthermore, the pore-fluid EC in 1RGW column was much lower than that in the 2RGW column, and thus less oversaturated. Collectively, the 1RGW column received lower amounts of dissolved Ca^{2+} and HCO_3^- than the 2RGW column, consequently the magnitude of calcite to precipitate in 1RGW column is expected to be much less noticeable and measurable. However, within the uncertainty, pCO_2 or F_{CO2} in the 2RGW column were not significantly higher than those in the 1RGW column (Figure 5.7B; Figure5. 8B; Figure 5.9; Figure 5.11). This might be due to the higher amount of water that is lost to evaporation.

4.4. Calcite precipitation and CO_2 emission in the field

For the pecan orchard, the top soil at 15cm from Pecan_Fine and Pecan_Coarse sites has similar soil moisture content before irrigation and reaches the same level after an irrigation event in three weeks, much faster than the column experiments (Figure 5.4C). Soils with finer texture (Pecan_Fine) have higher soil moisture content at saturation and also stay saturation longer than those with coarser texture (Pecan_Coarse). Thus, drying due to evapotranspiration loses more

water in Pecan_Fine soils. Indeed, the vegetation in the orchard will uptake soil water, drastically diminishing excess soil water, a process excluded in our column experiments. Abudu et al. (2016) estimated that pecan trees have an ET ranging from 1054-1167 mm per growing season. The soils have higher salinity and soil waters have higher pore fluid EC, driving more calcite precipitation at the Pecan_Fine site, as observed by soil analyses in previous chapters (Figure 5.5B). Thus, we expect to observe higher calcite-derived CO_2 emission in Pecan_Fine as shown in Figure 5.8C. However, soil respiration contributes CO_2 as well, thus F_{CO2} is controlled by both biological and abiotic process (Figure 5.8). Ortiz et al (2018b) analyzed soil gas CO_2 and showed using C isotopes that is a mixture of soil respired, calcite-derived and atmospheric CO_2.

The main differences in magnitude of F_{CO2} efflux between our greenhouse experiments and field measurements include temperature, biotic soil respiration and a much higher soil reservoir of calcites undergoing dissolution and precipitation. Ma et al. (2013) had detected high abiotic soil respiration rates as a result of the capacity of saline soils to emit or consume pedogenic carbonates. Furthermore, purely physical controls of CO_2 movement as a result of pressure pumping (Sanchez-Canete et al., 2013) and CO_2 dissolution and effusion from soil waters (Fa et al., 2016) can and should be considered as an important natural process that is augmented by salt loading through irrigation, such as dryland agricultural fields that are saline, rich in pedogenic carbonates.

4.5. Future directions

F_{CO2} data measured by LI820 and calculated by diffusivities using Equations 5.1 and 5.2 are different by several orders of magnitude. This difference is due to different time scales, but most likely the *Ds* calculation, that did not take texture into consideration. As a result, diffusion coefficient (*Ds*) was not that different between sand and clay. Concentration gradients should be better constrained using different boundary conditions at the sand/clay interface. When bulk soil

EC is converted to fluid EC, negative values were derived at relatively dry conditions, so either threshold behaviors are reached or different empirical values should be used. We propose that future work should consider the Brovelli and Cassini (2011) model. This study identified water loss through evaporation as an important parameter to control the soil moisture content, pore-water chemistry and therefore, the calcite precipitation and CO_2 production. Existing empirical models can be used and estimate evaporation rates.

To further characterize our experiments, gas samples can be collected to verify sensor CO_2 concentrations and trace $\delta^{13}C$. Soil samples could also be collected to physically observe calcite accumulations to facilitate mass-balance. Such data could provide information on gas movement, sources of CO_2 and driving mechanisms of calcite precipitation. In addition, multiple irrigation events can be administered to evaluate if calcite precipitation rates and CO_2 effluxes vary with more events.

5. CONCLUSION

The oversaturation of calcite in irrigation waters from the Rio Grande and ground water sources, lead to the precipitation of pedogenic calcite and consequently, emission of abiotic CO_2. However, with contribution of soil respired CO_2, it is almost impossible to study what controls the magnitude of calcite-derived abiotic CO_2 and how it will change in future scenarios. Here we studied CO_2 movement and production after flood-irrigation without interference of biological processes using flow-through columns, packed with different layers of sand and clay. Artificial irrigation solutions of different concentrations of dissolved calcium and bicarbonate were used but all were oversaturated with respect to calcite. CO_2 fluxes from this experiment are showed to be controlled by physical trapping and release due to water ponding, but also calcite-induced CO_2 emission, as water loss through evaporation increases pore-fluid EC and drives more

oversaturation. Similar CO_2 efflux data are collected from two sites in the pecan orchard, even though these sites are characterized by contrasting soil texture, salt buildup, and primary productivity of pecan trees and expected to have different soil respiration rates. Furthermore, within each site, CO_2 efflux does not simply decrease with a distance away from pecan trees. Both observations point to the importance of calcite-derived CO_2, and this is in agreement of C isotope data from soil CO_2 that shows soil CO_2 is from all three sources, soil respiration, calcite precipitation and atmosphere input.

Table 5.1. Characteristics of porous media, irrigation water, and columns in the flow-through experiments

Porous Media				
	pH	**EC (μS/cm)**	**TOC (%)**	**Grain Size (μm)**
Sand (SiO_2)	8.74	294.8	0.25	125-250
Clay (Bentonite)	9.09	2277		<3.90

Irriation Chemistry					
	pH	**EC (μS/cm)**	**$NaHCO_3$ (mg/L)**	**$CaCl_2$ (mg/L)**	**Saturation index (calcite)**
DI	6.27	2.15	0	0	0
1RGW	7.28	585	350	231	0.4
2RGW	7.22	1162	699	6461	1.8

Columns		
	Bulk density (g/cm^3)	**Porosity***
DI		
Sand	1.29	49.7%
1RGW		
Sand	1.86	27.0%
Clay	0.85	66.4%
Sand	1.01	60.3%
2RGW		
Sand	1.77	30.8%
Clay	0.85	66.4%
Sand	1.1	56.8%

* Porosity was calculated assuming particle density of 2.56 g/cm^3

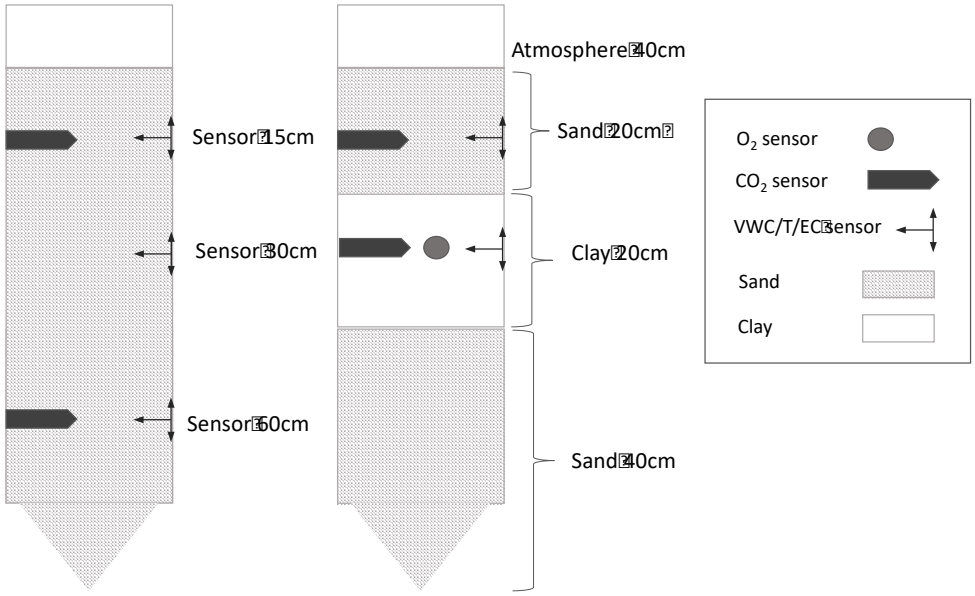

Figure 5.1. Experimental set-up of flow-through columns packed by different sediments (Sand, Left; Sand+Clay, Right). *Not to scale.

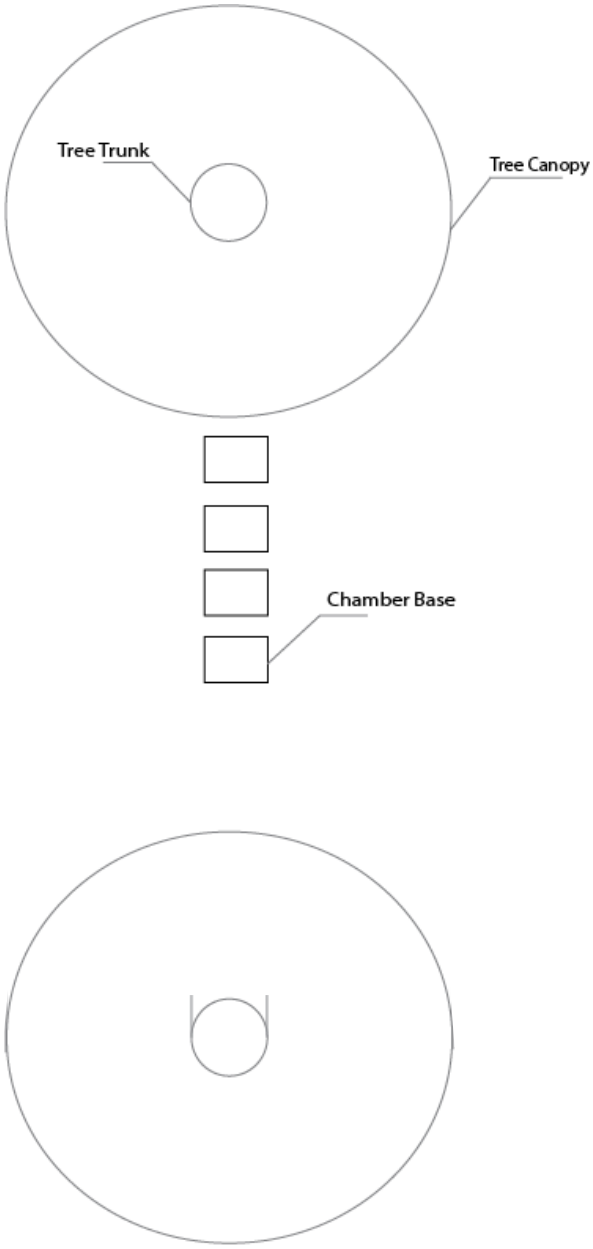

Figure 5.2. Diagram illustrating four sites between two trees in the pecan orchard, where F_{CO2} was measurements. Two sets of sites were selected: Pecan_Fine and Pecan_Coarse with different sizes of tree trunk and canopy. *Not to scale

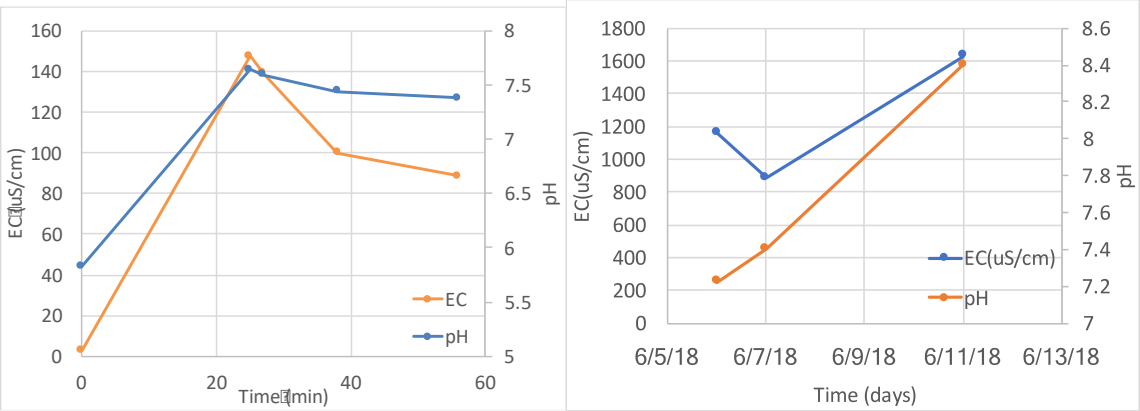

Figure 5.3. Changes in pH and EC with time in the outflow water of the DI+Sand experiment (A) and in the ponded water of the 2RGW Sand+Clay experiment (B).

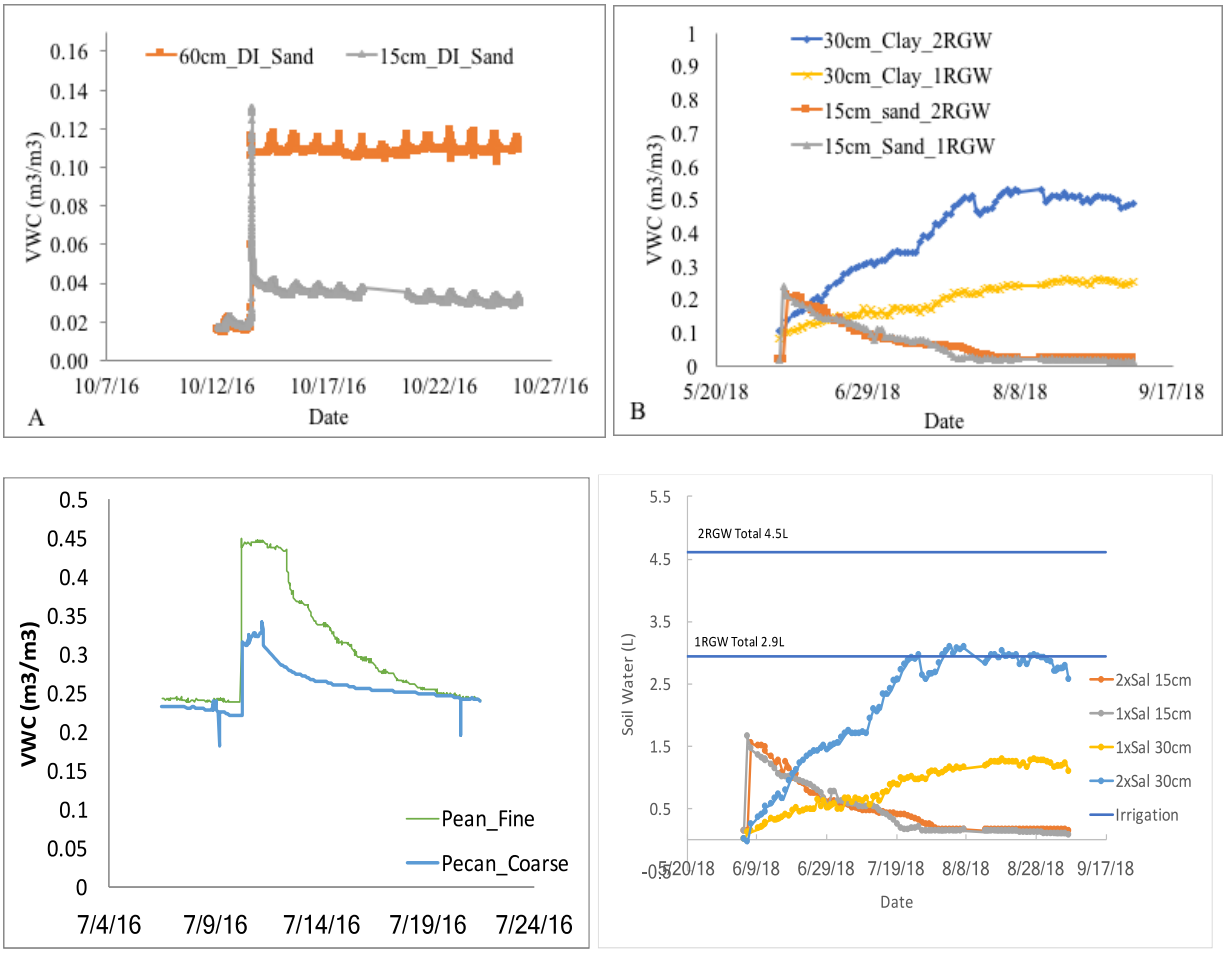

Figure 5.4. Volumetric water content in the DI+Sand column (A), Sand+Clay columns (1RGW, 2RGW) (B), pecan soils (15 cm) as a function of an irrigation event. Also plotted is amount of soil water in sand (labelled as 15 cm) and clay (labelled as 30 cm) for 1RGW and 2RGW with time. The horizontal reference lines indicate the total amount of water used for irrigation.

A.

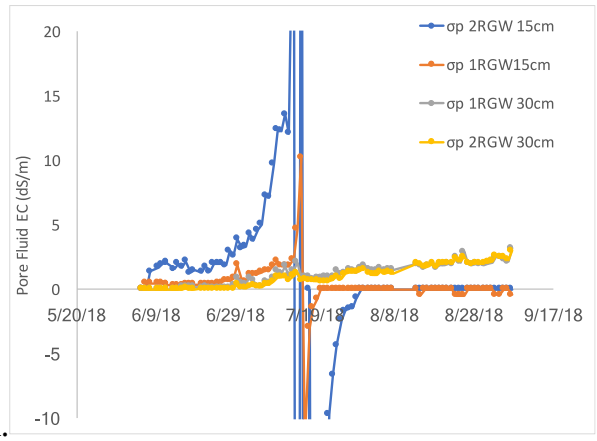

B.

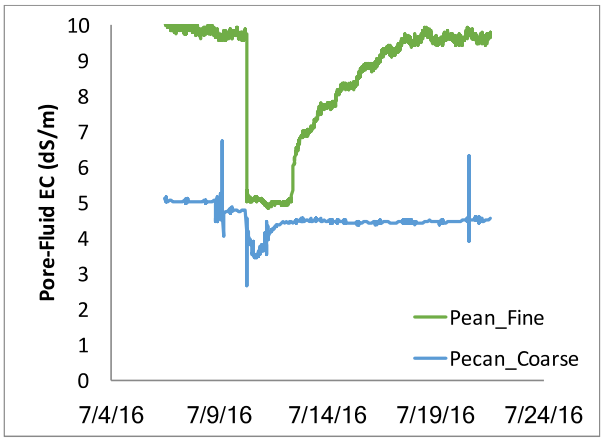

Figure 5.5. Pore fluid EC as a function of time after one irrigation event for 1RGW and 2RGW Columns (A) and the pecan soils of the Pecan_Fine and Pecan_Coarse (15 cm, B).

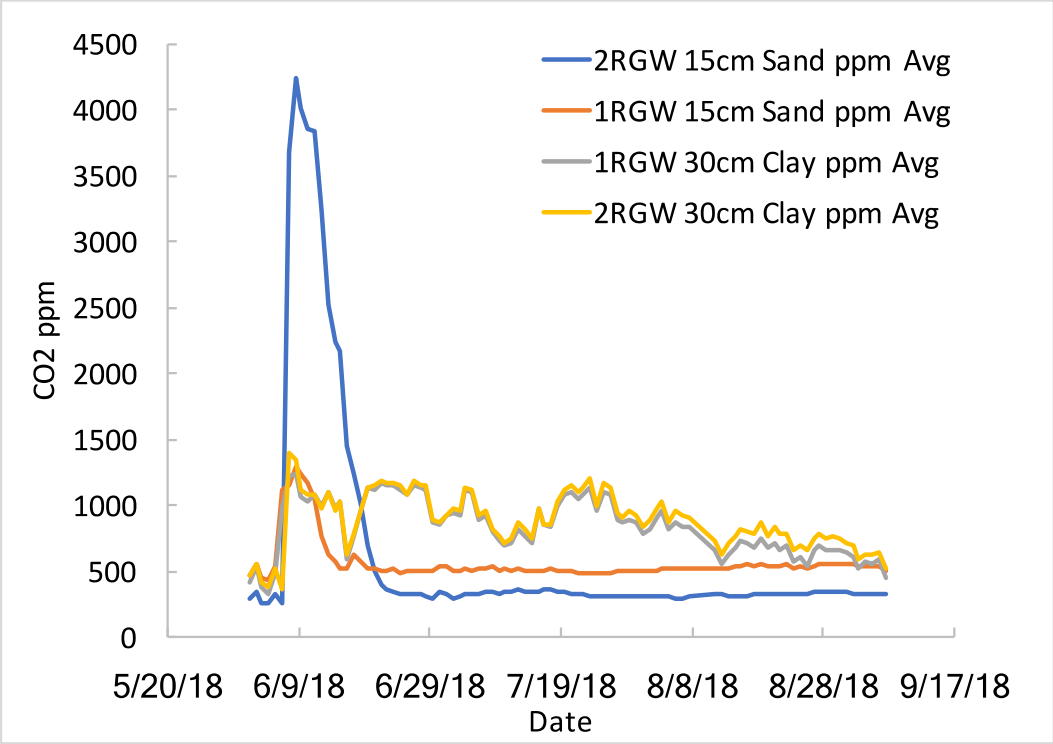

Figure 5.6. pCO_2 as a function of time after irrigation for the Sand+Clay column experiments.

A.

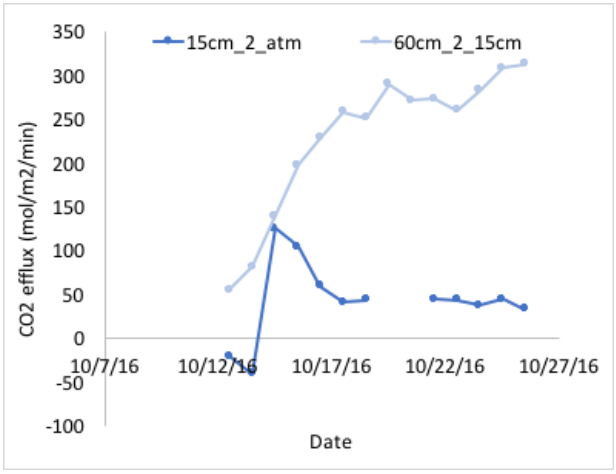

B.

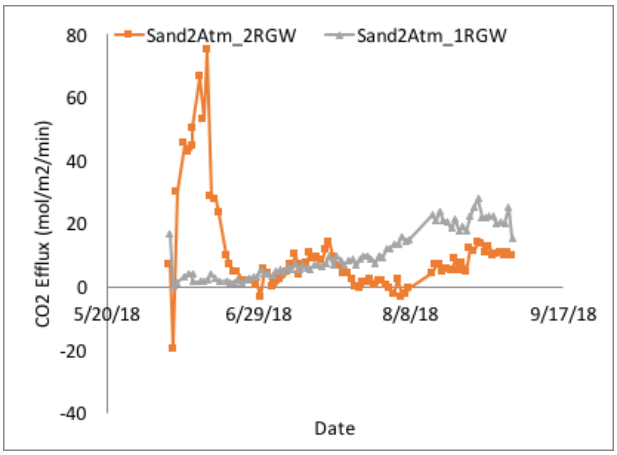

C.

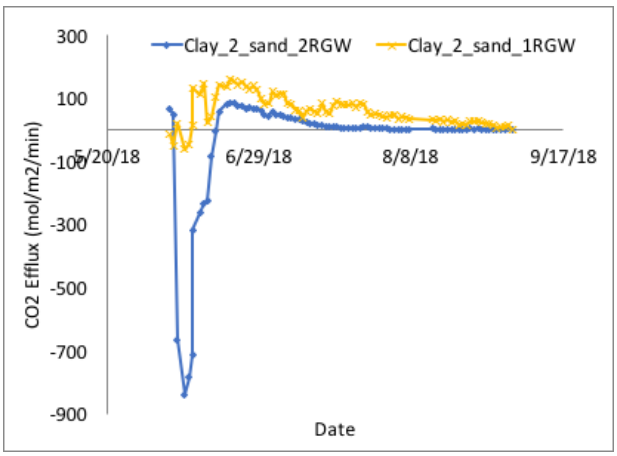

Figure 5.7. Calculated FCO_2 for DI+Sand column (A), for 1RGW and 2RGW columns from 15 cm sand to atmosphere (B) and from 30 cm clay to 15 cm sand (C).

A.

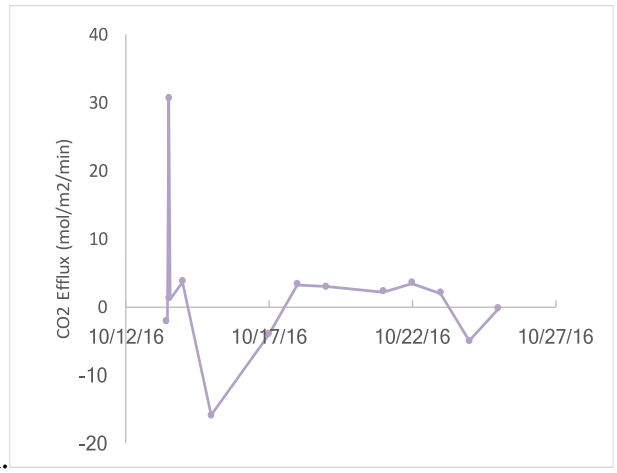
40
30
20
10
0
-10
-20
CO2 Efflux (mol/m2/min)
10/12/16
10/17/16
10/22/16
10/27/16

B.

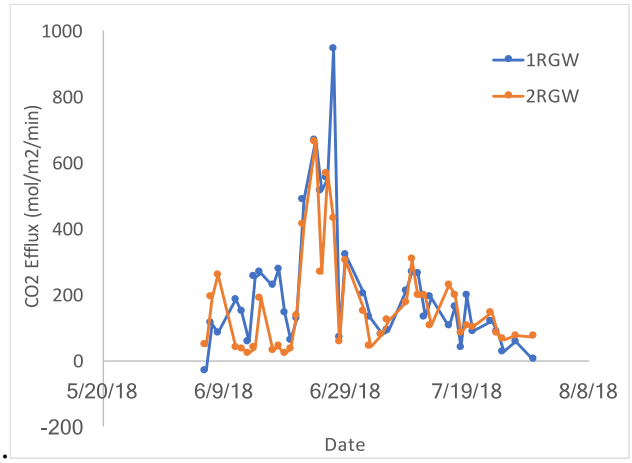
1000
800
600
400
200
0
-200
CO2 Efflux (mol/m2/min)
1RGW
2RGW
5/20/18
6/9/18
6/29/18
7/19/18
8/8/18
Date

C.

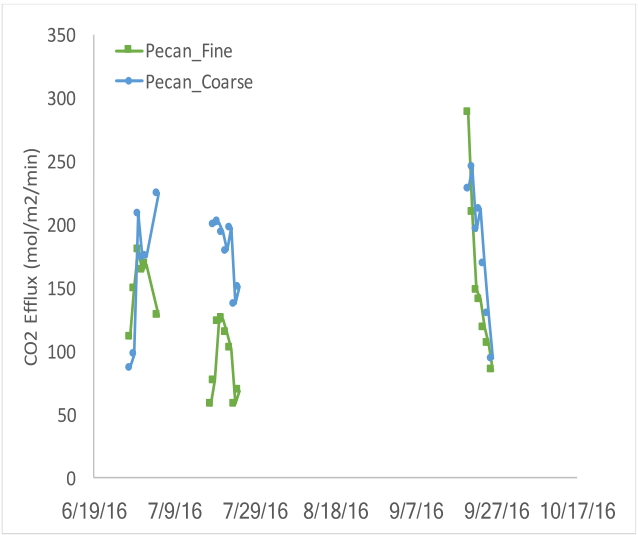
350
300
250
200
150
100
50
0
CO2 Efflux (mol/m2/min)
Pecan_Fine
Pecan_Coarse
6/19/16
7/9/16
7/29/16
8/18/16
9/7/16
9/27/16
10/17/16

D.

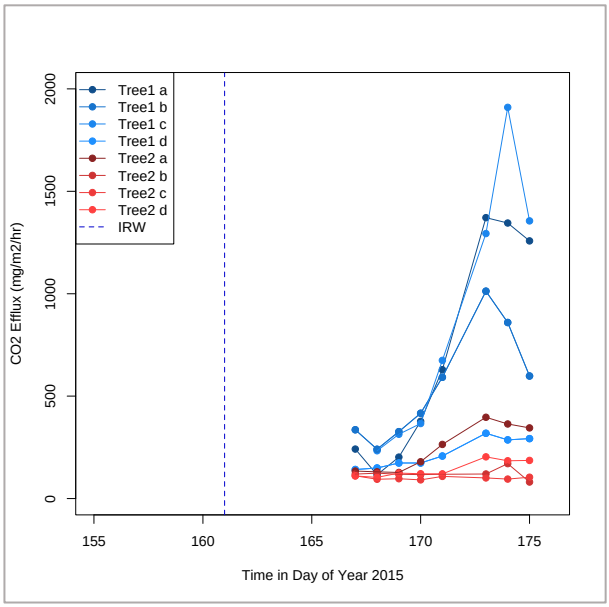

E.

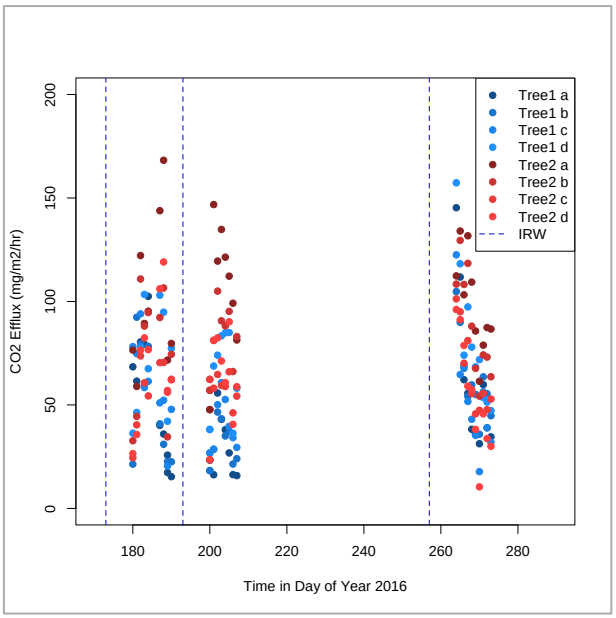

Figure 5.8. measured CO_2 efflux (F_{CO2}) for DI+Sand column (A), Sand+Clay columns (1RGW and 2RGW, B). F_{CO2} at the pecan orchard, averaged over 4 locations at the Pecan_Fine and and Pecan_Coarse sites (C) as well as at individual location for year 2015 and year 2016 (D, E). Tree1 and Tree2 correspond to Pecan_Fine and Pecan_Coarse, respectively. Furthermore, alphabetical labeling refers to roughly 1m distance from the base of the tree (a) to 4m from the base of the tree (d). Dashed vertical lines correspond to irrigation events.

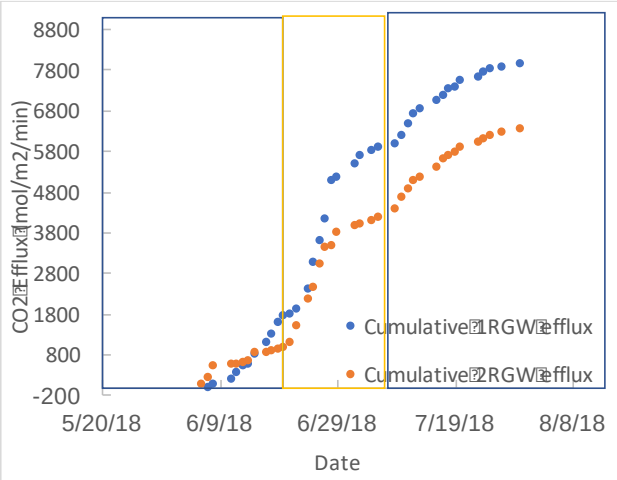

Figure 5.9. Cumulative curves of CO_2 efflux for 1RGW and 2RGW columns. The highlighted areas separate the three main times of CO_2 emission: water-atmosphere gas exchange (grey), drying of the water seals (yellow), and calcite-induced CO_2 emission (blue).

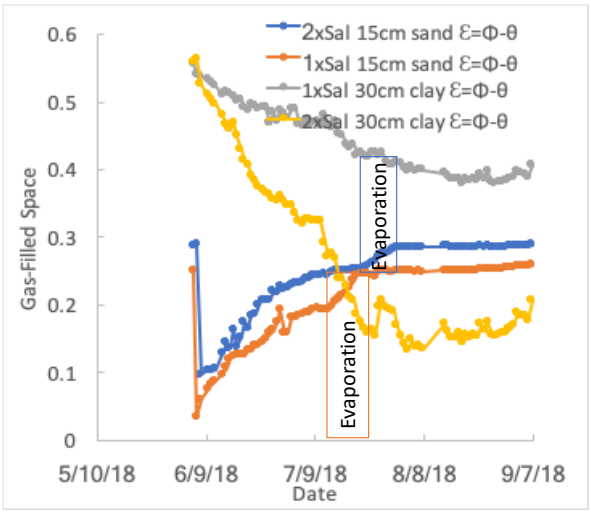

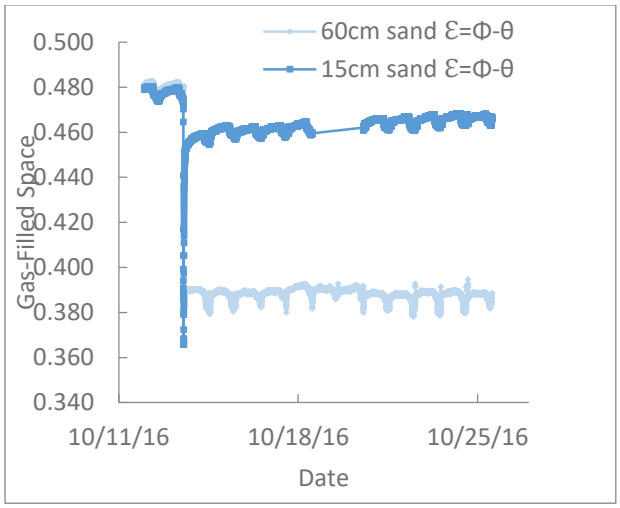

Figure 5.10. Change in gas-filled pore space of the Sand+Clay columns (1RGW and 2RGW; A) and the Sand column after irrigation (B). In the Sand+Clay columns gas-filled pore space increases as evaporation ensues for the sand layer, and stablizes approximately 30 days after flooding. For the clay layer, gas-filled pore space continues to decrease as water infiltrates and also stablizes approximately 30 days after irrigation. For the Sand column, gas-filled pore space decreases immediately after flooding for both depths, inceases within a day for both depths of 15 cm and 60 cm, and then remains low for the remainder of the experiment with diurnal fluctuation.

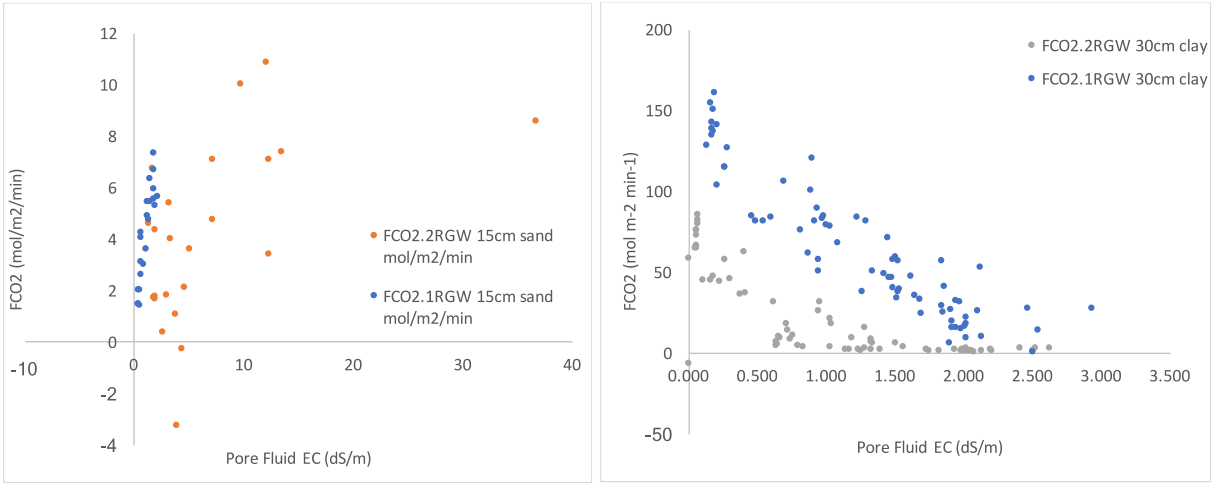

Figure 5.11. Correlations between pore-fluid EC for A) sand layers and B) and clay layers for 1RGW and 2RGW.

REFERENCES:

Bolpagni R., Pierobon E., Longhi,D., Nizzoli D., Bartoli M., Tomaselli M, Viaroli P., (2007) Diurnal exchanges of CO2 and CH4 across the water-atmosphere interphase in a water chestnut meadow (*Trapa natans* L.) *Aquatic Botany 87,* 43-48

Borrok, D.M., Engle, M.A. (2014) The role of climate in increasing salt loads in dryland rivers. Journal of Arid Environments 111, 7-13

Brovelli A. and Cassiani G. (2011) Combined estimation of effective electrical conductivity and permittivity for soil monitoring. *Water Resources Research 47,* W08510, doi:10.1029/2011WR010487

Cox C. et al. (2018) Soil quality changes due to flood irrigation in agricultural fields along the Rio Grande in western Texas. Applied Geochemistry 90, 87-100

Evans A. (2009), The Feeding of the Nine Billion: Global Food Security for the 21st Century, Chatham House report, 61 pp., The Royal Institute of international Affairs, Chatham House, London, U. K. [Available at http://www.chathamhouse.org.uk/publications/papers/view/-/id/694/.]

Fa K.Y., Zhang, Y.Q., Wu, B., Quin, S.G., Liu, Z, She, W.W. (2016) Patterns and possible mechanisms of soil CO2 uptake in sandy soil, *Science of the Total Environment 544,* 587-594

Falasca S.L., Ulberich A., and Acevedo A. (2014) Identification of Argentinian saline drylands suitable for growing Salicornia bigelovii for bioenergy, *International Journal of Hydrogen Energy* 39, 8692-8689

Garcia-Luque E., Forja J.M., Gomez-Parra A. (2005) Characterization of atmosphere-water exchange processes of CO2 in estuaries using dynamic simulation. *Journal of Marine Systems 58,* 98-106

Gaumont-Guay et al. (2006). Interpreting the dependence of soil respiration on soil temperature and water content in a boreal aspen stand. *Agricultural and Forest Meteorology 140,* 220-235

Gregory, P. J., and T. S. George (2011), Feeding nine billion: The challenge to sustainable crop production, *J. Exp. Bot*., 62, 5233–5239.

Guntinas M.E., Gil-Sotres F., Leiros M.C., Trasar-Cepeda C. (2009). CO2 emission from soils under different uses and flooding conditions. *Soil Biology and Biochemistry 41,* 2598-2601

Hall S. A. and Peterson J.A. (2013) Floodplain construction of the Rio Grande at El Paso, Texas, USA: response to Holocene climate change. *Quaternary Science Reviews* v 65 102-119

Hashimoto S. and Komatsu H. (2006) Relationships between soil CO2 concentration and CO2 production, temperature, water content, and gas diffusivity: implications for field studies through sensitivity analyses. *J. For. Res 11* (1), 41-50.

Hilhorst M.A. (2000) A Pore-water Conductivity Sensor. Soil Sci. Soc. Am. J. 64: 192201925

Kearney, J. (2010), Food consumption trends and drivers, Philos. Trans. R. Soc. B, 365, 2793–2807

Kuzyakov Y. (2006) Sources of CO2 efflux from soil and review of partitioning methods *Soil Biology & Biochemistry 38,* 425-448

Liss, P.S. (1973) Processes of gas exchange across an air-water interface. *Deep Sea Research and Oceanographic Abstracts (20)* 221-238

Ma, J., Wang, Z.Y., Stevenson B.A., Zheng X.J., Li, Y. (2013) An inorganic CO2 diffusion and dissolution process explains negative CO2 fluxes in saline/alkaline soils. *Scientific Reports 3:2025* doi:10.1038/srep02025

Millington, R.J., and J.M. Quirk. 1961. Permeability of porous solids. Trans. Faraday Soc. 57:1200–1207. doi:10.1039/tf9615701200

Ortiz, A.C. and Jin, L. (2018a) Physical and chemical controls of salt movement and accumulation in natural versus irrigated soils in arid-lands of southwestern U.S.: a case study in El Paso, TX.

Ortiz, A.C., Ogrinc N., Kaye J., Jin, L. (2018b) Accumulation of pedogenic carbonates in the irrigated agricultural soils of southwest U.S.: an important CO2 efflux from dryland to atmosphere?

Pla C., Cuezva S., Martinez-Martinez J., et al. (2017). Role of soil pore structure in water infiltration and CO2 exchange between the atmosphere and underground air in the vadose zone: A combined laboratory and field approach. Catena 149, 402-416

Rath, K., Rousk, J., 2015. Salt effects on the soil microbial decomposer community and their role in organic carbon cycling: a review. *Soil Biol. Biochem. 81*, 108–123.

Sanchez-Canete, E. P., Kowalski A.S., Serrano-Ortiz P., Perez-Priego, O., Domingo F. (2013). Deep CO2 soil inhalation/exhalation induced by synoptic pressure changes and atmospheric tides in a carbonated semiarid steppe. *Biogeosciences 10,* 6591-6600

Shrivastava P., Kumar R. (2015) Soil salinity: A serious environmental issue and plant growth promoting bacteria as one of the tools for its alleviation. *Saudi Journal of Biological Sciences v* 22 123-131

Szynkiewicz A., et al. (2015) Isotopic studies of the Upper and Middle Rio Grande. Part 2- Salt loads and human impacts in south New Mexico and west Texas. *Chemical Geology v.* 411 336-350

Tilman, D., C. Balzer, J. Hill, and B. L. Befort (2011), Global food demand and the sustainable intensification of agriculture, *Proc. Natl. Acad. Sci. U. S. A., 108*, 20,260–20,264.

Wang, Y., Deng C., Liu, Y., Niu Z., Li, Y.(2015) Identifying change in spatial accumulation of sol salinity in an inland river watershed, China *Science of the Total Environment 621,* 177-185

Williams A. J., et al. (2013) Hydrogeochemistry of the Middle Rio Grande aquifer system – Fluid mixing and salinization of the Rio Grande due to fault inputs, *Chemical Geology,* 351, 281-298

Wong V.N.L., et al. (2009) Carbon dynamics of sodic and saline soils following gypsum and organic material additions: A laboratory incubation. *Applied Soil Ecology (41)* 29-40

World Bank, World Development Report (2008), Agriculture for Development, Washington, D.C.

Xiao, X, Kuang X., Sauer T., et al. (2015) Bare soil carbon dioxide fluxes with time and depth determined by high-resolution gradient-based measurements and surface chambers, *Soil Science Society of America Journal 79,* 1073

Yu Y., Zhao C., Jia H., Niu B., Sheng, Y., Shi, F. (2017). Effects of nitrogen fertilizer, soil temperature and moisture on the soil-surface CO2 efflux and production in an oasis cotton field in arid northwestern China. *Geoderma 308,* 93-103

Zamanian K., Pustovoytov K., Kuzyakov Y. (2016) Pedogenic carbonates: Forms and formation processes. *Earth-Science Reviews 157* 1-17

Chapter 6: Conclusion

The results of this dissertation can provide a new conceptual model of driving mechanisms of soil salinization and C-cycling in our sample sites (Figure 6.1). Where field and experimental data are used, and include an expanded timeline of soil moisture, pore-fluid EC (instead of chemical reactions) and CO_2 before irrigation. This new model highlights field capacity of soils, dilution and dissolution of salts with pore-fluid EC as a proxy for such reactions and bi-directional flux of CO_2 upon flooding and CO_2 efflux as a result of water seal-drying and calcite precipitation.

From our findings in Chapter 1, we propose that continuous irrigation in unmanaged fields will lead to soil salinization and posit that diminished surface water availability will push farmers and stakeholders into using groundwaters for irrigation, which are higher in salinity. Their application would require extended use of soil amendments to preserve critical zone functions and stay agriculturally viable. This adds operation cost and makes farming economically vulnerable, challenging regional sustainability for the Rio Grande valley. Furthermore, soil-texture spatial heterogeneity in this river basin is bound to continue to control where salts precipitate. Additional site-specific amendments should be applied onto soils of high-clay content.

Findings from Chapter 2 show that pedogenic carbonate precipitation in agricultural fields is driven by Ca^{2+} loadings of irrigation practices and not by natural processes. To prevent caliche hardpans, continuous acidification of soils with urea and humic acids needs to remain a priority. Consequently, such soil acidification can be additionally beneficial, as they could convert soils into CO_2 sinks, rather than sources through the dissolution of existing $CaCO_3$.

Although we have quantified irrigation induced abiotic CO_2 as a previously unmeasured carbon flux into the atmosphere in Chapter 3, its relative impact on carbon emission mass balances might be negligible. Certainly, the majority of the CO_2 produced by this process must be uptaken

through the photosynthetic processes occurring in surrounding crops. The quantification of such cycling is open to investigation, which should include upscaling C-cycling with Eddy-covariance towers and chamber measurements.

We have learned from Chapter 4 that inorganic CO_2 fluxes resulting from calcite precipitation will be a function of soil moisture loss, as well as atmospheric pressure pumping. Lateral transport of water and soil gases should also be considered in the field as an additional physical control, which was not parameterized in this work. Impeded or sluggish fluid flow as a result of soil texture heterogeneity needs to be considered, particularly in fine and coarse texture boundaries. These must impact the difference in temporal responses of CO_2 efflux, which are much faster in the field than in 1D column experiments.

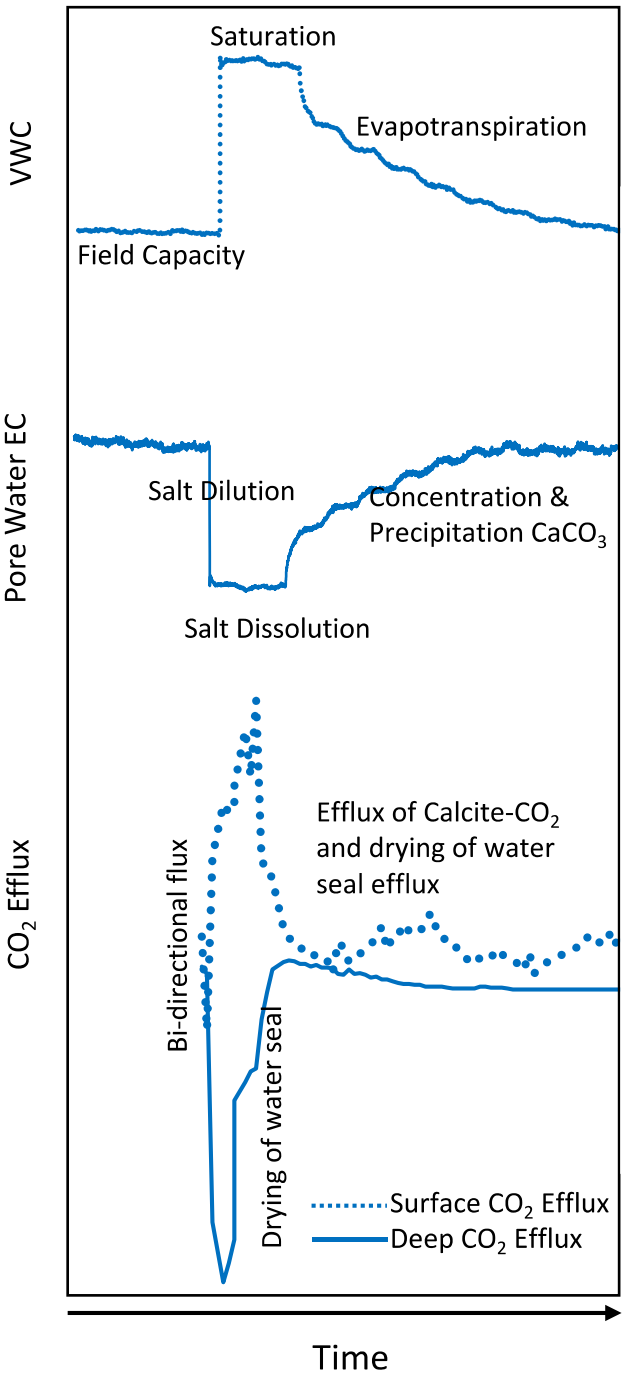

Figure 6.1. The revised conceptual model of field soil moisture, salt dissolution and precipitation and CO_2 efflux with an extended timeline of flooding events in agricultural fields.

Vita

Anna C. Ortiz earned her Bachelor of Science degree in Environmental Science from the University of Texas at El Paso in 2011. In 2014, she received her Master of Science degree in Environmental Science from UTEP. She joined UTEP's doctoral program in Geological Science in 2014.

Anna Ortiz was the recipient of a UTEP Graduate School Dodson Research Grant, UTEP's NSF-funded GK-12 Fellowship, the Geological Society of America Research Grant, the DOE Science Graduate Research Fellowship and UTEP's Hunt Rowling Scholarship.

She has presented her research at several meetings including the 2014 and 2015 American Geophysical Union conferences and the 2017 and 2018 Goldschmidt Conferences. Her work on critical-zone soil salinity will be published in the Biogeochemistry of the Critical Zone Book Volume.

The dissertation, "A combined field, experimental and modeling approach to understand the impacts of flood irrigation on pedogenic $CaCO_3$ and CO_2 dynamics in drylands" was supervised by Dr. Lixin Jin.

Contact Information: anna.ortizc@gmail.com